

Inaugural dissertation
for
obtaining the doctoral degree
of the
Combined Faculty of Mathematics, Engineering and Natural Sciences
of the
Ruprecht - Karls - University
Heidelberg

Presented by

M.Sc. Dimitrios Papagiannidis

born in Athens, Greece

Oral examination: 17.05.2022

Endoplasmic reticulum size and shape control in *Saccharomyces cerevisiae*

Referees: Prof. Dr. Bernd Bukau
Prof. Dr. Sebastian Schuck

I. Summary

Cells resize and reshape their organelles in response to changing physiological demands. This thesis focuses on the endoplasmic reticulum (ER), an organelle which, depending on cell type and physiological conditions, displays remarkable adaptability in both size and shape. Although much is known about the role of proteins in ER morphogenesis, the mechanisms controlling the biogenesis of its membrane, and hence size, are unclear. In this work, I build upon a genetic screen performed to identify genes involved in ER expansion in the budding yeast, *Saccharomyces cerevisiae*, and I focus on the poorly characterised ER membrane protein Ice2p. I show that Ice2p is required for and promotes ER expansion, and that it does so independently of the central determinant of ER homeostasis, the unfolded protein response (UPR). To further uncover the molecular role of Ice2p, I explore known genetic interactions and discover that Ice2p opposes the activity of Pah1p, which is a conserved phosphatidic acid phosphatase with a central role in the regulation of lipid synthesis in yeast. Specifically, I show that Ice2p interacts with and inhibits the conserved Spo7p-Nem1p complex, which normally dephosphorylates and activates Pah1p. By showing that Ice2p cooperates with pathways transcriptionally controlling lipid synthesis, and with the UPR to maintain cell homeostasis, I place Ice2 into a broader cellular context. Additionally, I present preliminary data approaching the physiological conditions during which cells use Ice2p-Pah1p to control the size of their ER. Finally, in the last part of the thesis, I follow up on the unexpected observation that the reticulon proteins, which are membrane proteins with a central and conserved role in ER morphogenesis, form cytosolic puncta after prolonged ER stress, a phenotype especially pronounced in cells lacking Ice2p. These data suggest that there are mechanisms controlling the membrane association of reticulon proteins, and as an extension ER shape. Overall, this thesis extends the understanding of mechanisms regulating the biogenesis of ER membrane as well as its morphogenesis and provides the ground for future work not only in yeast but also in higher eukaryotes.

II. Zusammenfassung

Zellen verändern die Größe und Form ihrer Organellen als Reaktion auf veränderte physiologische Anforderungen. Diese Arbeit konzentriert sich auf das Endoplasmatische Retikulum (ER), einem Organell, das je nach Zelltyp und physiologischer Bedingung eine bemerkenswerte Anpassungsfähigkeit in Bezug auf Größe und Form aufweist. Obwohl viel über die Rolle von Proteinen bei der Morphogenese des ERs bekannt ist, sind die Mechanismen, die die Biogenese seiner Membran und damit auch seine Größe kontrollieren, unklar. In dieser Arbeit baue ich auf einem genetischen Screening auf, das zur Identifizierung von Genen durchgeführt wurde, die an der ER-Erweiterung in der Hefe *Saccharomyces cerevisiae* beteiligt sind. Insbesondere konzentriere ich mich auf das derzeit nur wenig charakterisierte ER-Membranprotein Ice2p. Ich zeige, dass Ice2p für die ER-Erweiterung erforderlich ist und diese fördert, und zwar unabhängig von der Unfolded Protein Response (UPR), der zentralen Determinante der ER-Homöostase. Um die molekulare Rolle von Ice2p weiter aufzudecken, untersuchte ich bekannte genetische Interaktionen und entdeckte, dass Ice2p der Aktivität von Pah1p, einer konservierten Phosphatidsäurephosphatase, die eine zentrale Rolle bei der Regulierung der Lipidsynthese in Hefe spielt, entgegenwirkt. Ich zeige insbesondere, dass Ice2p mit dem konservierten Nem1p-Spo7p-Komplex, der normalerweise Pah1p dephosphoryliert und aktiviert, interagiert und diesen hemmt. Indem ich zeige, dass Ice2p in Signalwegen eine Rolle spielt, die die Lipidsynthese transkriptionell kontrollieren, und mit der UPR, um die Zellhomöostase aufrechtzuerhalten, stelle ich Ice2 in einen breiteren zellulären Kontext. Darüber hinaus präsentiere ich vorläufige Daten zu den physiologischen Bedingungen, unter denen Zellen Ice2p-Pah1p zur Kontrolle der Größe ihres ERs nutzen. Im letzten Teil der Arbeit gehe ich schließlich auf die unerwartete Beobachtung ein, dass die Retikulum-Proteine, bei denen es sich um Membranproteine handelt, die eine zentrale und konservierte Rolle bei der ER-Morphogenese spielen, nach längerem ER-Stress zytosolische Pünktchen bilden; ein Phänotyp, der in Zellen, denen Ice2p fehlt, besonders ausgeprägt ist. Diese Daten deuten darauf hin, dass es unbekannte Mechanismen geben könnte, die die Membranassoziation von Retikulumproteinen und damit auch die Form des ER kontrollieren. Insgesamt erweitert diese Arbeit das Verständnis der Mechanismen, die die Biogenese der ER-Membran sowie ihre Morphogenese regulieren, und bereitet somit die Grundlage für weiterführende Arbeiten sowohl in Hefe als auch in höheren Eukaryonten.

Table of Contents

<i>I. Summary</i>	<i>i</i>
<i>II. Zusammenfassung</i>	<i>ii</i>
<i>III. Acknowledgements</i>	<i>vi</i>
<i>IV. Contributions</i>	<i>vii</i>
<i>V. Yeast gene and protein nomenclature and list of abbreviations</i>	<i>viii</i>
<i>VI. List of Figures</i>	<i>ix</i>
<i>VII. List of Tables</i>	<i>x</i>
<i>1. Introduction</i>	<i>1</i>
1.1 The endoplasmic reticulum	1
1.1.1 Morphology of the ER.....	2
1.1.2 Form follows function.....	3
1.1.3 ER stress	5
1.1.4 Yeast as a model organism for ER size and shape.....	6
1.2 Lipid synthesis in yeast	7
1.2.1 Phospholipid synthesis pathways and interplay with lipid storage	7
1.2.2 Lipid metabolism regulation: precursor availability	8
1.2.3 Lipid metabolism regulation: enzyme availability.....	10
1.3 A screen to identify factors involved in ER expansion	11
1.3.1 Ice2p.....	11
1.4 Aims of this thesis	13
<i>2. Materials and Methods</i>	<i>14</i>
2.1 Materials	14
2.1.2 Growth media and plates.....	20
2.1.2 Enzymes, standards and kits.....	22
2.1.3 Antibodies	24
2.1.4 PAGE gel recipes	25
2.2 Methods	26
2.2.1 Plasmids	26

2.2.2 Yeast strains.....	29
2.2.3 Growth conditions and treatments.....	33
2.2.4 Light microscopy.....	34
2.2.5 Correlative light and electron microscopy (CLEM).....	35
2.2.6 Yeast cell lysis.....	36
2.2.7 Protein determination.....	38
2.2.8 Total membrane preparation.....	38
2.2.9 Subcellular fractionation.....	38
2.2.10 Microsome preparation.....	39
2.2.11 Immunoprecipitation.....	39
2.2.12 Co-immunoprecipitation.....	40
2.2.13 Pah1p dephosphorylation and phosphorylation in vitro.....	40
2.2.14 Proximity biotinylation assay.....	40
2.2.15 Western blotting.....	41
2.2.16 PhosTag-PAGE.....	41
2.2.17 Quantitative real-time PCR.....	42
2.2.18 Flow cytometry.....	43
2.2.19 Growth assays.....	44
2.2.20 Lipidomic analysis.....	44
3. Results.....	47
3.1 ER remodelling in yeast.....	47
3.1.1 Visualisation of the ER by fluorescence microscopy.....	47
3.1.2 Qualitative description of peripheral ER expansion.....	49
3.1.3 Quantitative description of cortical ER expansion.....	51
3.2 <i>ICE2</i> is required for and promotes ER expansion.....	52
3.2.1 <i>ICE2</i> is required for lipid synthesis-mediated ER expansion.....	52
3.2.2 <i>ICE2</i> is required for ER stress-mediated ER expansion.....	54
3.2.3 <i>ICE2</i> overexpression and ER expansion.....	58
3.3 Unravelling the molecular role of <i>Ice2p</i>.....	59
3.3.1 <i>Ice2p</i> acts independently of the reticulon proteins.....	59
3.3.2 <i>Ice2p</i> acts independently of lipid droplets.....	60
3.3.3 <i>ICE2</i> is functionally linked to phospholipid synthesis.....	61
3.3.4 <i>Ice2p</i> controls the phosphorylation status of Pah1p.....	65
3.3.5 <i>Ice2</i> interacts with and restricts the Spo7p-Nem1p complex.....	68

3.4 Inhibition of Spo7p-Nem1p by Ice2p promotes phospholipid synthesis and ER expansion	71
3.4.1 <i>ICE2</i> deletion promotes phospholipid synthesis	71
3.4.2 Ice2p promotes ER expansion by inhibiting Pah1p	74
3.5 How does <i>ICE2</i> coordinate with other pathways regulating ER homeostasis? ..	76
3.5.1 <i>ICE2</i> cooperates with <i>OPI1</i> to promote ER expansion.....	76
3.5.2 <i>ICE2</i> helps maintain cell homeostasis	77
3.6 Preliminary observations on the physiological role of the regulation of Pah1p .	78
3.6.1 Stress-induced and lipid synthesis-induced ER expansion	78
3.6.2 ER expansion upon exit from stationary phase	80
3.7 ER expansion by regulation of ER-tubulating proteins	82
4. Discussion and outlook.....	88
4.1 An updated model connecting lipid synthesis to ER membrane biogenesis	88
4.2 Revisiting existing literature on <i>ICE2</i>	91
4.2.1 Reported genetic interactions.....	91
4.2.2 <i>ICE2</i> and protein quality control	91
4.2.3 <i>ICE2</i> and its link to lipid droplets, ER inheritance and zinc homeostasis	92
4.3 The Pah1p/Lipin switch and ER expansion.....	93
4.3.1 The Pah1p/Lipin switch and ER stress.....	93
4.3.2 The Pah1p/Lipin switch and exit from stationary phase	94
4.4 How could Ice2p be regulated?	95
4.5 Conservation	96
4.6 ER morphogenesis factors and ER sheet formation.....	97
4.7 Control of ER size and shape – future directions.....	97
5. Bibliography	100

III. Acknowledgements

First of all I would like to thank Sebastian. Thank you for being my mentor and helping me to develop as a scientist. Thanks for all of the fruitful discussions, spontaneous meetings and grounding sessions.

I would also like to thank my TAC members, Bernd and Walter, for the valuable input during our meetings and for encouraging me to get out of my comfort zone.

Next, I would like to thank all members of the Schuck lab, past and present, for contributing to this incredible working atmosphere. In addition to that, I would like to thank Peter for the supervision during my Master thesis which evolved into a wonderful collaboration; Jasmin, for introducing me to the Schuck lab and for all our breakfast conversations; Tamas, for the constant challenging of every.single.new.result; Rolf for all the brainstorming sessions, about anything; Oli for all the music company, Sibi for the invaluable support – especially during the revisions – and both of you for making the shift system something to look forward to (!); Giulia for exploring the mysteries of Lipin together; Lis for the uncountable ethical dilemma resolutions; Aye and Niklas, for all of the discussions and, of course, the frequent C&C supply. I would also like to thank all ZMBH members for sharing reagents and know-how, and specifically Matthias and Daniel from the Knop lab. Außerdem möchte ich mich für die ständige Unterstützung durch das Team der Spülküche bedanken. Ich weiß wie viel Arbeit das ist, und ich hoffe Sie wissen, wie wertvoll ihre Arbeit für uns ist. Vielen Dank!

As it is quite obvious, climbing has been a central part of this experience, helping to keep me sane (or rather keeping me from getting completely insane) and motivated. Thanks to everyone who participated in this. Nils and Hanna, thanks for the additional supply of motivation and determination, which of course extended beyond climbing!

This experience would not have been possible without the unconditional support, in all shapes and forms, from all my friends and family (who are, in fact, one and the same).

Nic, what can I say. We started this journey together all the way back in 2014 during our Master studies, and found a way to share all its different phases leading up to the completion of our PhDs in sync. Let's see what the future brings us!

Last, I cannot even begin to explain (quite literally) how grateful I am to you, Sophie. Your endless curiosity, enthusiasm, energy, critical thinking and understanding have been a source of motivation, inspiration and support without which these last years would not have been a wonderful and productive experience.

IV. Contributions

A significant proportion of the results presented here were recently published in The EMBO Journal (Papagiannidis et al., 2021). This includes data presented in Figures 5B, 6, 7, 8, 9, 11, 12B-D,H, 13C-G, 14,15,16,17 and 18. Sebastian Schuck and Peter Bircham contributed to the conceptualisation of the study. All experiments were conceptualised and designed by me and some experiments were performed in collaboration with colleagues as also indicated in the main text and figure legends.

The growth assays presented in Figure 10A, Figure 11A and Figures 12 B,C,E-F were conceptualised, designed and performed in collaboration with Peter Bircham.

The imaging experiments presented in Figure 14H were initially performed by me and were repeated and quantified by Oliver Pajonk.

The lipidomics experiments presented in Figure 15 and Figure 16E (all steps after the cell lysis) were performed by Christian Luchtenborg and Britta Brügger.

The growth assays presented in Figure 18A were initially performed by me and were repeated by Giulia Ruffini.

The imaging experiment presented in Figure 20A was initially performed by me and was repeated by Oliver Pajonk under my supervision.

The CLEM experiment presented in Figure 23B was conceptualised, designed and performed in collaboration with Ayelen Valko. High-pressure freezing, freeze substitution, sectioning and post-staining was performed by Charlotta Funaya.

The imaging pulse-chase experiments presented in Figure 24 were conceptualised and designed in collaboration with Ayelen Valko and were performed by Artur Astapenka under our supervision.

All other experiments were carried out by me.

V. Yeast gene and protein nomenclature and list of abbreviations

Taking the *YFG* wild-type gene as an example, *yfg* refers to a mutant version and *yfg* Δ to a deletion mutant. Exceptions are the strain lacking all yeast reticulon and reticulon-like proteins, which is referred to as Δ *rtns*, and the strain unable to form lipid droplets, which is referred to as Δ *LD*. *Yfgp* refers to the corresponding wild-type protein and *yfgp* to a mutant version.

APS	Ammonium persulfate
CDP-DAG	Cytidine diphosphate diacylglycerol
CLEM	Correlative light and electron microscopy
DAG	Diacylglycerol
DTT	Dithiothreitol
EE	Ergosterol esters
EM	Electron microscopy
ER	Endoplasmic reticulum
ERAD	ER associated degradation
FastAP	Alkaline phosphatase
G418	Geneticin
HPF	High pressure freezing
LD	Lipid droplet
MDH	Monodansylpentane
OD	Optical density
PA	Phosphatidic acid
PAGE	Polyacrylamide gel electrophoresis
PC	Phosphatidylcholine
PE	Phosphatidylethanolamine
PI	Phosphatidylinositol
SDS	Sodium dodecyl sulfate
TAG	Triacylglycerol
Tm	Tunicamycin
UPR	Unfolded protein response
UPRE	UPR response element
YNB	Yeast nitrogen base

VI. List of Figures

Figure 1. Phospholipid synthesis pathways in yeast	8
Figure 2. Phosphoregulation of Pah1p	9
Figure 3. Visualisation of the ER in yeast	48
Figure 4. Qualitative description of ER expansion	50
Figure 5. Quantitative description of cortical ER expansion	51
Figure 6. ICE2 is required for ER expansion upon activation of phospholipid synthesis	53
Figure 7. ICE2 is required for ER stress-induced ER expansion	55
Figure 8. ICE2 is required for ER stress-induced ER expansion	57
Figure 9. ICE2 overexpression promotes ER expansion independently of and without activating the UPR.....	58
Figure 10. ICE2 acts independently of the reticulons	60
Figure 11. ICE2 acts independently of lipid droplets	61
Figure 12. ICE2 is functionally linked to SPO7, NEM1 and PAH1	63
Figure 13. Ice2p opposes Pah1p dephosphorylation by inhibiting the Spo7p-Nem1p complex.....	67
Figure 14. Ice2p interacts with and spatially restricts the Spo7p-Nem1p complex	70
Figure 15. Inhibition of the Spo7p-Nem1p complex by Ice2p promotes phospholipid synthesis	73
Figure 16. Ice2p promotes ER expansion by regulating the phosphorylation status of Pah1p.....	75
Figure 17. ICE2 cooperates with OPI1 to promote ER expansion	76
Figure 18. ICE2 cooperates with the UPR to maintain cell homeostasis.....	77
Figure 19. Preliminary data on role of the regulation of Pah1p during ER stress	79
Figure 20. Preliminary data on role of the regulation of Pah1p during exit from stationary phase	81
Figure 21. Rtn1-only puncta are not specific to the ER stressor or fluorescent protein used	83
Figure 22. Yop1p also forms Sec63-negative puncta after prolonged ER stress	84
Figure 23. Rtn1-only puncta are not membrane bound.....	86

Figure 24. Cytosolic Rtn1-only puncta are formed by molecules that were initially membrane inserted	87
Figure 25. Model for pathways controlling ER membrane biogenesis	90

VII. List of Tables

Table 1. Drugs and chemical compounds used in this study.....	14
Table 2. Buffers and solutions used in this study.....	15
Table 3. Synthetic complete amino acid mix	19
Table 4. Media for liquid cultures.....	20
Table 5. Plates	21
Table 6. Enzymes used in this study.....	22
Table 7. Standards and kits used in this study	23
Table 8. Antibodies used in this study.....	24
Table 9. Recipes for PAGE gels	25
Table 10. Plasmids used in this study	26
Table 11. Oligonucleotides used in this study	27
Table 12. Strains used in this study	29

1. Introduction

One of the key requirements for life is the ability to respond and adapt to changing environmental conditions. This holds true across different layers of complexity; from behavioural adaptation, such as dressing warmly or lighting a fire to keep warm; physiological adaptation, such as constricting of blood vessels to minimise heat loss; down to the molecular scale, with single cell adaptation to local environments. The “ultimate goal” of these adaptations is the maintenance of homeostasis, and as an extension, life.

Eukaryotic cells are characterised, apart from their name-giving nucleus, by the presence of various subcellular membrane-bound compartments, termed organelles. Each organelle comprises a specialised environment where designated biochemical reactions can take place. As an adaptive response to different physiological conditions, cells modulate the function of their organelles. This modulation often extends to the size and shape of the organelles, in accordance with the principle “form follows function”. The focus of this thesis is the remodelling of endoplasmic reticulum (ER), and specifically the biogenesis of the ER membrane.

1.1 The endoplasmic reticulum

Initial reports of the ER date back to 1902 when Emilio Veratti first described in detail the geometrical arrangement of a reticulate apparatus on histological sections of muscle fibres (Veratti, 1961), although the first observations of this organelle are thought to date even earlier – back to 1890 – by, among others, Santiago Ramón y Cajal (Mazzarello et al., 2003). These initial observations were, however, not followed up. The ER was then re-discovered in 1945 by Porter and colleagues in electron micrographs of cultured cells from chick embryos (Porter et al., 1945). During the following decade, as electron microscopy and sample preparation kept improving, the ER was described in more detail mainly by Keith Porter and George Palade (Palade, 1955, 1956), two of the fathers of cell biology (Jamieson, 2008; Schekman, 2008). From early on it became evident that the shape and size of the endoplasmic reticulum can drastically vary between different cell types (Palade and Porter, 1954; Porter and Palade, 1957).

1.1.1 Morphology of the ER

The ER forms the nuclear envelope and extends into the cytosol forming the so-called peripheral ER; a continuum of structures, ranging from cylindrical tubules to flat membrane cisternae (termed ER sheets), forming an interconnected network. Besides tubules and sheets, intermediate structures have been described, such as fenestrated sheets (Puhka et al., 2012), tubular matrices (Nixon-Abell et al., 2016) and nanoholes (Bahmanyar et al., 2018; Schroeder et al., 2019). Moreover, it was recently reported that two different types of tubules exist (Wang et al., 2021a). The peripheral ER assumes its shape with the help of various proteins, with mechanisms that are to a very large extent conserved from yeast to humans. The best understood class of ER shaping proteins are the reticulon and reticulon-like proteins, which localise to and help form high curvature ER, namely ER tubules and the edges of ER sheets (Voeltz et al., 2006). Yeast has two reticulons and one reticulon-like protein, namely Rtn1p, Rtn2p and Yop1p. These proteins have a characteristic membrane topology which contributes to the formation of ER tubules. The so-called reticulon homology domain (RHD) is composed of two membrane domains which are proposed to form a wedge-like structure. This, in combination with a conserved amphipathic helix of the RHD (Brady et al., 2015; Wang et al., 2021b) and the fact that reticulon and reticulon-like proteins can oligomerise (Hu et al., 2008; Shibata et al., 2008), leads to the formation and stabilisation of highly curved ER.

Although sufficient to promote tubule formation (Voeltz et al., 2006), the action of the reticulon and reticulon-like proteins alone is necessary but insufficient to achieve the complex network structure of the ER. Another class of proteins contributing to ER morphogenesis are the atlastins, dynamin-like GTPases which mediate homotypic ER fusion (Hu et al., 2009b; Orso et al., 2009). In yeast this function is carried out by Sey1p (Anwar et al., 2012). The combination of the tubulating function of the reticulons with the fusion function of the atlastins is sufficient to produce a tubular network *in vitro* (Powers et al., 2017). Although not required for the formation of a tubular network *in vitro*, the protein Lunapark, which localises at and stabilises three-way junctions of ER tubules, is important for the ER structure *in vivo* (Chen et al., 2012).

When it comes to the formation of ER sheets, much less is known. It has been proposed that the stabilisation of ER sheet edges by reticulon and reticulon-like proteins is sufficient for the formation of ER sheets (Shibata et al., 2010; Shemesh et al., 2014). No ER sheet-forming

protein has been identified to date, although different proteins have been proposed to stabilise ER sheets or act as luminal spacers, including ribosomes (Shibata et al., 2006, 2010; Prinz et al., 2000), or, in higher eukaryotes, CLIMP63 (Klopfenstein et al., 2001), p180 and kinectin (Shibata et al., 2010), and NOMO (Amaya et al., 2021). In yeast, ER sheets are thought to form when the tubulating capacity of the cells, as mediated by the reticulons, is exceeded by the amount of ER membrane (Schuck et al., 2009). The amount of ER membrane is not only linked to ER shape, as in the example of yeast, but also to ER size.

Apart from the amount of ER membrane, its lipid composition has also been linked to different ER morphologies. It was recently observed that an increase in phosphatidylinositol (PI) levels correlate with ER sheet formation, at least in *C.elegans* (Bahmanyar et al., 2014; Bahmanyar, 2015).

1.1.2 Form follows function

Why would an organelle assume different morphologies? The ER carries out a variety of different functions. It is involved in protein synthesis, which includes protein translation and translocation, post-translational modification and folding, lipid synthesis and, in higher eukaryotes, calcium storage (Schwarz and Blower, 2016). Different parts of the ER are associated with different functions.

ER sheets, which are commonly referred to as “rough ER”, are densely studded with ribosomes and are specialised in protein synthesis and folding (Voeltz et al., 2002; Schwarz and Blower, 2016). Membrane proteins of the secretory pathway as well as luminal proteins and proteins to be secreted are co-translationally or post-translationally translocated into the ER (Aviram and Schuldiner, 2017). Targeting to the ER is dictated by cis-encoded signal sequences and can be achieved through different pathways. The canonical route involves the Sec61p translocon and the contribution of the ER luminal chaperone BiP (Kar2p in yeast) (Rapoport, 2007). Other pathways are the GET pathway, for tail anchored proteins (Schuldiner et al., 2008), and the SND pathway (Aviram and Schuldiner, 2017). In the case of transmembrane domains of co-translationally targeted proteins, their topology is defined during their co-translational translocation. A combination of the activity of chaperones with the increased luminal space of ER sheets contributes to protein folding. Moreover, the biochemical environment of the ER allows posttranslational modifications such as disulfide

bond formation and protein glycosylation. Proteins that move through the secretory pathway do so in transport carriers that bud off from the ER and are targeted to the Golgi.

In contrast, ER tubules, which are less densely studded with ribosomes, are referred to as “smooth ER”. ER tubules are thought to be required for lipid synthesis, another process in which the ER plays a central part (Voeltz et al., 2002). Many phospholipid synthesis enzymes display an ER localisation (Jacquemyn et al., 2017). Once synthesised, lipids can be transferred to other organelles as components of transport carriers or through contact sites between the ER and the target organelle. Contact sites of the ER with other organelles have roles that extend beyond lipid transfer, such as lipid synthesis, organelle dynamics and organelle biogenesis (Phillips and Voeltz, 2016).

The specialisation of ER subdomains to different functions becomes evident in physiological examples. Ensuring proper ER shape and size is a central part in cell differentiation. Specialised protein secreting cells, like pancreatic acinar cells, salivary gland acinar cells and plasma cells, are characterised by an extensive ER network predominantly composed of ER sheets (Fawcett, 1981; Zucker-Franklin, 1988; Lee et al., 2005; Trezise and Nutt, 2021). On the other hand, steroid hormone secreting cells like Leydig cells are characterised by an extensive ER network, but are predominantly composed of ER tubules (Fawcett, 1981; Benton et al., 1995; Li et al., 2019). The ER, therefore, assumes different morphologies to accommodate the specialised functions of different cell types.

Defects in ER shape and function lead to different diseases. Disruption of the highly dynamic tubular ER network of neurons, for example, has been associated with neurodegenerative diseases (Renvoisé and Blackstone, 2010; Westrate et al., 2015). Mutations in the ER shaping proteins ATL1, an atlastin, and REEP1, a reticulon-like protein, are linked to Hereditary Spastic Paraplegia (Blackstone, 2012; Westrate et al., 2015) and alterations in the contact sites between the ER and mitochondria are linked to Alzheimer's disease (Hedskog et al., 2013). Moreover, viruses can hijack host's ER functions and alter its structure not only to accommodate the translation of their genome, but also to achieve cell entry, genome replication and cell exit (Inoue and Tsai, 2013; Ravindran et al., 2016).

1.1.3 ER stress

Disruption of the processes carried out in the ER leads to what is termed ER stress. ER stress is sensed and countered by cells to restore homeostasis.

The most studied type of ER stress is the one caused by accumulation of misfolded proteins. This can be caused by errors during translation, the expression of constitutively misfolded proteins, disruption of the folding process due to inability to form post-translational modifications or exposure to environmental stresses such as elevated temperature. The initial cellular response to misfolded proteins at the ER is their degradation, following a pathway called ER associated degradation (ERAD). ERAD involves the recognition and ubiquitination of misfolded proteins, their retrotranslocation to the cytosol and their proteasomal degradation (Ruggiano et al., 2014; Wu and Rapoport, 2018; Sun and Brodsky, 2019). The inability of cells to cope with the load of misfolded proteins leads to the activation of the unfolded protein response (UPR). The UPR is a transcriptional program that leads to an increase of chaperone levels and the expansion of the ER, thereby increasing the folding capacity of the organelle; the upregulation of ERAD and protein degradation; and in mammalian cells, the arrest of general protein translation, which reduces the load of the protein folding machinery (Ron and Walter, 2007; Walter and Ron, 2011). In yeast, the UPR is a linear pathway which involves the ER transmembrane protein Ire1p and the transcription factor Hac1p. Accumulation of misfolded proteins leads to activation of Ire1p by mechanisms that are under debate. There are two prevailing models. The first model suggests that at steady state Ire1p is bound to and kept inactive by Kar2p. Accumulating misfolded proteins compete with Ire1p for binding of Kar2p, leading to dissociation of Kar2p and activation of Ire1p (Okamura et al., 2000; Bertolotti et al., 2000). The second suggests that Ire1p can directly bind misfolded proteins and that these act as activating ligands (Gardner and Walter, 2011).

Activation of Ire1p involves initial dimer formation, trans-autophosphorylation and subsequent higher order oligomer formation. Apart from a kinase, Ire1p is also an endonuclease. When active, Ire1p mediates the unconventional splicing of the *HAC1*-mRNA which, in turn, activates the transcription of genes containing a UPR response element (UPRE; Mori et al., 1998). In higher eukaryotes the UPR consists of, in addition to the IRE1 pathway, two additional branches. These are mediated by the proteins PERK and ATF6 (Ron and Walter, 2007; Walter and Ron, 2011). Apart from decreasing the protein folding load of

the organelle, the mammalian UPR branches also reduce the protein load by either Ire1p-mediated mRNA degradation (Hollien and Weissman, 2006) or the arrest of protein translation (Ron and Walter, 2007; Walter and Ron, 2011). In some cases, after prolonged ER stress, apoptosis is also induced.

Cells can also activate the UPR in response to perturbations in the physicochemical properties of the ER membrane, conditions which are referred to as lipid bilayer stress (Ernst et al., 2018; Radanović and Ernst, 2021). Remarkably, some of these conditions are sensed by Ire1p, such as the depletion of inositol (Cox et al., 1997), increased degree of lipid saturation (Volmer et al., 2013) and altered lipid packing density (Halbleib et al., 2017).

In addition to the UPR, ER stress also leads to activation of both macro and micro ER-phagy pathways, through which aberrant proteins or excess ER domains are degraded (Fregno and Molinari, 2018; Schuck, 2020). In a study published in 2009, Schuck et al showed that ER membrane expansion can alleviate misfolded protein-induced ER stress independently of the UPR (Schuck et al., 2009). This study not only confirms the increased luminal space of the ER as a contributing factor to ER folding, but also highlights the relevance of ER expansion in conditions of ER stress.

1.1.4 Yeast as a model organism for ER size and shape

The peripheral ER in yeast is localised directly underneath the plasma membrane, thereby facilitating the assessment of ER morphology by fluorescence microscopy. The function of the ER can be interfered pharmacologically. Treatment of yeast cells with DTT, which disrupts disulfate bond formation, and tunicamycin, which blocks protein glycosylation, both lead to protein misfolding in the ER, causing ER stress and, as an extension, ER expansion. Moreover, the ease of yeast genetic manipulations allows studying the role of individual proteins on endogenous levels, as well as high throughput studies. These features, together with the fact that the mechanisms determining the morphology of the ER are to a large extent conserved make yeast an ideal model organism to study ER morphogenesis.

1.2 Lipid synthesis in yeast

In order for cells to expand their ER, they need to produce more membrane and, as an extension, more membrane phospholipids. Understanding the mechanisms that govern ER expansion, therefore, requires understanding of the phospholipid synthesis pathways.

1.2.1 Phospholipid synthesis pathways and interplay with lipid storage

Yeast cells grown in minimal media rely on the so-called cytidine diphosphate diacylglycerol (CDP-DAG) pathway for the production of the different phospholipid species (Figure 1). In this pathway phosphatidic acid (PA) serves as a precursor for all membrane phospholipids. In brief, PA is converted to CDP-DAG by Cds1p (Shen et al., 1996) which is, in turn, either converted to PI by Pis1p (Nikawa and Yamashita, 1984; Nikawa et al., 1987) or to phosphatidylserine (PS) by Cho1p (Atkinson et al., 1980; Kiyono et al., 1987). PS serves as a precursor of phosphatidylethanolamine (PE), with reactions mediated by Psd1p (Clancey et al., 1993) and Psd2p. PE is converted to phosphatidylcholine (PC) by Cho2p and Opi3p (Kodaki and Yamashita, 1987).

In the presence of exogenous ethanolamine or choline, yeast cells activate the Kennedy pathway which, as opposed to the CDP-DAG pathway, is conserved between yeast and humans. In this pathway diacylglycerol (DAG) serves as a precursor for the main membrane phospholipids PE and PC (Carman and Henry, 1989; Kwiatek et al., 2020).

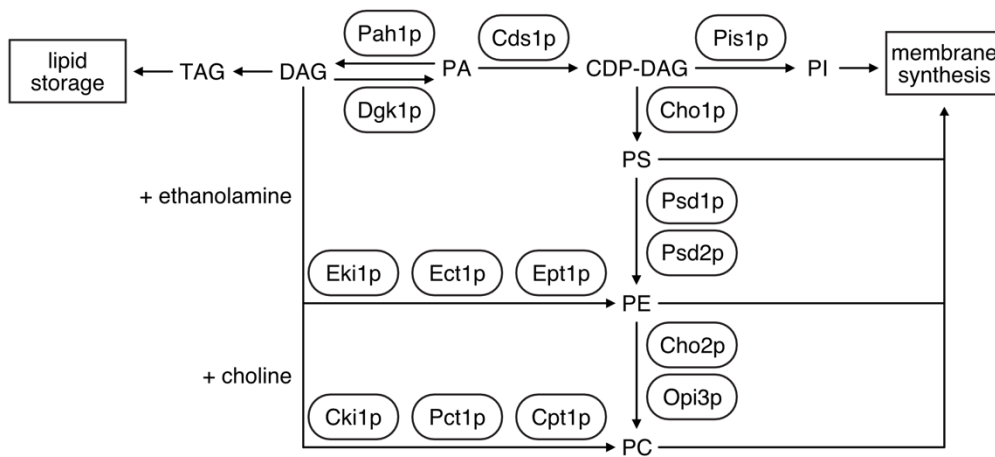


Figure 1. Phospholipid synthesis pathways in yeast

Schematic depicting the phospholipid synthesis pathways in yeast together with their interplay with the production of the storage lipid TAG. TAG: triacylglycerol, DAG: diacylglycerol, CDP-DAG: cytidine diphosphate diacylglycerol, PI: phosphatidylinositol, PS: phosphatidylserine, PE: phosphatidylethanolamine, PC: phosphatidylcholine. Modified from (Papagiannidis et al., 2021).

In addition to membrane phospholipids, PA is also the precursor of triacylglycerol (TAG), which together with the other neutral lipid class, ergosterol esters (EE), is stored in lipid droplets. This places PA at the bifurcation point where cells decide whether to produce either membrane or storage lipids, making PA homeostasis crucial for cell physiology.

The two enzymes that are most relevant for this are Pah1p, which uses PA as a substrate to produce DAG (Han et al., 2006), and Dgk1p (Han et al., 2008), which catalyses the opposite reaction. Pah1p therefore promotes lipid storage whereas Dgk1p promotes membrane synthesis. The other enzymes that either produce PA, namely the lysoPA acyltransferases Slc1p, Slc4p and Loa1p and the phospholipase D, or use it as substrate, such as Cds1p or the PA phosphatases Lpp1p, Dpp1p and App1p only play a minor role in PA homeostasis (Klug and Daum, 2014; Kwiatek et al., 2020).

1.2.2 Lipid metabolism regulation: precursor availability

Since PA can both be used for membrane and storage lipid synthesis, the interconversion of PA to DAG at the ER, mediated by Pah1p and Dgk1p, is under strict regulation.

In proliferating cells, when lipid metabolism is focused on membrane biogenesis, Pah1p displays a cytosolic localisation, is heavily phosphorylated and inactive (Figure 2). Pah1p can

be phosphorylated in 38 different sites by a plethora of different kinases and in response to stimuli such as nutrient availability. Most of these phosphorylations have an inhibitory effect on Pah1p by promoting its cytosolic localisation, promoting its degradation or inhibiting its enzymatic activity (Carman and Han, 2019; Kwiatek et al., 2020). Despite the high number of phosphosites, a core of 7 to 8 sites are the most relevant for activity of Pah1p (O'Hara et al., 2006; Su et al., 2014). Although Pah1p can be phosphorylated by many kinases, there is only one described Pah1p phosphatase, the Spo7p-Nem1p complex (Siniossoglou et al., 1998; Santos-Rosa et al., 2005). Nem1p is an ER transmembrane phosphatase and Spo7p, another ER membrane protein, is its obligate activator. Pah1p activation requires its interaction with the Spo7p-Nem1p complex. This interaction is mediated by the acidic tail of Pah1p, leads to Pah1p dephosphorylation, enzymatic activation and further stabilisation of its interaction with the ER membrane (Karanasios et al., 2013, 2010). There, Pah1p has access to its substrate, PA, and dephosphorylates it to DAG. Active Pah1p is rapidly degraded, presumably to avoid lipotoxicity caused by accumulation of DAG (Hsieh et al., 2016). The activity of the Spo7p-Nem1p complex is also regulated by phosphorylation. Specifically, Spo7p-Nem1p is inhibited by PKA-mediated phosphorylation (Su et al., 2018) and by mTOR-mediated phosphorylation (Dubots et al., 2014). Finally, activity of Dgk1p is also positively regulated by phosphorylation (Qiu et al., 2016).

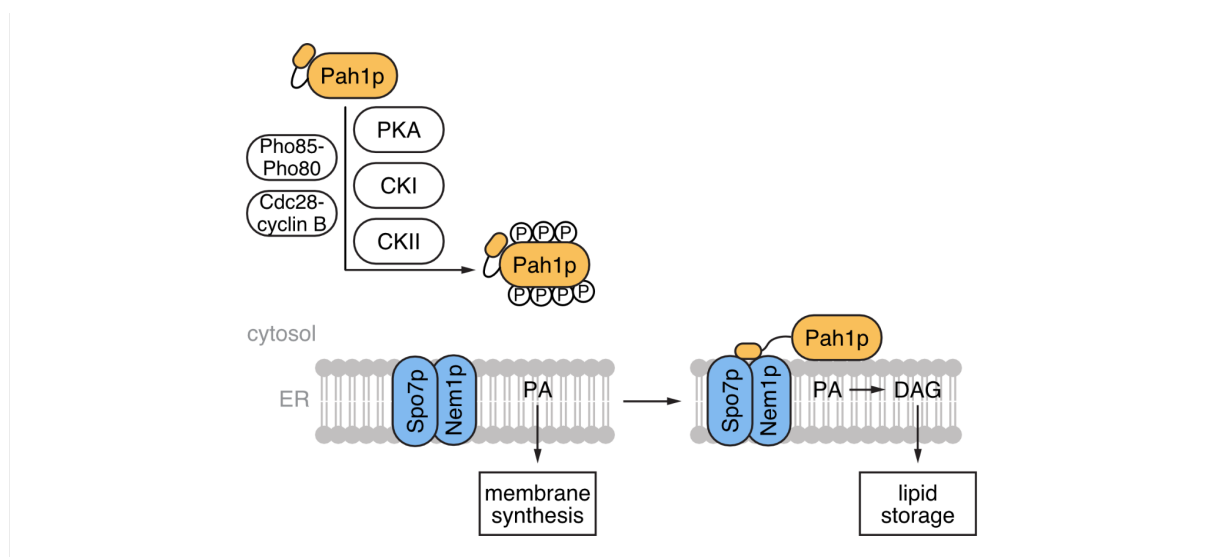


Figure 2. Phosphoregulation of Pah1p

Schematic depicting the phosphoregulation of Pah1p. Inactive Pah1p is heavily phosphorylated and displays a cytosolic localisation. Pah1p can be phosphorylated by the kinases Pho85-Pho80, Cdc28-cyclin B, PKA, CKI and CKII. Activation of Pah1p requires its interaction with and dephosphorylation by the Spo7p-Nem1p phosphatase complex. Active Pah1p associates with the ER membrane and dephosphorylates phosphatidic acid (PA) to diacylglycerol (DAG). Modified from (Papagiannidis et al., 2021).

1.2.3 Lipid metabolism regulation: enzyme availability

PA plays a central role also in the transcriptional regulation of phospholipid synthesis enzymes by controlling the activity of a transcriptional repressor (Henry and Patton-Vogt, 1998; Carman and Henry, 2007). Many genes of the phospholipid synthesis pathways contain variants of a specific activator sequence of their promoters, the UAS_{INO} sequence, with a consensus of 5' CATGTGAAAT 3'. In addition, genes involved in fatty acid synthesis and genes that encode for permeases mediating the uptake of phospholipid precursors are also under the same transcriptional control (Schüller et al., 1992; Hasslacher et al., 1993; Carman and Henry, 2007; Kwiatek et al., 2020). The UAS_{INO} sequence can be recognised and bound by the Ino2p-Ino4p complex, a transcriptional activator (Carman and Henry, 1989; Kodaki et al., 1991; Ambroziak and Henry, 1994; Bachhawat et al., 1995). Opi1p, a transcriptional repressor, can bind Ino2p and inhibit the Ino2p-Ino4p complex (White et al., 1991). The localisation of Opi1p is crucial for this regulation. In actively proliferating cells, Opi1p is tethered to the ER membrane and has therefore no access to the nucleus. This tethering is mediated by Scs2p (Loewen et al., 2003; Loewen and Levine, 2005) and enhanced with the additional binding of Opi1p to PA (Loewen et al., 2004; Hofbauer et al., 2018). In conditions of low PA concentration, Opi1p is released from the ER membrane and translocates to the nucleus, where it represses the Ino2p-Ino4p complex (Loewen et al., 2004).

This regulatory circuit leads to the co-regulation of genes encoding lipid synthesis genes and matches that to the availability of the main phospholipid precursor, PA. In addition, this pathway is under metabolic and growth phase control. Presence of exogenous molecules including inositol, ethanolamine and choline leads to the transcriptional repression of phospholipid synthesis genes and the activation of the Kennedy pathway (Carman and Henry, 1999). Growth of cells to stationary phase also leads to transcriptional repression (Homann et al., 1987; Lamping et al., 1994), as does depletion of zinc from the medium (Iwanyshyn et al., 2004). Interestingly, depletion of zinc activates the *PIS1* gene, encoding for the PI synthase Pis1p (Han et al., 2005).

Transcription of *PAH1* is controlled by the same elements but with opposite effects. This means that *PAH1* transcription is activated upon growth to stationary phase (Pascual et al., 2013) and upon depletion of zinc from the medium (Soto-Cardalda et al., 2012). Moreover, Pah1p can itself display a transcriptional repressor activity. Specifically, active Pah1p

associates with and represses the transcription of the UAS_{INO}-containing genes *INO1*, *INO2* and *OPI3* (Santos-Rosa et al., 2005).

1.3 A screen to identify factors involved in ER expansion

A screen was recently performed in the Schuck lab which aimed to identify genes required for ER expansion (Papagiannidis et al., 2021). The idea of the screen was to acutely induce ER membrane expansion thereby avoiding adaptations to long term ER expansion. Moreover, we aimed to induce ER expansion without causing ER stress. To this end, the coding sequence of *ino2*(L119A)p, hereafter referred to as *ino2**, was placed under the control of an artificial expression system that can be induced upon treatment with estradiol (Pincus et al., 2014). Expression of *ino2** leads to ER expansion (Schuck et al., 2009; Papagiannidis et al., 2021) since *ino2**p cannot be recognised by Opi1p (Heyken et al., 2005). This inducible ER expansion system, which does not activate the UPR (Papagiannidis et al., 2021), was introduced into a gene deletion library of non-essential genes. In addition, the ER of the resulting strains was labelled with two fluorescently tagged proteins. Sec63p was tagged with mNeon and served as a general ER marker. Furthermore, Rtn1p was tagged with mCherry and served as a high curvature ER marker. Cells were treated with estradiol and subsequently imaged by high throughput microscopy. A combination of visual inspection and computational analysis led to the identification of mutants unable to expand their ER. Of those, the *ice2Δ* mutant showed the strongest underexpansion phenotype.

1.3.1 Ice2p

The *ICE2* gene encodes for an ER transmembrane protein, which is predicted to contain ten transmembrane domains with no identifiable cytosolic or ER luminal domain (Alli-Balogun and Levine, 2021). Since the first study on *ICE2* in 2005 (Estrada de Martin et al., 2005), many studies have tried to ascribe a role to Ice2p. Specifically, Ice2p has been suggested to be important for the maintenance or formation of the so-called cortical ER (which refers to the peripheral ER just beneath the plasma membrane), cortical ER inheritance (Estrada de Martin et al., 2005; Loewen et al., 2007), protein targeting to the inner nuclear membrane (Murthi

and Hopper, 2005), signal peptide-independent protein translocation into the ER (Hosomi et al., 2020), ER-plasma membrane contact sites (Loewen et al., 2007; Quon et al., 2018), zinc homeostasis (Ruotolo et al., 2008; North et al., 2012), PC synthesis (Tavassoli et al., 2013), UPR signalling (Cohen et al., 2017) and lipid droplet breakdown during exit from stationary phase (Markgraf et al., 2014). Despite the number of studies on Ice2p, its role on the molecular level still remains unclear. The complexity of the function of *ICE2* is also evident from the large number of genetic interactions it displays (Usaj et al., 2017).

1.4 Aims of this thesis

ER homeostasis is an integral part of cell physiology. While the mechanisms that ensure the proteostasis of the ER are understood in great detail, the mechanisms that control ER membrane biogenesis remain to a large extent unclear. The overall aim of this thesis was to define the molecular mechanisms that control ER size and shape and can be divided into two main parts. In the first part, I followed up on a screen to identify new mechanisms of ER membrane expansion control. My specific aims were:

- a) Validation of the importance of *ICE2* for ER membrane expansion
- b) Determination of the molecular role of Ice2p in the context of ER expansion
- c) Exploration of the interplay between Ice2p and other mechanisms mediating ER expansion, namely the UPR and the transcriptional regulation of lipid synthesis enzymes
- d) Identification of physiological conditions under which Ice2p-dependent ER expansion is relevant

In the second part of the thesis, I aimed to further characterise an observation I made regarding the localisation of ER-tubulating proteins in the context of ER stress. Specifically, I explored a new process that may reflect the regulation of the activity of ER-tubulating proteins in the context of ER sheet formation.

2. Materials and Methods

2.1 Materials

2.1.1 Drugs and Chemical compounds

Table 1. Drugs and chemical compounds used in this study

Drug/Compound	supplier	Catalogue no.
Dithiothreitol (DTT)	AppliChem (Darmstadt, Germany)	A1101
Tunicamycin	Merck (Darmstadt, Germany)	654380–50 MG
β -estradiol	Sigma (Taufkirchen, Germany)	E8875
PMSF	Applichem	A0999
cOmplete protease inhibitors	Roche (Mannheim, Germany)	04693116001
PhosSTOP	Roche	4906845001
cOmplete protease inhibitors (EDTA free)	Roche	04693132001
NaN_3	Merck	106688
DNA stain G	Serva (Heidelberg, Germany)	39803.01
Geneticin (G418)	Biochrom (Cambridge, UK)	A 2912
Hygromycin B	Invivogen (Toulouse France)	ant-hm-5
Nourseothricin (ClonNat)	Werner BioAgents (Jena, Germany)	5.003.00
Autodot (monodansylpentane (MDH))	BioCat (Heidelberg, Germany)	SM1000b
Ampicillin	AppliChem	A0839

Biotin	Sigma	B4639
FLAG peptide	Frauke Melchior	n.a
PhosTag acrylamide	FUJIFILM Wako Chemicals (Neuss, Germany)	AAL-107
TEMED	Applichem	A1148

2.1.2 Buffers and solutions

Table 2. Buffers and solutions used in this study

Buffer/solution	Composition
Bis-Tris-HCl (4x)	1.4 M in water
Acrylamide mix (30%, 29:1)	30% (w/v) acrylamide 0.8% (w/v) N,N'-methylen-bisacrylamide
Acrylamide mix (30%, 37.5:1)	29.2% (w/v) acrylamide 0.8 % (w/v) N,N'-methylen-bisacrylamide
Amino acid mix	2% in water (autoclaved)
Ammonium persulfate (APS)	10 % (w/v) in water
B88 buffer	20 mM HEPES-KOH pH 6.8 0.25 M sorbitol 150 mM KOAc 5 mM Mg(OAc) ₂
Betaine	5 M in water containing 0.5% (w/v) Orange G
Biotinylation assay lysis buffer	50 mM Tris pH 7.5 0.4% (w/v) SDS 2% (v/v) Triton X-100 150 mM NaCl 5 mM EDTA 1 mM DTT Complete protease inhibitors

Biotinylation assay wash buffer 1	10 % (w/v) SDS
Biotinylation assay wash buffer 2	50 mM HEPES pH 7.4 500 mM NaCl 1 mM EDTA 1% (v/v) Triton X-100 0.1% (w/v) sodium deoxycholate
Biotinylation assay wash buffer 3	50 mM Tris pH 7.5 50 mM NaCl 0.1% (v/v) Triton X-100
Blotting buffer	25 mM Tris 192 mM glycine 20% (v/v) ethanol or methanol
Colony PCR buffer (10x)	200 mM Tris-HCl, pH 8.8 100 mM (NH ₄) ₂ SO ₄ 100 mM KCl 25 mM MgCl ₂
cOmplete protease inhibitors (25x)	1 tablet in 2 ml water
Dephosphorylation buffer	50 mM Tris pH 7.1 150 mM NaCl 100 mM NaOAc 100 mM MgCl ₂ 1 mM DTT 0.1 mg/ml BSA Complete protease inhibitors
Dithiothreitol (DTT)	1 M in water
DNA loading dye (6x)	50 % (v/v) glycerol 10% (v/v) 10x TAE buffer 0.05 (w/v) Orange G
dNTPs	10 mM of each in water
Galactose (10x)	20% (w/v) in water, filter sterilised
Glucose (10x)	20% (w/v) in water, autoclaved
Glycerol (2x)	30% (w/v) in water, autoclaved
Homemade ECL solution	100 mM Tris-HCl, pH 8.5 1.25 mM Luminol 0.2 mM p-Coumaric acid 0.9% (v/v) H ₂ O ₂ , freshly added

Hypo-osmotic lysis buffer	50 mM HEPES-HCl pH 7.5 1 mM EDTA 200 mM sorbitol 1 mM PMSF Complete protease inhibitors
Immunoisolation lysis buffer	20 mM Tris pH 8 150 mM KCl 5 mM MgCl ₂ 1 % (v/v) Triton X-100 1 mM PMSF cOmplete protease inhibitors (EDTA-free) PhosSTOP
Lipidomics lysis buffer	50 mM HEPES pH 7.5 0.5 mM EDTA
Lithium acetate	1 M in water, filter sterilised
Luminol	250 mM luminol in DMSO
Modified SDS-PAGE sample buffer	0.06 M Tris-HCl pH 6.8 5% glycerol 2% SDS 4% β-mercaptoethanol 0.0025% bromophenol blue
NaN ₃	1 M in water
p-Coumaric acid	90 mM p-Coumaric acid in DMSO
Phenylmethylsulfonyl fluoride (PMSF)	1 M in water
PhosSTOP (10x)	1 tablet in 1 ml water
PhosTag solution	5 mM in 3 % (v/v) methanol
Polyethylene glycol (PEG) 3350	50% (w/v) in water, filter sterilised
Ponceau S	0.1% Ponceau S 5% (v/v) acetic acid
Raffinose (10x)	10% (w/v) in water, filter sterilised
Reducing buffer	100 mM Tris-HCl pH 9.4 10 mM NaN ₃

Reynold's lead citrate	2.7% (w/v) lead nitrate 3.5% (w/v) sodium citrate dihydrate 160 mM sodium hydroxide
Salmon sperm DNA	10 mg/mL in water
SDS-PAGE running buffer	25 mM Tris 0.1% (w/v) SDS 192 mM glycine
SDS-PAGE sample buffer (4x)	278 mM Tris, pH 6.8 44.4% (v/v) glycerol 4.4% (w/v) LDS 0.02% (w/v) bromophenol blue 0.1 volumes β -mercaptoethanol, freshly added
Separating gel buffer	2M Tris, pH 8.8
Sodium dodecyl sulfate (SDS)	15% (w/v) in water
Spheroplast buffer	50 mM Tris-HCl pH 7.5 1 M sorbitol
Stacking gel buffer	0.5 M Tris, pH 6.8
Standard lysis buffer	50 mM HEPES pH 7.5 0.5 mM EDTA
Sucrose gradient buffers	20 mM HEPES-KOH pH 7.4 50 mM KOAc 2 mM EDTA 1.2 M or 1.5 M sucrose
TAE buffer (50x)	2 M Tris 1 M acetic acid 50 mM EDTA
TBS/Tween (TBST)	10 mM Tris, pH 7.4 150 mM NaCl 0.1% (v/v) Tween
TES buffer	10 mM Tris-HCl pH 7.5 10 mM EDTA 0.5 % SDS
Transformation mix	33% (w/v) polyethylene glycol (PEG) 3350 100 mM lithium acetate 0.28 μ g/ml freshly boiled salmon sperm DNA
Tunicamycin	1 mg/mL in DMSO

Yeast nitrogen base w/o ammonium sulfate (YNB)	6.9% (w/v) in water, autoclaved
Zn-PhosTag blotting buffer	25 mM Tris 192 mM glycine 10% (v/v) methanol
Zn-PhosTag running buffer	100 mM Tris 100 mM MOPS 5 mM sodium bisulfite 0.5 % (w/v) SDS
ZnCl ₂	10 mM in water, filter sterilised
β-estradiol	10 mM in ethanol
MnCl ₂	10 mM in water, filter sterilised

Table 3. Synthetic complete amino acid mix

Component	Amount	Component	Amount
adenine	0.5 g	isoleucine	2 g
alanine	2 g	leucine	4 g
para-aminobenzoic acid	0.2 g	lysine	2 g
arginine	2 g	methionine	2 g
asparagine	2 g	phenylalanine	2 g
aspartic acid	2 g	proline	2 g
cysteine	2 g	serine	2 g
glutamic acid	2 g	threonine	2 g
glutamine	2 g	tyrosine	2 g

glycine	2 g	tryptophan	2 g
histidine	2 g	uracil	2 g
inositol	2 g	valine	2 g

Amino acid mixes for drop-out media were prepared as described in Table 3 but omitting the corresponding amino acid(s).

2.1.2 Growth media and plates

Table 4. Media for liquid cultures

Medium	Composition
SCD	0.69% (w/v) YNB 0.2% (w/v) amino acid mix 2% (w/v) glucose
SC raffinose	0.69% (w/v) YNB 0.2% (w/v) amino acid mix 2% (w/v) raffinose
SC raffinose/galactose	0.69% (w/v) YNB 0.2% (w/v) amino acid mix 2% (w/v) raffinose 2 % (w/v) galactose
YPD	1% (w/v) yeast extract 2% (w/v) peptone 2% (w/v) glucose
LB	1% (w/v) tryptone 0.5% (w/v) yeast extract 1% (w/v) NaCl

Table 5. Plates

Plates	Composition
SCD plates	SCD 2% (w/v) agar
SCD tunicamycin plates	SCD 2% (w/v) agar 0.2 µg/ml Tunicamycin
LB ampicillin plates	LB 2% (w/v) agar 100 µg/ml ampicillin
YPD antibiotic plates	YPD 1% (w/v) agarose 20 µg/ml G418 or 100 µg/ml Hygromycin B or 10 µg/ml CloNat

Dropout plates were prepared using the appropriate dropout amino acid mix. Antibiotics and tunicamycin were added after the rest of the medium was cooled down to 50°C. Agarose allowed lower antibiotic concentrations.

2.1.2 Enzymes, standards and kits

Table 6. Enzymes used in this study

Enzyme	Supplier
Alkaline phosphatase (FastAP)	Thermo Fisher Scientific (Waltham, Massachusetts)
Zymolyase T100	Biomol (Hamburg, Germany)
BglII	Thermo Fisher Scientific
PmeI	New England Biolabs (NEB; Ipswich, Massachusetts)
PacI	NEB
AscI	NEB
BssHII	NEB
SacI	NEB
SpeI	NEB
Taq DNA Polymerase	Sigma
Opti Taq DNA polymerase	Roboklon (Berlin, Germany)
Q5 High-Fidelity DNA polymerase	NEB
DpnI	NEB
T4 DNA ligase	NEB

Table 7. Standards and kits used in this study

Kit	Supplier
BCA assay kit	Thermo Fisher Scientific
GeneRuler 1kb Plus DNA Ladder	Thermo Fisher Scientific
NucleoSpin Plasmid Mini-Prep Kit	Macherey-Nagel (Düren, Germany)
NucleoSpin Gel and PCR Clean up	Macherey-Nagel
PageRuler Plus Prestained Protein Ladder	Thermo Fisher Scientific
NEBuilder HiFi DNA Assembly Master Mix	NEB
RevertAid First Strand cDNA synthesis kit	Thermo Fisher Scientific
SensiFAST SYBR No-ROX kit	Bioline (Meridian Bioscience, Ohio, US)
SuperSignal West Femto maximum sensitivity substrate	Thermo Fisher Scientific

2.1.3 Antibodies

Table 8. Antibodies used in this study

Antibody	source	Catalogue no. / ref
anti-mCherry (1C51)	Abcam (Cambridge, UK)	ab125096
anti-mouse-HRP	Pierce (Waltham, Massachusetts)	31462
Anti-Pgk1 (22C5)	Abcam	ab113687
anti-rabbit-HRP	Pierce	31462
anti-HA (3F10)	Roche	11867423001
anti-rat-HRP	Jackson ImmunoResearch (Cambridge, UK)	712-035-153
anti-Sec61 (Sec61C)	Peter Walter	(Schuck et al., 2009)
anti-FLAG M2 agarose beads	Sigma	A2220
anti-FLAG (M2)	Sigma	F1804
anti-Dpm1(5C5A7)	Invitrogen (Waltham, Massachusett)	A-6429
streptavidin agarose beads	Pierce	20347
streptavidin-HRP	Pierce	21130
anti-mNeonGreen (32F6)	Chromotek (Planegg, Germany)	32f6-100

2.1.4 PAGE gel recipes

Table 9. Recipes for PAGE gels

10 % SDS-PAGE separating gel		4 % stacking gel	
H ₂ O	2.7 ml	H ₂ O	1.2 ml
separating gel buffer	1.2 ml	stacking gel buffer	0.5 ml
30% acrylamide mix (37.5:1)	2.0 ml	30% acrylamide mix (37.5:1)	0.27 ml
15% SDS	40 µl	15% SDS	13 µl
10% APS	60 µl	10% APS	20 µl
TEMED	6 µl	TEMED	2 µl
8% Zn-PhosTag-PAGE separating gel (50 µM)		8% Mn-PhosTag-PAGE separating gel (50 µM)	
H ₂ O	3.014 ml	H ₂ O	2.714 ml
separating gel buffer	1.2	Bris-Tris-HCl	1.5
30% acrylamide mix (29:1)	1.6 ml	30% acrylamide mix (29:1)	1.6 ml
PhosTag solution (5 mM)	60 µl	PhosTag solution (5 mM)	60 µl
Mn ₂ Cl (10 mM)	60 µl	Zn ₂ Cl (10 mM)	60 µl
10% APS	60 µl	10% APS	60 µl
TEMED	6 µl	TEMED	6 µl

2.2 Methods

2.2.1 Plasmids

Table 10. Plasmids used in this study

Plasmid	Alias	Source
pRS315	pRS315	(Szoradi et al., 2018)
pRS415-P _{ADH1} - <i>ICE2</i>	pSS761	(Papagiannidis et al., 2021)
pFA6a-mNeon-kanMX6	pSS445	(Schäfer et al., 2020)
pFA6a-kanMX6	pSS034	(Longtine et al., 1998)
pFA6a-His3MX6	pSS036	(Longtine et al., 1998)
pFA6a-natNT2	pSS032	(Janke et al., 2004)
pFA6a-kanMX4	pYM3	(Knop et al., 1999)
pFA6a-mCherry-klTRP1	pSS880	this study (Katharina Schaeff)
pFA6a-mNeon-klTRP1	pSS904	this study (Katharina Schaeff)
pFA6a-hphNT1	pSS033	(Janke et al., 2004)
pFA6a-3HA-His3MX6	pSS042	(Longtine et al., 1998)
pFA6a-6HA-hphNT1	pSS642	(Janke et al., 2004)
pFA6a-mCherry-TRP1	pSS062/pPW2403	Greg Tully, Peter Walter
pFA6a-mNeon-HISMX6	pSS447	(Papagiannidis et al., 2021)
pFA6a-mCherry-His3MX6	pSS063/pPW2404	Greg Tully, Peter Walter
pRS404-GPD-mCherry- <i>UBC6</i>	pSS962	(Schäfer et al., 2020)
pFA6a-mNeon-natNT2	pSS733	Matthias Meurer, Michael Knop
pNH605-ADH-GEM-P _{GAL} - <i>ino2(L119A)</i>	pSS475	(Papagiannidis et al., 2021)
pNH605-ADH-GAL4-ER-M2	pSS130/pDEP151	David Pincus
pNH604-P _{GAL} -Hac1i	pSS624	(Pincus et al., 2014)
YCplac111- <i>PAH1</i> -PrtA	pSS1005	(O'Hara et al., 2006)
YCplac111- <i>PAH1</i> -3HA	pSS1045	this study
YCplac111- <i>pah1(D398A D400A)</i> -GFP	pSS971	(Karanasios et al., 2010)
YCplac111- <i>pah1(D398A D400A)</i> -3HA	pSS1046	this study
YCplac111- <i>pah1(7A)</i> -PrtA	pSS1006	(O'Hara et al., 2006)
YCplac111- <i>pah1(7A)</i> -PrtA	pSS1044	this study

YCplac111- <i>pah1(7A)</i> - 3HA	pSS1047	this study
pRS305-Hac1-splicing-reporter	pSS275/pDEP005	(Pincus et al., 2010)
pFA6a-kanMX6-P _{GAL1}	pSS049	(Longtine et al., 1998)
pFA6a-TRP1-P _{GAL1}	pSS050	(Longtine et al., 1998)
pFA6a-mNeon-HA-kiTRP1	pSS741	this study (Katharina Schaeff)
pFA6a-mNeon-HA-HISMX6	pSS695	this study (Katharina Schaeff)

Table 11. Oligonucleotides used in this study

Oligo	Sequence
pFA6a-kiTRP fw	TAATTAAGGCGCGCCAGATCTaaagtgaacgatcattcacta
pFA6a-kiTRP rev	gaattcgagctcgtttaaacTAAGAGGTGAAAGATCTTAATTAG
Pac-neon	AATTAATTAACatggtttctaagggtgaagaag
neon-Ascl	AAGGCGCGCcttactgtacaattcgtccatac
HA-stop-pFA6a fw	taccatacagatgttctgactatgcgTAAGGCGCGCCACTTCTAAAT
neon-HA rev	cgcatagtcaggaacatcgtatgggtaCTTGTACAATTCGTCCATAACC
YCplac111_Pah1-3HA_fw	gtatgacgtcccggactatgcaggatcctatccatagacgttccagattacgctTAAAGATTCTTGT AGCCG
YCplac111_Pah1-3HA_rev	catagtccgggacgtcatacggatagcccgatagtcaggaacatcgtatgggtaATCTTCGAATT CATCTTCG
Pah1(7A)_P178L mut fw	GAATCCTCTACAACGACACCACtAGATTCAGTTGAAGAGAGGAAGC
Pah1(7A)_P178L mut rev	GCTTCTCTCTTCAACTGAATCTaGTGGTGTCTGTTGTAGAGGATTC
Pah1_+235_fw	CTGGAGAAGCCTATTTTCG
Pah1_+2322_rev	GAAGATGCTCTCCTCGATTTAG
Pah1_+2296_fw	AGAACTAAATCGAGGAGAGC
Pah1_+297_rev	CAACTCGTCAGGGACATC
TAF10 fw (qPCR)	GGATCAGGTCTTCCGTAGCG
TAF10 rev (qPCR)	AGGCTGTTGCTGTCCTTGC
INO1 fw (qPCR)	ACTTTGTCGTCTCTGGTTGGG
INO1 rev (qPCR)	CTTCACCAAGGACATCTTCGC

Oligonucleotides used to generate PCR products for gene deletion or tagging were designed according to (Longtine et al, 1998; Janke et al, 2004) and are not listed. All oligonucleotides were purchased from Sigma-Aldrich or Integrated DNA Technologies (IDT) and stored as 100 μ M stock solutions in water.

2.2.1.1 Molecular cloning

DNA segment amplification and plasmid linearization by PCR was performed using the OptiTaQ Polymerase or the Q5 High-Fidelity Polymerase (Table 6) according to the manufacturer's manuals. Site directed mutagenesis was performed using the Q5 High-Fidelity polymerase and following the Stratagene Quikchange site-directed mutagenesis. Parental plasmids were degraded by incubation of reactions with DpnI. Restriction digest reactions were performed using restriction enzymes from Thermo Fisher Scientific or NEB according to the manufacturer's manuals. Linearised backbones were dephosphorylated by incubation of digestion reaction with FastAP at 37°C for 1 h. PCR products and digested DNA fragments were separated on 1% agarose gels in 2x TAE buffer and purified by gel extraction using the NucleoSpin Gel and PCR Clean-up kit. Linearised vectors were re-ligated or ligated with DNA fragments either by Gibson assembly, using the NEBuilder HiFi DNA Assembly Master Mix, or by ligation, using the T4 DNA ligase, according to the manufacturer's manuals. Chemo-competent *Escherichia coli* (DH5 α) bacteria were transformed to amplify the resulting plasmids. Plasmids from single bacterial colonies were retrieved using the NucleoSpin Plasmid kit and verified by Sanger sequencing by Microsynth Seqlab or GATC.

To generate pSS880, kITRP1 was amplified from pYM3 with primers pFA6a-kITRP fw/rev and combined by Gibson assembly with pSS063 (Table 10) linearized with BgIII/PmeI.

To generate pSS904, neon was amplified from pSS445 (Table 10) with primers Pac-neon/neon-Ascl, digested with PacI/Ascl and cloned into the PacI/BssHIII site of pSS880. To generate pSS740, pSS741 and pSS445, plasmids pSS733, pSS904 and pSS445 (Table 10) were linearised with primers HA-stop-pFA6a fw/neon-HA rev in order to include an HA tag and were re-ligated by Gibson assembly. To generate pSS1045 and pSS1046, pSS1005 and pSS971 (Table 10) were linearized with primers YCplac111_Pah1-3HA_fw and YCplac111_Pah1-3HA_rev in order to exclude the PtA or GFP tag and include a 3xHA tag and were re-ligated by Gibson assembly. To generate pSS1044, L178P mutation of pSS1006 (Table 10) was corrected by site directed mutagenesis using primers Pah1(7A)_P178L mut fw/rev. To generate pSS1047, segment containing the 7A mutations was amplified from

pSS1044 using primers Pah1_+235_fw and Pah1_+2322_rev and was combined with Gibson assembly with pSS1045 linearized with primers Pah1_+2296_fw and Pah1_+297_rev.

2.2.2 Yeast strains

Table 12. Strains used in this study

Strain genotype	Alias	Source
<i>leu2-3,112 trp1-1 can1-100 ura3-1 his3-11,15</i>	SSY122	(Szoradi et al., 2018)
<i>SEC63-mNeon::kan RTN1-mCherry::HIS3 leu2::GEM-P_{GAL1}-ino2(L119A)-LEU2</i>	SSY1405	(Papagiannidis et al., 2021)
<i>SEC63-mNeon::kan RTN1-mCherry::HIS3 leu2::GEM-P_{GAL1}-ino2(L119A)-LEU2 ice2Δ::nat</i>	SSY1603	(Papagiannidis et al., 2021)
<i>SEC63-mNeon::kan RTN1-mCherry::HIS3 leu2::GEM-LEU2</i>	SSY2328	(Papagiannidis et al., 2021)
<i>SEC63-mNeon::kan RTN1-mCherry::HIS3</i>	SSY1404	(Papagiannidis et al., 2021)
<i>SEC63-mNeon::kan RTN1-mCherry::HIS3 ice2Δ::nat</i>	SSY2356	(Papagiannidis et al., 2021)
<i>SEC63-mNeon::kan RTN1-mCherry::HIS3 opi1Δ::hph</i>	SSY2595	(Papagiannidis et al., 2021)
<i>SEC63-mNeon::kan RTN1-mCherry::HIS3 opi1Δ::hph ice2Δ::nat</i>	SSY2811	(Papagiannidis et al., 2021)
<i>his3::P_{GPD}-TagBFP-hph trp1::4xUPRE-GFP-TRP1</i>	SSY2306	(Papagiannidis et al., 2021)
<i>his3::P_{GPD}-TagBFP-hph trp1::4xUPRE-GFP-TRP1 ice2Δ::nat</i>	SSY2312	(Papagiannidis et al., 2021)
<i>his3::P_{GPD}-TagBFP-hph leu2::HAC1-GFP-splicing-reporter-LEU2</i>	SSY2309	(Papagiannidis et al., 2021)
<i>his3::P_{GPD}-TagBFP-hph leu2::HAC1-GFP-splicing-reporter-LEU2 Δice2Δ::nat</i>	SSY2313	(Papagiannidis et al., 2021)
<i>YMG1 SEC63-mNeon::URA3 RTN1-mCherry::kan</i>	SSY2228	(Papagiannidis et al., 2021)
<i>YMG1 SEC63-mNeon::URA3 RTN1-mCherry::kan hac1Δ::nat</i>	SSY2331	(Papagiannidis et al., 2021)
<i>SEC63-mNeon::kan</i>	SSY1034	This study (Sebastian Schuck)
<i>leu2-3,112 trp1-1 can1-100 ura3-1 his3-11,15 ade2-1</i>	SSY001	(Schuck et al., 2014)
<i>yop1Δ::kan</i>	SSY285	This study (Sebastian Schuck)
<i>yop1Δ::kan rtn1Δ::HIS3</i>	SSY317	This study (Sebastian Schuck)
<i>yop1Δ::kan rtn1Δ::HIS3 rtn2Δ::nat</i>	SSY319	This study (Sebastian Schuck)
<i>yop1Δ::kan rtn1Δ::HIS3 rtn2Δ::nat ADE2</i>	SSY1786	This study (Sebastian Schuck)

<i>yop1Δ::kan rtn1Δ::HIS3 rtn2Δ::nat SEC63-mNeon::TRP1</i>	SSY2235	This study
<i>yop1Δ::kan rtn1Δ::HIS3 rtn2Δ::nat ice2Δ::hph</i>	SSY1734	This study (Sebastian Schuck)
<i>yop1Δ::kan rtn1Δ::HIS3 rtn2Δ::nat ice2Δ::hph ADE2</i>	SSY1787	This study (Sebastian Schuck)
<i>yop1Δ::kan rtn1Δ::HIS3 rtn2Δ::nat ice2Δ::hph SEC63-mNeon::TRP1</i>	SSY2236	This study
<i>YMG1 dga1Δ::TRP1 lro1Δ::HIS3 are1Δ::TRP1 are2Δ::HIS3</i>	YMG5	(Velázquez et al., 2016)
<i>YMG1 SEC63-mNeon::URA3 RTN1-mCherry::kan ice2Δ::nat</i>	SSY2229	(Papagiannidis et al., 2021)
<i>YMG5 SEC63-mNeon::URA3 RTN1-mCherry::kan ice2Δ::nat</i>	SSY2230	(Papagiannidis et al., 2021)
<i>YMG5 SEC63-mNeon::URA3 RTN1-mCherry::kan</i>	SSY2256	(Papagiannidis et al., 2021)
<i>YMG1 ADE2 SEC63-mNeon::URA3 RTN1-mCherry::kan leu2::GEM-P_{GAL1}-ino2(L119A)-LEU2</i>	SSY2598	(Papagiannidis et al., 2021)
<i>YMG1 ADE2 SEC63-mNeon::URA3 RTN1-mCherry::kan leu2::GEM-P_{GAL1}-ino2(L119A)-LEU2 ice2Δ::nat</i>	SSY2599	(Papagiannidis et al., 2021)
<i>YMG5 ADE2 SEC63-mNeon::URA3 RTN1-mCherry::kan leu2::GEM-P_{GAL1}-ino2(L119A)-LEU2</i>	SSY2600	(Papagiannidis et al., 2021)
<i>YMG5 ADE2 SEC63-mNeon::URA3 RTN1-mCherry::kan leu2::GEM-P_{GAL1}-ino2(L119A)-LEU2 ice2Δ::nat</i>	SSY2601	(Papagiannidis et al., 2021)
<i>SEC63-mNeon::kan RTN1-mCherry::HIS3 nem1Δ::hph</i>	SSY2482	(Papagiannidis et al., 2021)
<i>SEC63-mNeon::kan RTN1-mCherry::HIS3 ice2Δ::nat nem1Δ::hph</i>	SSY2484	(Papagiannidis et al., 2021)
<i>SEC63-mNeon::kan RTN1-mCherry::HIS3 spo7Δ::hph</i>	SSY2481	(Papagiannidis et al., 2021)
<i>SEC63-mNeon::kan RTN1-mCherry::HIS3 ice2Δ::nat spo7Δ::hph</i>	SSY2483	(Papagiannidis et al., 2021)
<i>SEC63-mNeon::kan RTN1-mCherry::HIS3 pah1Δ::hph</i>	SSY2807	(Papagiannidis et al., 2021)
<i>SEC63-mNeon::kan RTN1-mCherry::HIS3 ice2Δ::nat pah1Δ::hph</i>	SSY2808	(Papagiannidis et al., 2021)
<i>SEC63-mNeon::kan RTN1-mCherry::HIS3 dgk1Δ::nat</i>	SSY2480	This study
<i>SEC63-mNeon::kan RTN1-mCherry::HIS3 dgk1Δ::nat nem1Δ::hph</i>	SSY2485	This study
<i>SEC63-mNeon::kan RTN1-mCherry::HIS3 dgk1Δ::nat spo7Δ::hph</i>	SSY2486	This study
<i>SEC63-mNeon::kan RTN1-mCherry::HIS3 dgk1Δ::hph ice2Δ::nat</i>	SSY2539	This study
<i>SEC63-mNeon::kan RTN1-mCherry::HIS3 pah1Δ::hph dgk1Δ::nat</i>	SSY2822	This study
<i>PAG1-3HA::HIS3</i>	SSY2592	(Papagiannidis et al., 2021)
<i>PAH1-3HA::HIS3 ice2Δ::nat</i>	SSY2594	(Papagiannidis et al., 2021)

<i>PAH1-3HA::HIS3 nem1Δ::nat</i>	SSY2593	(Papagiannidis et al., 2021)
<i>ura3::P_{ADH1}-ICE2-LEU2</i>	SSY2597	This study
<i>PAH1-3HA::HIS3 ura3::P_{ADH1}-ICE2-LEU2</i>	SSY2602	This study
<i>PAH1-3HA::HIS3 ice2Δ::nat nem1Δ::hph</i>	SSY2718	(Papagiannidis et al., 2021)
<i>nem1Δ::nat PAH1-3FLAG::kan</i>	SSY3065	(Papagiannidis et al., 2021)
<i>pep4Δ::TRP1 prb1Δ::HIS3 pah1Δ::nat</i>	SSY3053	(Papagiannidis et al., 2021)
<i>pep4Δ::TRP1 prb1Δ::HIS3 pah1Δ::hph ice2Δ::nat</i>	SSY3074	(Papagiannidis et al., 2021)
<i>pep4Δ::TRP1 prb1Δ::HIS3 pah1Δ::hph nem1Δ::nat</i>	SSY3075	(Papagiannidis et al., 2021)
<i>pep4Δ::TRP1 prb1Δ::HIS3 pah1Δ::hph nem1Δ::nat ice2Δ::kan</i>	SSY3095	(Papagiannidis et al., 2021)
<i>NEM1-3HA::HIS3 pah1Δ::hph</i>	SSY3140	(Papagiannidis et al., 2021)
<i>NEM1-3HA::HIS3 pah1Δ::hph ice2Δ::nat</i>	SSY3141	(Papagiannidis et al., 2021)
<i>ice2Δ::nat PAH1-3FLAG::kan</i>	SSY3096	(Papagiannidis et al., 2021)
<i>ICE2-3HA::HIS</i>	SSY2421	(Papagiannidis et al., 2021)
<i>SPO7-3HA::HIS3</i>	SSY2910	(Papagiannidis et al., 2021)
<i>NEM1-3HA::HIS3</i>	SSY2913	(Papagiannidis et al., 2021)
<i>SPO7-3FLAG::kan</i>	SSY3183	(Papagiannidis et al., 2021)
<i>ICE2-3HA::HIS3 SPO7-3FLAG::kan</i>	SSY3184	(Papagiannidis et al., 2021)
<i>ICE2-3HA::HIS3 SPO7-3FLAG::kan nem1Δ::hph</i>	SSY3197	(Papagiannidis et al., 2021)
<i>NEM1-3FLAG::kan</i>	SSY3195	(Papagiannidis et al., 2021)
<i>ICE2-3HA::HIS3 NEM1-3FLAG::kan</i>	SSY3196	(Papagiannidis et al., 2021)
<i>NEM1-3HA::HIS3 ice2Δ::nat</i>	SSY2914	(Papagiannidis et al., 2021)
<i>NEM1-3HA::HIS3 ura3::P_{ADH1}-ICE2-LEU2</i>	SSY2915	(Papagiannidis et al., 2021)
<i>NEM1-3HA::HIS3 spo7Δ::hph</i>	SSY2945	(Papagiannidis et al., 2021)
<i>ICE2-TurboID-3myc::kan</i>	SSY2978	(Papagiannidis et al., 2021)
<i>ICE2-TurboID-3myc::kan PAH1-3HA::HIS3</i>	SSY2979	(Papagiannidis et al., 2021)
<i>ICE2-TurboID-3myc::kan PAH1-3HA::HIS3 spo7Δ::nat</i>	SSY3117	(Papagiannidis et al., 2021)
<i>ICE2-TurboID-3myc::kan PAH1-3HA::HIS3 nem1Δ::nat</i>	SSY3118	(Papagiannidis et al., 2021)
<i>SPO7-3HA::HIS3 ura3::P_{ADH1}-ICE2-LEU2</i>	SSY2912	(Papagiannidis et al., 2021)

<i>ICE2-mScarlet::kan SPO7-mNeon::nat</i>	SSY3244	(Papagiannidis et al., 2021)
<i>ICE2-mScarlet::kan NEM1-mNeon::nat</i>	SSY3245	(Papagiannidis et al., 2021)
<i>ura3::P_{TEF}-mCherry-UBC6-URA3 SPO7-neon::nat</i>	SSY2916	(Papagiannidis et al., 2021)
<i>ura3::P_{TEF}-mCherry-UBC6-URA3 NEM1-neon::nat</i>	SSY2917	(Papagiannidis et al., 2021)
<i>ura3::P_{TEF}-mCherry-UBC6-URA3 SPO7-neon::nat ice2Δ::hph</i>	SSY3238	(Papagiannidis et al., 2021)
<i>ura3::P_{TEF}-mCherry-UBC6-URA3 NEM1-neon::nat ice2Δ::hph</i>	SSY3239	(Papagiannidis et al., 2021)
<i>ICE2-mScarlet::kan SEI1-neon::HIS</i>	SSY3318	(Papagiannidis et al., 2021)
<i>PAH1-3HA SEC63-mNeon::kan RTN1-mCherry::HIS3</i>	SSY2841	(Papagiannidis et al., 2021)
<i>pah1(7A)-3HA SEC63-mNeon::kan RTN1-mCherry::HIS3</i>	SSY2842	(Papagiannidis et al., 2021)
<i>PAH1-3HA SEC63-mNeon::kan RTN1-mCherry::HIS3 ura3::P_{ADH1}-ICE2-LEU2</i>	SSY2843	(Papagiannidis et al., 2021)
<i>pah1(7A)-3HA SEC63-mNeon::kan RTN1-mCherry::HIS3 ura3::P_{ADH1}-ICE2-LEU2</i>	SSY2844	(Papagiannidis et al., 2021)
<i>PAH1-3HA SEC63-mNeon::kan RTN1-mCherry::HIS3 ice2Δ::nat</i>	SSY2970	(Papagiannidis et al., 2021)
<i>SEC63-mNeon::kan RTN1-mCherry::HIS3 ura3::P_{ADH1}-ICE2-LEU2</i>	SSY2588	(Papagiannidis et al., 2021)
<i>SEC63-mNeon::kan RTN1-mCherry::HIS3 ura3::P_{ADH1}-ICE2-LEU2 opi1Δ::hph</i>	SSY2596	(Papagiannidis et al., 2021)
<i>SEC63-mNeon::kan RTN1-mCherry::HIS3 hac1Δ::hph</i>	SSY2805	(Papagiannidis et al., 2021)
<i>SEC63-mNeon::kan RTN1-mCherry::HIS3 ice2Δ::nat hac1Δ::hph</i>	SSY2806	(Papagiannidis et al., 2021)
<i>SEC63-mNeon::kan RTN1-mCherry::HIS3 PAH1-6HA::hph</i>	SSY2804	this study
<i>SEC63-mNeon::kan RTN1-mCherry::HIS3 PAH1-6HA::hph leu2::GEM-P_{GAL1}-ino2(L119A)-LEU2</i>	SSY2840	this study
<i>SEC63-mNeon::kan RTN1-mCherry::HIS3 PAH1-6HA::hph leu2::GEM-LEU2</i>	SSY2835	this study
<i>SEC63-mNeon::kan RTN1-mCherry::HIS3 PAH1-6HA::hph leu2::GEM-LEU2 trp1::P_{ADH1}-HAC1'-TRP1</i>	SSY2845	this study
<i>leu2::Hac1-GFP-splicing-reporter-LEU2</i>	SSY2487	this study (Rolf Schmidt)
<i>SEC63-mCherry::TRP1</i>	SSY583	this study (Sebastian Schuck)
<i>SEC63-mCherry::TRP1 ADE2</i>	SSY1403	this study (Jasmin Schäfer)
<i>SEC63-mCherry::TRP1 RTN1-mNeon::HIS3</i>	SSY2711	this study
<i>Yop1-mCherry::HIS3</i>	SSY2645	this study
<i>Yop1-mCherry::HIS3 RTN1-mNeon::TRP1</i>	SSY2713	this study
<i>ice2Δ::nat</i>	SSY1757	this study (Sebastian Schuck)

<i>ice2Δ::nat Yop1-mCherry::HIS3</i>	SSY2646	this study
<i>ice2Δ::nat Yop1-mCherry::HIS3 RTN1-mNeon::TRP1</i>	SSY2714	this study
<i>ADE2 ura3::P_{GPD}-mCherry-UBC6-URA3</i>	SSY1212	this study (Jasmin Schäfer)
<i>ADE2 ura3::P_{GPD}-mCherry-UBC6-URA3 RTN1-neon::nat</i>	SSY2814	this study
<i>ADE2 ura3::P_{GPD}-mCherry-UBC6-URA3 RTN1-neon::nat Δice2::hph</i>	SSY3198	this study
<i>SEC63-mNeon::kan YOP1-mCherry::HIS3</i>	SSY2648	this study
<i>SEC63-mNeon::kan TRP1::P_{GAL1}-RTN1-mCherry::HIS3</i>	SSY3399	this study (Artur Astapenka under my supervision)
<i>SEC63-mNeon::kan TRP1::P_{GAL1}-RTN1-mCherry::HIS3 ice2Δ::nat</i>	SSY3400	this study (Artur Astapenka under my supervision)

Chromosomal modifications were introduced using PCR products or linearized plasmids according to (Longtine et al, 1998; Janke et al, 2004). For the transformations, yeast cells grown to an OD₆₀₀ of 1 in 5 ml YPD were washed once with water. The transforming DNA (PCR product, linearized plasmid or non-linearized plasmid) was added to the pellet, cells were resuspended in 360 μl of transformation mix and heat-shocked at 42°C for 40min. Cells were then pelleted and resuspended in 1 ml YPD. One-hundred μl of the cell suspension was then plated on the appropriate selective plate. In cases of selection with antibiotics, cells were recovered at 30°C for 6 h before plating. Resulting strains were verified either by colony PCR, using the Sigma Taq Polymerase and the 10x colony PCR mix, fluorescence microscopy or flow cytometry. Strains were frozen down as saturated cultures in 15 % (w/v) glycerol.

2.2.3 Growth conditions and treatments

Yeast cells were grown at 30°C in YPD, SCD, SCD-lacking the appropriate amino acid for auxotrophic selection of centromeric plasmids.

For transformations, 5 ml YPD was inoculated and cells were grown overnight. In the morning, cells were diluted to an OD₆₀₀ of 0.4 in 5 ml fresh YPD and were grown for 4 h.

For experiments performed with cells grown to exponential phase (OD₆₀₀ between 0.2 and 1), 5 ml of medium was inoculated and cells were grown during the day. An overnight culture was then prepared such that cells reached exponential phase the next morning. For the experiments where cells were grown to stationary phase, the exponentially growing cells were let to grow for 48 h without further dilution.

For experiments involving strain $\Delta LD\ ice2\Delta$ and for the lipidomics experiments 5 ml medium was inoculated and cells were grown overnight. The next morning cells were diluted to exponential phase and were grown overday before being diluted again, aiming to reach exponential phase the next morning.

For treatment with DTT, tunicamycin (Tm) and estradiol, exponential phase cultures were diluted to an OD₆₀₀ of 0.2 (DTT and Tm) or 0.05 (estradiol) before being treated with the indicated concentration for the indicated time.

For staining of lipid droplets with monodansylpentane (MDH), cells harvested from 1 ml were resuspended in 20 μ l 50 μ M MDH, incubated at room temperature for 10 min and washed once with water.

2.2.4 Light microscopy

All microscopy experiments were performed with cultures grown in SCD medium. Just before imaging cells were harvested, mounted on a coverslip and were overlaid with an agarose pad prepared from 1 % (w/v) agarose in SCD.

For experiments presented in Figures 3, 4, 5, 6, 7, 8, 9, 10, 12, 14H, 17, 20, 21, 23, and 24(C,D), cells were imaged at room temperature using a DMI8 inverted microscope (Leica, Wetzlar, Germany) equipped with a CSU-X1 spinning-disk confocal scanning unit (Yokogawa, Musashino, Japan) and an ORCA-Flash 4.0 LT camera (Hamamatsu, Hamamatsu, Japan). A HC PL APO 63x/1.40-0.60 or a HC PL APO 100x/1.4 CS2 oil objective lens (Leica) was used.

For experiments presented in Figures 14(I,J), 22, and 24(A,B), cells were imaged at room temperature using a an IX81 inverted microscope (Olympus, Hamburg, Germany) equipped with an ORCA-R2 camera (Hamamatsu), a PL APO 100x/1.45 oil DIC objective lens (Olympus) and a Lumencor Spectra X illumination system.

2.2.4.1 Image processing

For images that were presented in the figures, background subtraction was performed in Fiji (Schindelin et al., 2012) using the rolling ball method, with a radius of 50 or 150.

2.2.4.2 Image quantification

To avoid bias, image files were anonymized before analysis with the "Blind Analysis Tools" plugin in Fiji (<https://imagej.net/plugins/blind-analysis-tools>).

For the cortical ER morphology quantifications presented in Figures 5B, 6A, 6C, 7A, 9A, 11B, 11C, 16A, 16B, and 17B both bright field and fluorescence images of cortical sections were used, as described in (Papagiannidis et al., 2021). Bright field images were used for cell segmentation. To enhance the contrast of the cell periphery, a Gaussian blur (sigma = 2) was applied, followed by image downscaling ($x = y = 0.5$). Next, a tubeness filter (sigma = 1) was applied, followed by image upscaling to the original resolution. Cells were segmented using CellX (Dimopoulos et al., 2014) and out of focus cells were removed manually. The cell segmentation mask, together with the background-subtracted Rtn1p-mCherry and Sec63p-mNeon images were used for cortical ER morphology quantification using a semi-automatic tool developed by Peter Bircham (<https://github.com/SchuckLab/ClassifiER> (Papagiannidis et al., 2021)). At least 100 and up to 1000 cells per condition and replicate were quantified. The same was the case for the quantification of percentage of cells displaying the Rtn1-only puncta phenotype presented in Figures 8C, 16C, and 21A.

For the quantification of Nem1p and Spo7p foci presented in Figure 14I maximum intensity projections of five optical slices spaced 1 μm apart were used. At least 400 cells per condition in each biological replicate were quantified.

2.2.5 Correlative light and electron microscopy (CLEM)

Cells were grown to exponential phase and were treated with 8 mM DTT for 2 h (section 2.2.3). Rtn1-only puncta phenotype was assessed with wide-field fluorescence microscopy (section 2.2.4) before high pressure freezing (HPF). For the HPF cells were collected by filtration. To prevent cells from drying, the filter was kept on a YPD plate. Cells were then loaded on 0.2-mm-deep aluminum carriers (Engineering Office M. Wohlwend, Sennwald, Switzerland). Specifically, cell suspension was loaded on the deep cavity of carrier A using a cut tip and subsequently the flat side of carrier B was placed on top. HPF was performed by Charlotta Funaya with a HPM010 high-pressure freezer (Bal-Tec, Liechtenstein). Freeze substitution was performed exactly as by (Schäfer et al., 2020). Specifically, "Freeze substitution was done with an EM AFS2 automated freeze substitution system (Leica Microsystems, Wetzlar, Germany). Samples were kept in dry acetone containing 0.1% uranyl acetate at -90°C for 24 h. The temperature was increased to -45°C at a rate of $5^{\circ}\text{C}/\text{h}$ and

maintained at -45°C for another 5 h. Samples were washed with dry acetone for 3×10 min and incubated in 10% Lowicryl resin in dry acetone for 2 h and in 25% resin for another 2 h. Samples were transferred to 50% resin, and the temperature was increased to -35°C at a rate of $5^{\circ}\text{C}/\text{h}$ and maintained at 35°C for another 2 h. Samples were transferred to 75% resin, and the temperature was increased to -25°C at a rate of $5^{\circ}\text{C}/\text{h}$ and maintained at -25°C for another 2 h. Samples were incubated in 100% resin at -25°C for 3×10 h. UV polymerization was done at -25°C for 24 h, the temperature was increased to 20°C under UV light within 9 h, and polymerization was continued for another 24 h" (Schäfer et al., 2020). Sections of 90 nm were prepared by Charlotta Funaya using a Leica UC6 ultramicrotome and sections were collected on carbon-coated 200 mesh copper grids (Electron Microscopy Sciences, Hatfield, PA). Grids were then placed on a carrier between coverslips in PBS (Kukulski et al., 2012) and were imaged with the wide-field fluorescence microscope at 100x magnification (section 2.2.4). Focus was determined using the DIC channel (focus point was the one with the minimum contrast) and fluorescence images were acquired using 100% intensity and 1s of exposure. After imaging grids were washed with PBS and stained with 3% uranyl acetate and Reynold's lead citrate by Charlotta Funaya as a preparation for electron microscopy. Electron microscopy was performed using a Jeol JEM-1400 (Jeol Ltd., Tokyo, Japan) transmission electron microscope operating at 120 kV using the SerialEM software package (Mastronarde, 2005) and a bottom mount 4k by 4k pixel digital camera (TemCam F416; TVIPS, Gauting, Germany). Cells of interest were imaged based on the fluorescence microscopy images and with the help of the imprinted letters on the finder grids. Fluorescence and electron microscopy images were correlated based on morphological features using the ICY software and the ec-CLEM plug-in (Paul-Gilloteaux et al., 2017).

2.2.6 Yeast cell lysis

2.2.6.1 Bead beating

Cells (5 ODs; 1 OD of cells is defined as the equivalent of 1 ml of a culture with OD_{600} of 1 and corresponds to approximately 2×10^7 cells) were harvested at 3,000 xg for 5 min and washed once with distilled water. Pellets were either snap frozen and stored at -80°C or processed immediately. All steps were performed on ice unless stated otherwise. Pellets were resuspended in 200 μl standard lysis buffer (Table 2) supplemented with 1 mM PMSF and cOmplete protease inhibitors and transferred into pre-cooled 2 ml screw cap tubes

containing 0.7 g 1 mm glass beads. Cells were lysed by vortexing for 40 s at 6 m/s using a FastPrep 24 (MP Biomedical). To collect the lysates, the screw cap tubes were pierced at the bottom using a flamed needle, were firmly placed on top of 1.5 ml microfuge tubes and centrifuged at 1,000 xg for 10 seconds. Twenty μ l 15% (w/v) was then added and samples were incubated at 65°C for 5 min. Samples were then centrifuged at 4°C at maximum speed using a tabletop centrifuge and clarified lysates were transferred to new microfuge tubes. For treatment of whole cell lysates with alkaline phosphatase (Table 6), cells were lysed in sample buffer with or without PhosSTOP (Table 2). Samples without PhosSTOP were treated with Alkaline phosphatase (5 μ l per 100 μ l lysate) at 37°C for 1 h and SDS was added after the treatment.

2.2.6.2 Post-alkaline extraction

Post-alkaline extraction was performed according to (Kushnirov, 2000). Cultures of exponentially growing cells (5 ODs) were harvested as before and resuspended in 200 μ l distilled water. One volume of 0.2 M NaOH was added and samples were incubated at room temperature for 5 min. Cells were then centrifuged at room temperature at 1,000 xg for 5 min and pellets were resuspended in 100 μ l modified SDS-PAGE sample buffer (Table 2). Samples were then incubated at 65°C for 3 min and briefly spun down. Seven to 10 μ l were used to load on gels.

2.2.6.3 Osmotic lysis

Cells (20 ODs) were harvested at room temperature and washed once with distilled water. Cells were resuspended in 4 ml reducing buffer (Table 2). Cells were pelleted at room temperature at 1,000 xg for 5 min, were resuspended in 4 ml reducing buffer containing 10 mM DTT and incubated at 30°C for 5 min. Cells were pelleted like before, resuspended in 1 ml spheroplast buffer and were treated with 4 μ l zymolyase T100 (Table 6) at 30°C for 10 min. To monitor if the zymolyase treatment worked, a 25 μ l aliquot per sample before and after zymolyase treatment was diluted in 975 μ l water and the OD₆₀₀ was measured. Treatment was considered successful when the OD₆₀₀ dropped below 10% of the original. In case that was not the case, the incubation time was prolonged. The rest of the steps were performed at 4°C. Spheroplasts were transferred in a conical tube, regardless of the sample volume. This was done to facilitate the subsequent steps. Spheroplasts were collected at 4°C at 1,000 xg for 5 min and were washed 3x with 1 ml ice cold spheroplast buffer. Washing was performed with a cut 1 ml tip while avoiding the formation of air bubbles. After the last washing step

spheroplasts were resuspended in 1 ml hypo-osmotic lysis buffer (Table 2) and were incubated on ice for 10 min. Lysates were homogenised using a Dounce homogenizer with a clearance of 0.01 - 0.06 mm (Kimble Chase, New Jersey, United States) with 40 strokes using a tight pestell. Homogenised lysates were cleared at 3,000 xg for 5 min.

2.2.7 Protein determination

Protein concentrations were determined using the BCA assay in 96 well-plates. First, a reference series was prepared in duplicate with 0 to 10 µg BSA in 150 µl water. Samples were added in wells and volume was adjusted to 150 µl, also in duplicates. Sample volumes were selected such that the resulting protein concentrations were within the linear range of the standard curve. BCA reagents A and B (Table 7) were mixed at a ratio 50:1 and 150 µl was added per well, avoiding the formation of air bubbles. Plates were incubated at 30°C for at least 20 min and not more than 2 h and absorbance was measured at 562 nm using a TECAN sunrise (TECAN, Männedorf, Switzerland) or a PHERAstar FSX (BMG LABTECH, Ortenberg, Germany) reader. If needed, protein concentrations of different samples were normalised using the corresponding buffer.

2.2.8 Total membrane preparation

Total membrane preparation was performed in order to increase the concentrations of Spo7p, Nem1p and Ice2p in the samples used for Figures 14A and 14G. Cells (20 ODs) were lysed following the bead beating protocol (section 2.2.6.1) but without addition of SDS and with the clearing spin at 3,000 xg. Cleared lysate was then centrifuged at 4°C at 16,000 xg for 15 min. Supernatant (S16) was removed and pellet (P16) was washed once with lysis buffer and centrifuged like before. P16 was then resuspended in lysis buffer (same volume as the cleared lysate) containing 1.5 % (w/v) SDS, incubated at 65°C for 5 min and prepared for Western blotting.

2.2.9 Subcellular fractionation

For the experiment presented in Figure 21A, cells (100 ODs) were lysed following the osmotic lysis protocol (section 2.2.6.3) and total membrane preparation was performed as above, with the exception that the S16 fraction was kept (carefully removed without disturbing the pellet) and treated like the P16 fraction downstream of washing. Cell lysis by bead beating resulted

in a fraction of Rtn1p being present in the S16 regardless of cell treatment (data not shown), this is why the osmotic lysis protocol was used.

2.2.10 Microsome preparation

Microsomes were prepared according to (Lyman and Schekman, 1995) from strains lacking *PAH1*, *PEP4*, *PRB1* and additional genes as indicated. Reasoning behind the *pah1Δ* background was twofold. First, *PAH1* deletion ensured that all strains had the same ER morphology. Second, the subsequent in vitro assay (section 2.2.13) was not contaminated with endogenous Pah1p. *PEP4* and *PRB1* were deleted to avoid protein degradation during the subsequent in vitro assay. Cells (500 ODs) were lysed following the osmotic lysis protocol (section 2.2.6.3) with minor modifications. Specifically, spheroplasts were resuspended in hypo-osmotic lysis buffer to a concentration of 100 ODs/ml, and clearing spin was performed twice. Total membrane preparation was performed (section 2.2.8) and P16 was resuspended in 170 μ l ice cold B88 buffer, resulting in approximately 200 μ l.

A two-step sucrose gradient was prepared at 4°C in ultracentrifuge tubes (Ultra-Clear™ Centrifuge tubes from Beckman Coulter (Krefeld, Germany), 11 x 60 mm) as follows: 1.9 ml 1.5 M sucrose buffer (Table 2) was gently overlaid with 1.9 ml of 1.2 M sucrose buffer, ensuring a sharp interphase. Interphase position was marked with a marker on the tube.

Sample was gently loaded on top of the two-step sucrose gradient and ultracentrifugation was performed at 150,000 xg at 4°C for 1.5 h, using a pre-cooled SW-60 rotor. Microsomes appeared as a cloudy band around the two-step sucrose gradient interphase. Microsomes (around 300 μ l) were collected, diluted with 5 volumes of B88 buffer and centrifuges at 16,000 xg at 4°C for 15min. Pellets (hardly visible) were resuspended in 1 volume B88 buffer and pelleted again as above. Pellets were then resuspended in 50 μ l dephosphorylation buffer (Table 2) and dispersed by sonication (Elmasonic P sonicator (Elma, Singen, Germany), 100% power, 37 frequency, 3 cycles of: 20s on, 20s off while samples were kept on ice). For figure xyz, pellets were resuspended in 1x SDS-PAGE sample buffer (Table 2) and prepared for western blotting (section 2.2.15).

2.2.11 Immunoprecipitation

Cells (10 ODs) were lysed following the bead beating protocol (section 2.2.6.1) but in 200 μ l immunoisolation lysis buffer (Table 2). After lysate was retrieved, beads were washed with another 300 μ l lysis buffer. Lysates (500 μ l in total) were cleared at 16,000 xg at 4°C for 2 min

and Pah1p-FLAG was immunoprecipitated using anti-FLAG agarose beads (Table 8) at 4°C for 30 min on a rotating wheel. Beads were washed 3 times at room temperature for 5 min with immunoisolation lysis buffer (Table 2) and once with dephosphorylation buffer (Table 2). For each washing step, as well as for bead equilibration in lysis buffer before using, beads were centrifuged at 2,000 xg for 2 min. Pah1p-FLAG was eluted twice with 50 µl 0.2 mg/ml FLAG peptide in dephosphorylation buffer (Table 2) at room temperature for 5 min.

2.2.12 Co-immunoprecipitation

Cells (100 ODs) were lysed following the osmotic lysis protocol (section 2.2.6). Homogenised lysates were cleared at 500 xg at 4°C for 2 min and were incubated with 0.5 % (v/v) Triton X-100 at 4°C for 30 min to solubilise membrane proteins. Insoluble material was removed by ultracentrifugation at 100,000 xg for 30 min and the supernatant was incubated with anti-FLAG agarose beads as before (section 2.2.11). Beads were washed as above twice with hypo-osmotic lysis buffer (Table 2) containing 0.5 % (v/v) Triton X-100 and once with hypo-osmotic lysis buffer. To elute bound proteins, beads were resuspended in 1x SDS-PAGE sample buffer and incubated at 65°C for 5 min. As a loading control, 15 µg of total cell lysates (section 2.2.6.1) was used. This corresponded to 3% of the protein amount that was used as input for the immunoprecipitation (approximately 500 µg total protein).

2.2.13 Pah1p dephosphorylation and phosphorylation in vitro

To monitor the dephosphorylation of Pah1p, 50 µl of immunisolated Pah1p-FLAG (section 2.2.11) from *nem1Δ* cells was mixed with 50 µl prepared microsomes (section 2.2.10) from different deletion mutants as indicated. Reactions were incubated at 30°C for 30 min and were stopped with the addition of SDS sample buffer to 1x and subsequent incubation at 65°C for 5 min. To assess the presence of a potential kinase activity in the above assay, immuno-isolated Pah1p-FLAG from *nem1Δ* or *ice2Δ* cells was incubated with microsomes prepared from *nem1Δ* cells as above.

2.2.14 Proximity biotinylation assay

Cells were lysed following the bead beating protocol (section 2.2.6.1), but in the biotinylation assay lysis buffer (Table 2). Clarified lysates were incubated at 4°C for 1 h with streptavidin agarose beads (Table 8). Beads were washed as above (section 2.2.11), twice at 4°C for 5 min with the biotinylation assay lysis buffer, and twice at room temperature for 5 min with

each of the three biotinylation assay wash buffers (Table 2). To elute bound proteins, beads were resuspended in 1x SDS-PAGE sample buffer containing 2 mM biotin and incubated at 65°C for 10 min.

2.2.15 Western blotting

Samples were prepared for SDS-PAGE by addition of 4xSDS-PAGE sample buffer (Table 2) to 1x unless otherwise specified. Samples were incubated at 65°C for 5 min, briefly spun down and either snap frozen and stored at -20°C or immediately used. Equal volumes of samples (freshly prepared or thawed on ice) and marker (Table 7) were loaded on 10% SDS-PAGE gels (section 2.1.4) and run at room temperature at 200 V until the running front ran out. Proteins were blotted on nitrocellulose membranes at 4°C at 100 V for 1 h. Membranes were then rinsed with TBST (Table 2) and incubated for 5 min in Ponceau S solution (Table 2) to assess blotting efficiency. Membranes were destained with TBST and blocking was performed at room temperature for 30 min in TBST containing 5% (w/v) nonfat dry milk with gentle agitation. The same buffer was used for antibody incubation. Incubation with primary antibodies (Table 8) was performed overnight unless otherwise specified. Membranes were then washed 3 x 5 min at room temperature and were incubated with the HRP-coupled secondary antibodies (Table 8) at room temperature for 1 h. Membranes were washed again and were developed using the homemade ECL solution. For that, membranes were incubated for 1 min at room temperature with ECL (Table 2) while being protected from light. For experiment presented in Figure 14F, SuperSignal West Femto maximum sensitivity substrate (Table 7) was used. Membranes were then placed between two sheets of transparent foil and chemiluminescence was detected using an ImageQuant LAS 4000 imaging system (GE Healthcare, Chalfont St Giles, UK).

2.2.16 PhosTag-PAGE

Samples were prepared as described above and equal volumes were added on either Zn-PhosTag (section 2.1.4) gels (Figure 13C) or Mn-PhosTag gels (rest). Each pocket of the gels was loaded with the same volume of sample, marker (Table 7) plus sample buffer (Table 2) or just sample buffer. When possible, there was a well loaded with sample buffer between the marker and sample wells, and two consecutive wells loaded with marker. Although markers run irregularly on the PhosTag gels (Nagy et al., 2018), they were used to assess the overall running behaviour and timing.

For the Zn-PhosTag gels, gels were run using the Zn-PhosTag running buffer at room temperature for 2 h at 200 V. After running, gels were washed 3 x 10 min in PhosTag blotting buffer (Table 2) containing 1 mM EDTA to chelate the metal ions and 2 x 20 min in PhosTag blotting buffer to remove EDTA. Blotting was performed using the Zn-PhosTag blotting buffer at 100 V at 4°C for 3 h, making sure the blotting buffer was kept cold. Membranes were processed as before (section 2.2.15).

For the Mn-PhosTag gels, gels were run using the normal running buffer (Table 2) at 80 V at 4°C for 20min and at 15 mA/gel for approximately 5 h. Washing of gels and blotting was performed as above but using the regular blotting buffer (Table 2).

2.2.17 Quantitative real-time PCR

Cells were grown to exponential phase and were either treated with 800 nM estradiol to induce the expression of *ino2^p* or left untreated (2.2.3). Five ODs were pelleted at 1,000 xg for 5 min at 4°C, washed once with cold water, snap frozen and stored at -80°C. RNA was isolated through hot phenol extraction (Collart and Oliviero, 2001). All steps were performed under the fume hood. All surfaces (including working surface, pipettes, tip boxes etc) were treated with RNase AWAY (Sigma) and filter tips were used. Frozen pellets were resuspended in 400 µl ice cold TES buffer (Table 2). Four hundred µl acid phenol was added, samples were vortexed for 10 s using a Vortex Genie 2 (Bender and Hobein, Zurich, Switzerland) and incubated at 65°C for 1 h. During this incubation time, samples were vortexed as above every 10 min. Samples were then placed on ice for 5 min and centrifuged at 4°C at 16,000 xg for 5 min. The aqueous phase (top) was transferred into a new microfuge tube without touching the interphase. Four hundred µl acid phenol was added, samples were vortexed once as before and incubated on ice for 5 min before being centrifuged as above. Aqueous phase was again transferred into a new microfuge tube and 400 µl of chloroform was added. After another round of vortexing, incubation on ice and centrifugation, 300 µl of the aqueous phase (top) was transferred to a new microfuge tube. To precipitate the RNA, 30 µl of NaOAc together with 750 µl of ice-cold 100% ethanol were added and samples were vortexed and centrifuged as before. After this step RNA pellets (which became visible at the bottom of the tubes) were washed with 1 ml ice-cold 70% ethanol and centrifuged as above. Ethanol was then removed completely and tubes were left open for residual ethanol to evaporate. Pellets were then fully resuspended in 30 µl RNase-free water (Carl Roth, Karlsruhe, Germany) and RNA concentrations were determined using a NanoDrop spectrometer.

cDNA was then synthesised using 500 ng total RNA, Oligo(dT)₂₃ primers and the RevertAid First Strand cDNA synthesis kit (Table 7) according to the manufacturer's protocols. qPCR reactions were prepared on ice in 384-well microtiter plates (Greiner, Kremsmünster, Austria) in technical triplicates. Microtiter plate layouts were marked on the plates to avoid pipetting errors. One master mix per primer pair was prepared by mixing 5 µl 2x SensiFAST SYBR No-ROX Mix (Table 7) with 1 µl 2.5 µM of each primer (Table 11) per reaction. Seven µl of the master mix was then added on the corresponding wells, followed by 3 µl of pre-diluted cDNA (corresponding to 5 ng RNA per reaction). Plates were then carefully sealed and briefly spun down. qPCRs were run on a LightCycler II 489 (Roche) with the following conditions: i) pre-incubation at 95°C for 2 min, ii) 40 cycles of denaturing at 95°C for 5 s followed by annealing at 60°C for 10 s and extending at 72°C for 30 s with a single acquisition at the end of the extending phase and iii) a 5 min melting curve in which the temperature was steadily ramped to 97°C.

qPCR results were analysed as follows: i) Cp of each sample was determined using the 2nd derivative maximum method with the LightCycler II 480 software and average values of technical replicates. cDNA amounts of genes of interest were normalised to the housekeeping gene *TAF10* by subtracting the mean Cp of the housekeeping gene from the mean Cp of the gene of interest. Resulting values (ΔC_p) are on a log₂ scale due to the exponential increase of product during the PCR and were converted to normalised cDNA amounts on a linear scale by determining $2^{-\Delta C_p}$. Samples were compared by dividing the $2^{-\Delta C_p}$ value of the treated sample by the $2^{-\Delta C_p}$ of the untreated one.

2.2.18 Flow cytometry

Flow cytometry was used to measure the UPR activity. For Figures 7B-E, exponentially growing cells expressing cytosolic BFP and either the transcriptional or splicing reporter were treated with 8 mM DTT or 1 µg/ml tunicamycin for the indicated amount of time. Fluorescence was measured using a FACS Canto flow cytometer (BD Biosciences, Franklin Lakes, New Jersey) equipped with a high-throughput sampler. An isogenic strain without the corresponding UPR reporter was used as a background GFP fluorescence control. Cytosolic BFP was used to normalise for differences in protein translation capacity and background subtracted GFP/BFP values were normalised to the untreated wild-type condition. For Figure 20C, cells expressing the UPR-GFP transcriptional UPR reporter were grown to stationary phase (section 2.2.3). Fluorescence was measured as above at indicated amount of time after

dilution to fresh medium. Again, a strain without expressing the UPR reporter was used as a background control. This time, forward scatter (FSC) values were used to normalise to cell size, although for future repetitions of this preliminary experiment the cytosolic BFP should be used.

2.2.19 Growth assays

2.2.19.1 Growth assays in liquid culture

For growth assays 5 ml SCD was inoculated and cells were grown overnight. Saturated cultures were diluted to an OD₆₀₀ of 0.05 and 500 µl per strain was transferred to a 48-well plate in triplicates. Using a Tecan Infinite M1000 Pro plate reader, cultures were grown at room temperature, to avoid condensation, for 24 h and absorbance at 600 nm was measured in 5-minute intervals. A combination of linear and orbital shaking was applied to ensure cells remain in suspension throughout the assay. The area under the curve was calculated with the R package Growthcurver (Sprouffske and Wagner, 2016) and used as a measure for cell growth. For the growth assays presented in Figure 18A cells were grown to exponential phase instead of saturation and growth assays were performed at 30°C using a Tecan Spark Cyto plate reader.

2.2.19.2 Spotting assays

For spotting assays 5 ml SCD was inoculated and cells were grown overnight to saturation. The next morning, cultures were diluted to an OD₆₀₀ of 0.1 and were let to grow for 5 h. Cultures were then diluted to an OD₆₀₀ of 0.2 and 100 µl per strain was transferred to a 96-well plate. Five-fold serial dilutions were made and cells were spotted on SCD plates with and without 0.2 µg/ml tunicamycin (section 2.1.2) . Plates were incubated at 30°C for 1.5 h before being imaged.

2.2.20 Lipidomic analysis

Pre-cultures were inoculated and cells were grown overnight. The next morning, cells were diluted in fresh medium (1 in 100) and cells were grown overday before being diluted again in fresh medium in order to reach exponential phase the next morning. Cells were lysed following the bead beating protocol (section 2.2.6.1), but in the lipidomics lysis buffer (Table 2). Lipid extraction and measurements were performed by Christian Luchtenborg and Britta

Brügger at the BZH. "Aliquots corresponding to 1500-2000 pmol total lipid were subjected to acidic Bligh and Dyer extractions, except for ergosteryl esters which were recovered by neutral extractions. Lipid extractions were performed in the presence of internal lipid standards. Sample amounts were adjusted to ensure that all lipid standard to lipid species ratios were in a linear range of quantification. Typically, the range of standard to species ratios were within a range of >0.1 to <10. Following this approach, a relative quantification of lipid species was performed. Lipid standard were added from a master mix containing 40 pmol d7-PC mix (15:0/18:1-d7, Avanti Polar Lipids), 25 pmol PI (17:0/20:4, Avanti Polar Lipids), 25 pmol PE and 15 pmol PS (14:1/14:1, 20:1/20:1, 22:1/22:1, semi-synthesized as described in (Özbalci et al., 2013)), 20 pmol DAG (17:0/17:0, Larodan), 20 pmol TAG (D7-TAG-Mix, LM-6000 / D5-TAG 17:0,17:1,17:1, Avanti Polar Lipids), 20 pmol PA (PA 17:0/20:4, Avanti Polar Lipids), 5 pmol PG (14:1/14:1, 20:1/20:1, 22:1/22:1, semi-synthesized as described in (Özbalci et al., 2013)), 40 pmol ergosteryl ester (15:0 and 19:0, semi-synthesized as described in (Gruber et al., 2018)) and 20 pmol t-Cer (18:0, Avanti Polar Lipids). Lipids recovered in the organic extraction phase were evaporated by a gentle stream of nitrogen. Prior to measurements, lipid extracts were dissolved in 10 mM ammonium acetate in methanol, diluted 1:10 and transferred into Eppendorf twin.tec 96-well plates. Mass spectrometric measurements were performed in positive ion mode on an AB SCIEX QTRAP 6500+ mass spectrometer equipped with chip-based (HD-D ESI Chip, Advion Biosciences) nano-electrospray infusion and ionization (Triversa Nanomate, Advion Biosciences) as described (Özbalci et al., 2013). The following precursor ion scanning (PREC) and neutral loss scanning (NL) modes were used for the measurement of the various lipid classes: +PREC 184 (PC), +PREC282 (t-Cer), +NL141 (PE), +NL185 (PS), +NL277 (PI), +NL189 (PG), +NL115 (PA), +NL77 (ergosterol), +PREC379 (ergosteryl ester). Ergosterol was quantified following derivatization to ergosterol acetate in the presence of 200 pmol of the internal standard (22E)-Stigmasta-5,7,22-trien-3-beta-ol (Aldrich, R202967) using 100 µl acetic anhydride/chloroform (1:12 v/v) overnight under argon atmosphere (Ejsing et al., 2009). Mass spectrometry settings: Resolution: unit, low mass configuration; data accumulation: 400 MCA; curtain gas: 20; Interface heater temperature: 60; CAD: medium. Data evaluation was done using LipidView (Sciex) and ShinyLipids, a software developed in house." (Papagiannidis et al., 2021)

“Progress in cell biology is most beautifully revealed when complex cellular events become understood at the level of the molecular machines that orchestrate them.”

Peter Walter and David Ron

3. Results

3.1 ER remodelling in yeast

The qualitative and quantitative assessment of the expansion state of the ER was one of the fundamental aspects of this thesis. In the section below, the yeast ER as observed by fluorescence microscopy is presented along with the metrics used to quantify its expansion state, setting the scene for the experiments that follow.

3.1.1 Visualisation of the ER by fluorescence microscopy

As in all eukaryotic cells, the ER in yeast forms the nuclear envelope and extends into the cytosol forming the peripheral ER. The peripheral ER in yeast is confined to the space just beneath the plasma membrane and is termed cortical ER. To visualise and assess both qualitatively and quantitatively the ER in live cells by fluorescence microscopy, I used two ER membrane proteins that were endogenously tagged with fluorescent proteins. Sec63p, which plays a role in protein translocation into the ER and has been used as a general ER marker in live cells (Prinz et al., 2000), was tagged with mNeonGreen (mNeon; Shaner et al., 2013). Rtn1p, which is a member of the ER-shaping reticulon proteins (Voeltz et al., 2006), was tagged with mCherry; Shaner et al., 2004) and served as a high-curvature ER marker. Together, these markers allowed me to visualise the ER and to differentiate between its different subdomains.

In mid-sections of wild-type exponentially growing cells, the peripheral ER appears as a dotted profile close to the plasma membrane, while in cortical sections the “network” nature of the ER can be appreciated (Figure 3). In particular, Rtn1p-mCherry showed the scaffold of the network whereas Sec63-neon additionally highlighted ER sheets.

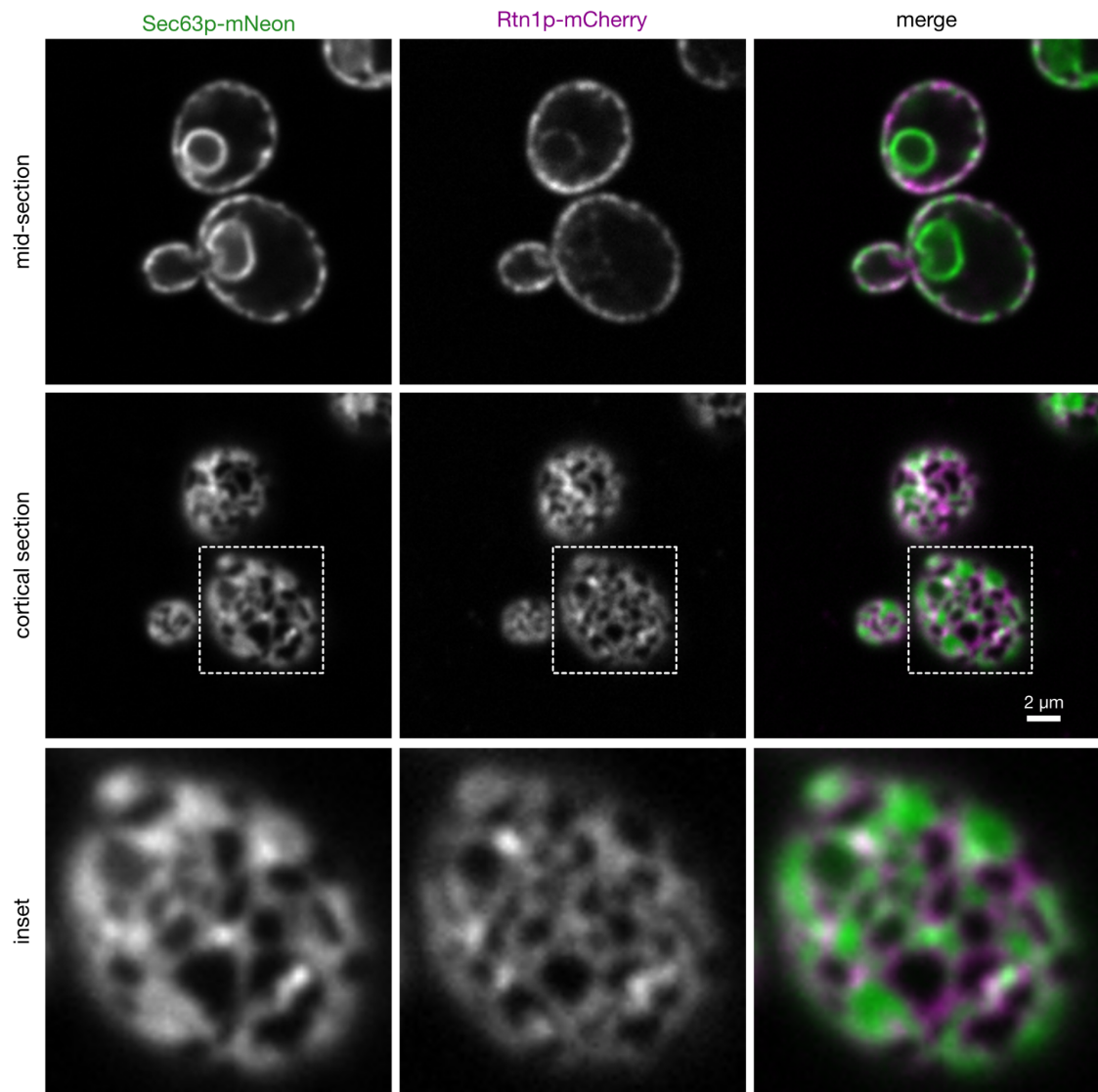


Figure 3. Visualisation of the ER in yeast

Sec63p-mNeon and Rtn1p-mCherry fluorescence microscopy images of mid and cortical sections of wild-type (wt; SSY1405), exponentially growing cells. The boxed areas are shown at higher magnification in the lower panel.

3.1.2 Qualitative description of peripheral ER expansion

The ER in yeast is remodelled as a response to different conditions. Accumulation of misfolded proteins in the ER constitutes a state of ER stress, leading to the activation of the UPR and ER expansion (Walter and Ron, 2011). To induce ER stress, I treated cells with DTT, which leads to the reduction of disulfide bonds and subsequent protein misfolding.

Treatment of cells with 8 mM DTT led to ER expansion within 45 min. In mid-sections, ER expansion was apparent from the formation of longer profiles around the cell periphery. Prolonged DTT treatment caused the appearance of additional ER stretches in the cytosol (Figure 4). In cortical sections, the area occupied by fluorescence signal increased with time of DTT treatment.

In addition to ER stress, activation of lipid synthesis also leads to ER expansion (Schuck et al., 2009). This can be achieved, for example, by deleting the transcriptional repressor Opi1p, or by expressing *ino2^{*}p*, a mutant version of Ino2p which can no longer be recognised and inhibited by Opi1p (Heyken et al., 2005). To compare ER expansion as a result of activated lipid synthesis to ER expansion caused by stress, I expressed *ino2^{*}p* using induction conditions phenocopying *OPI1* deletion (Papagiannidis et al., 2021). Expression of *ino2^{*}p* led to ER expansion resembling early time points of ER stress (Figure 4), in that there were longer profiles around the cell periphery in mid-sections and an increased area occupied by fluorescence signal in cortical sections. In contrast to ER expansion after prolonged ER stress, *ino2^{*}p* expression did not lead to the formation of cytosolic ER stretches.

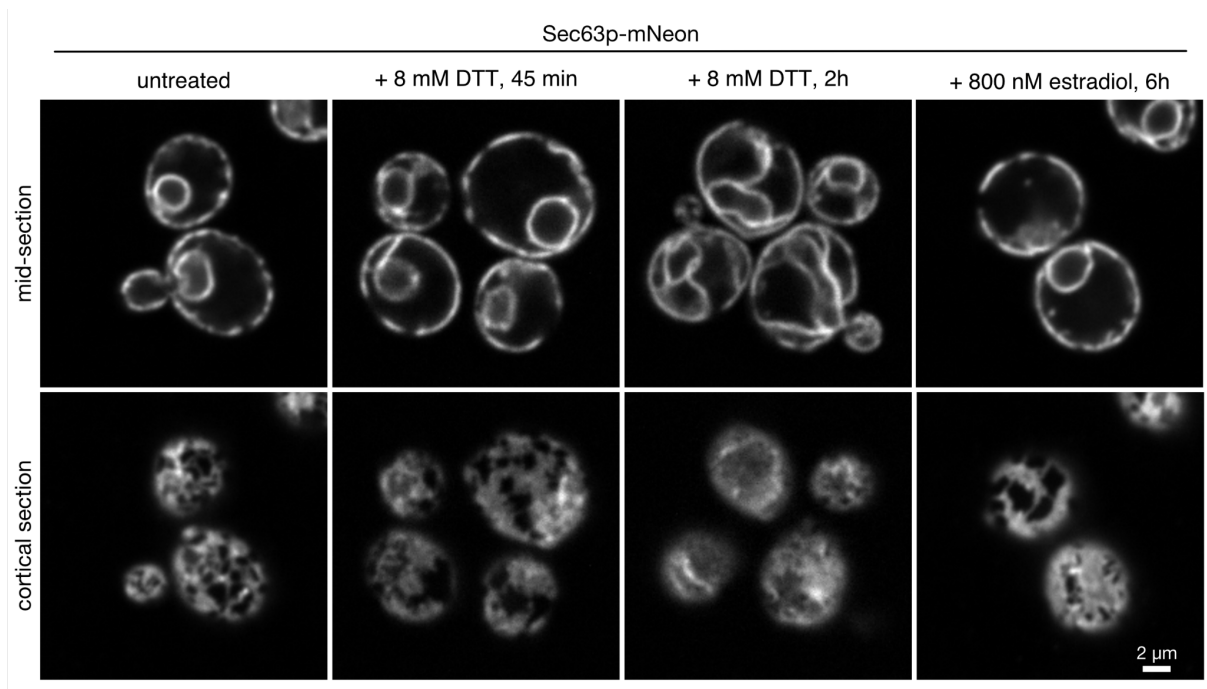


Figure 4. Qualitative description of ER expansion

Sec63p-mNeon fluorescence microscopy images of mid and cortical sections of wild-type (wt; SSY1405), exponentially growing cells. Cells were untreated (left), treated with 8 mM DTT for the indicated amount of time to induce ER stress (middle) or treated with 800 nM estradiol for 6 h in order to induce *ino2** expression (right). Images of untreated cells are the same as in Figure 3.

3.1.3 Quantitative description of cortical ER expansion

To quantitatively describe the expansion state of the ER based on fluorescence microscopy images of cortical sections, Peter Bircham developed a semi-automated image analysis tool (Figure 5A; Papagiannidis et al., 2021). This tool allows the quantification of the percentage of the cell periphery that is covered by ER and the relative contribution of ER sheets and tubules on the single cell level. It thus enables the quantitative description of the expansion state of the ER of cell populations.

Quantification of wild-type exponentially growing cells showed that, as reported before (Hu et al., 2008; Schuck et al., 2009; West et al., 2011), around 50% of the cell periphery is covered by ER, mostly by tubules (Figure 6A). Upon treatment with estradiol to induce *ino2** expression, the ER progressively expanded; not only did the total coverage of the ER increase, but also the relative proportion of ER sheets, consistent with previous work (Figure 5B; Schuck et al., 2009).

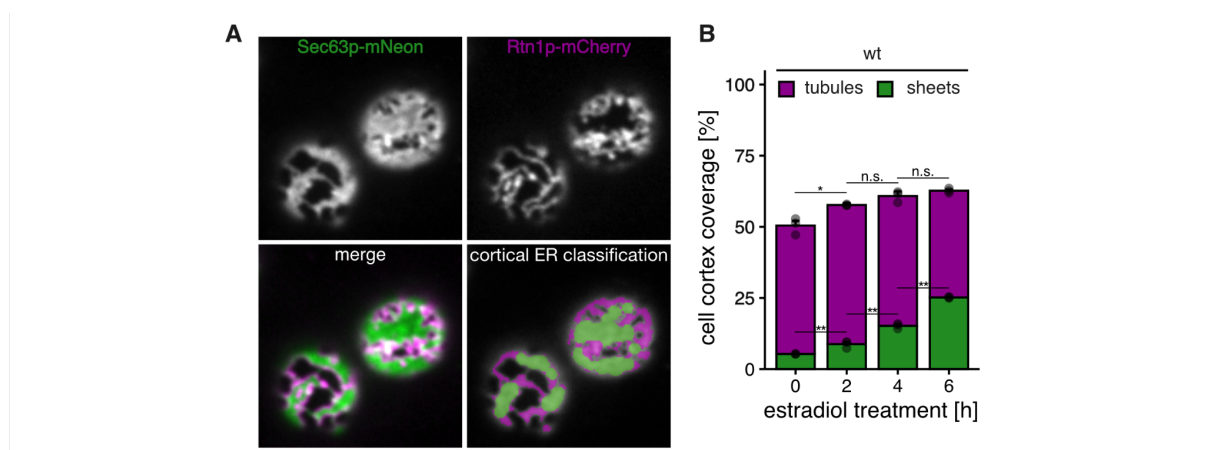


Figure 5. Quantitative description of cortical ER expansion

A. Sec63p-mNeon and Rtn1p-mCherry fluorescence microscopy images (top) of cortical sections of wild-type (wt; SSY1405), exponentially growing cells that were treated with 800 nM estradiol for 6 h to induce *ino2** expression. Merge (bottom left) together with the classification of cortical ER structures (bottom right) as tubules (purple) or sheets (green) are also shown. Modified from (Papagiannidis et al., 2021). **B.** Quantification of cortical ER structures of wild-type (SSY1405), exponentially growing cells that were either untreated or treated with 800 nM estradiol to induce *ino2** expression for the indicated amount of time. Mean values representing the percentage of the cell cortex covered by tubules (purple) or sheets (green), as well as the corresponding values of independent biological replicates are plotted ($n=3$). Error bars are standard error of the mean (s.e.m) of the total cell cortex area covered by ER (upper) or by sheets (lower). Asterisks indicate statistical significance compared with the corresponding previous time point, as judged by a two-tailed Student's t-test assuming equal variance. ** $P < 0.01$; * $P < 0.05$; n.s., not significant.

3.2 *ICE2* is required for and promotes ER expansion

The first step of this journey was for me to validate that *ICE2* is important for ER expansion also in the strain background used in our lab (W303, as opposed to the Y8205 background (Tong and Boone, 2007) that was used for the ER biogenesis screen (Papagiannidis et al., 2021)).

3.2.1 *ICE2* is required for lipid synthesis-mediated ER expansion

To validate the effect of *ICE2* on ER morphology, I first deleted *ICE2* and assessed ER morphology as described above with and without inducing ER expansion. Deletion of *ICE2* led to underexpanded ER already at steady state; the peripheral ER of untreated *ice2Δ* cells covered nearly as much area as the ER of wild-type cells, but the proportion of ER sheets was reduced (Figure 6A).

In contrast to wild-type cells, expression of *ino2** in *ice2Δ* cells did not lead to ER expansion; neither the total area covered by ER nor the proportion of ER sheets increased (Figure 6A). A possible explanation for this phenotype could be that *ino2**-induced activation of Ino2p-Ino4p signalling is impaired in *ice2Δ* mutants. To address this possibility, I measured the mRNA levels of *INO1*. *INO1* is a target gene of Ino2p-Ino4p (Hirsch and Henry, 1986), typically used to assess Ino2p-Ino4p activity (Carman and Henry, 1999). *INO1* mRNA levels were reduced in untreated *ice2Δ* cells compared to the wild-type (Figure 6B). Estradiol-induced *ino2** expression, however, led to activation of Ino2p-Ino4p both in *ice2Δ* and wild-type cells, as evident from the more than 100-fold increase in the mRNA levels of *INO1*. Of note, *ino2**-driven activation of Ino2p-Ino4p was higher in the absence of *ICE2*. This result shows that the inducible Ino2p-Ino4p system is intact in *ice2Δ* cells.

To rule out the possibility that Ice2p does not impair ER expansion altogether but simply causes a delay, I assessed the ER of cells lacking *OPI1* with thereby constitutively active Ino2p-Ino4p. *ICE2* deletion still impaired ER expansion in *opi1Δ* cells (Figure 6C) which normally display a constitutively expanded ER (Schuck et al., 2009).

Taken together, these results show that Ice2p is important for ER expansion in conditions of transcriptionally activated phospholipid synthesis.

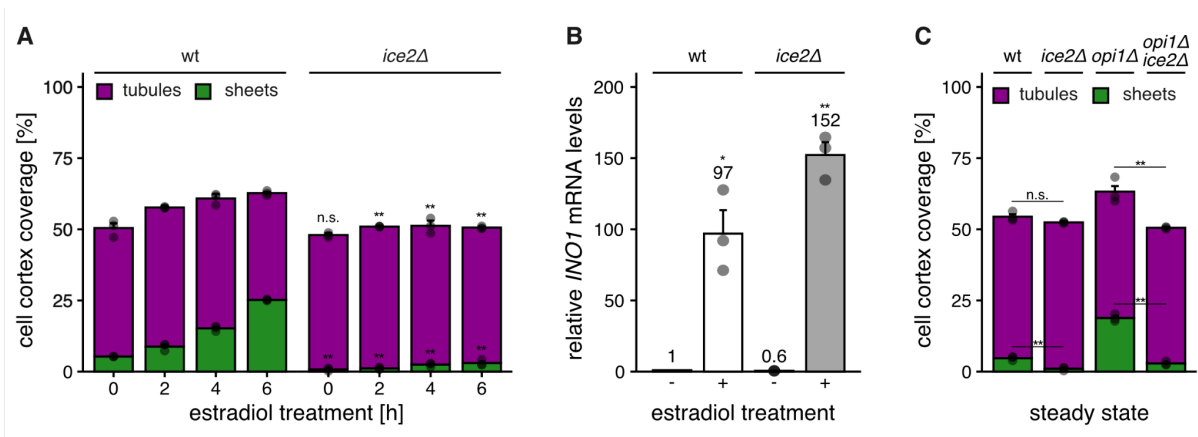


Figure 6. *ICE2* is required for ER expansion upon activation of phospholipid synthesis

A. Quantification of cortical ER structures of wild-type (wt; SSY1405) and *ice2Δ* (SSY1603) exponentially growing cells that were either untreated or treated with 800 nM estradiol to induce *ino2** expression for the indicated amount of time. Mean values representing the percentage of the cell cortex covered by tubules (purple) or sheets (green), as well as the corresponding values of independent biological replicates are plotted ($n=3$). Error bars are standard error of the mean (s.e.m) of the total cell cortex area covered by ER (upper) or by sheets (lower). Asterisks indicate statistical significance compared with the corresponding wild-type, as judged by a two-tailed Student's t-test assuming equal variance. ** $P < 0.01$; n.s., not significant. Left part of the plot (corresponding to the wild-type) is identical to Figure 5B, apart from the statistical information. **B.** Relative *INO1* mRNA levels of wild-type (SSY1405) and *ice2Δ* (SSY1603) exponentially growing cells that were either untreated or treated with 800 nM estradiol for 6 h to induce *ino2** expression, as measured by quantitative real-time PCR. Mean values as well as the corresponding values of independent biological replicates are presented ($n=3$). Data were normalised to untreated wild-type. Error bars are s.e.m and asterisks indicate statistical significance compared with the corresponding untreated condition, as judged by a two-tailed Student's t-test assuming equal variance, apart from the test against the normalised value for the wild-type where unequal variance was assumed. **C.** Quantification of cortical ER structures of wild-type (SSY1404), *ice2Δ* (SSY2356), *opi1Δ* (SSY2811) and *opi1Δ ice2Δ* (SSY2595) exponentially growing cells. Mean values representing the percentage of the cell cortex covered by tubules (purple) or sheets (green), as well as the corresponding values of independent biological replicates are plotted ($n=3$). Error bars are s.e.m of the total cell cortex area covered by ER (upper) or by sheets (lower). Asterisks indicate statistical significance compared with the corresponding wild-type, as judged by a two-tailed Student's t-test assuming equal variance. ** $P < 0.01$; n.s., not significant.

3.2.2 *ICE2* is required for ER stress-mediated ER expansion

As a next step, I assessed whether *ICE2* is important for ER expansion in conditions of ER stress.

After treatment with DTT the ER of wild-type cells expanded (Figure 7A), as expected (Schuck et al., 2009). Remarkably, after extensive DTT treatment the proportion of ER sheets increased at the expense of ER tubules, suggesting tubule-to-sheet conversion. In *ice2Δ* cells the picture looked different. At early time points after DTT treatment there was essentially no ER expansion observed. At later time points, however, the ER of *ice2Δ* cells expanded, as judged both by an increase in the total percentage of cell periphery covered by ER and the increase of the proportion of ER sheets. This observation suggested that stress-induced ER expansion in *ice2Δ* cells is delayed but not blocked.

To test whether UPR signalling is intact in *ice2Δ* cells, I employed two independent UPR activation reporters. The *HAC1* mRNA splicing reporter, which reports on the splicing activity of Ire1p (Pincus et al., 2010), and the UPRE-GFP reporter, which reports on the transcriptional activity of Hac1p (Jonikas et al., 2009). The readout of these experiments was GFP fluorescence as measured by flow cytometry, which increases in both cases upon UPR activation. Compared to the wild-type, *ICE2* mutants showed reduced UPR activation after treatment with the ER stressors DTT and tunicamycin, which blocks protein glycosylation (Figures 7B-7E). This could therefore be an explanation of the delayed ER expansion observed in *ICE2* deletion mutants.

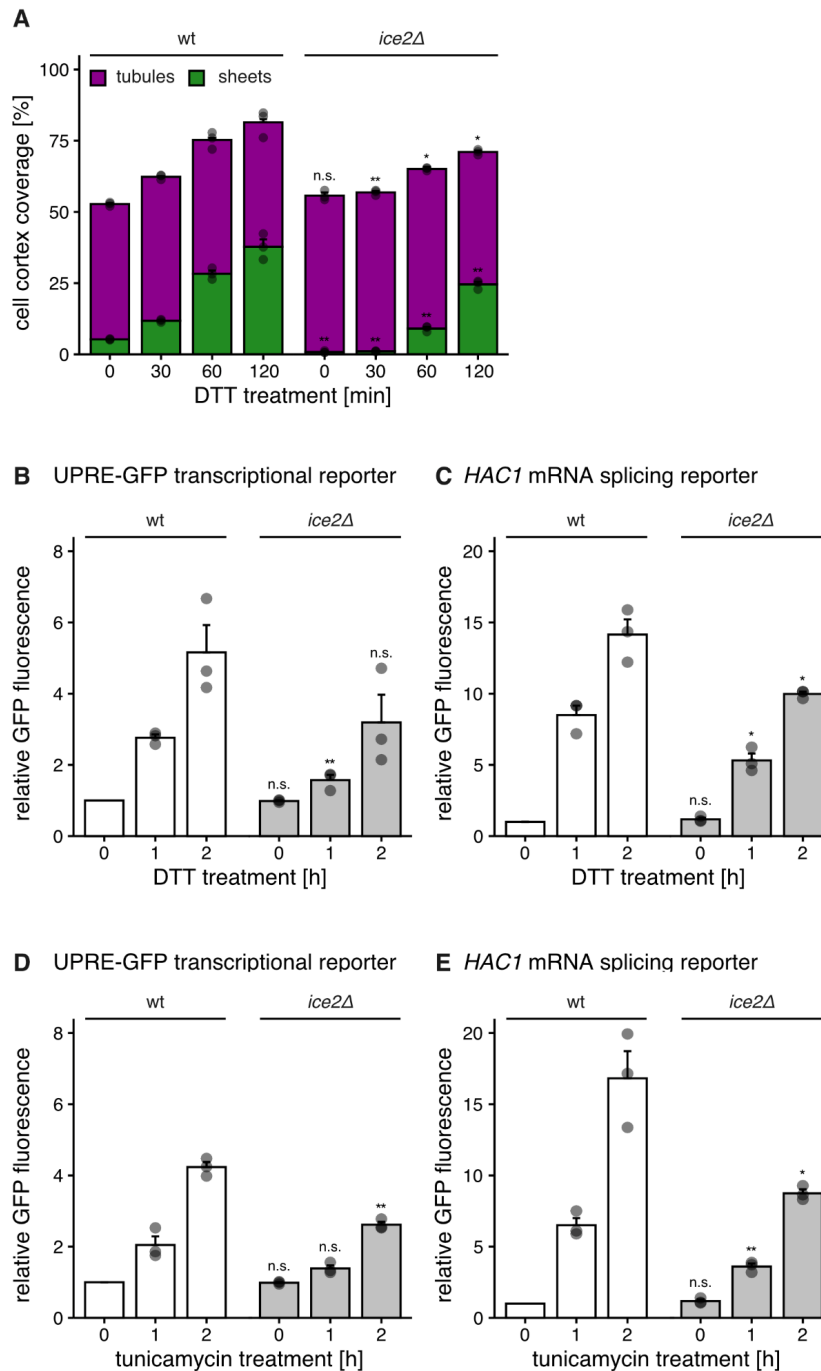


Figure 7. *ICE2* is required for ER stress-induced ER expansion

A. Quantification of cortical ER structures of wild-type (wt; SSY1405) and *ice2Δ* (SSY1603) exponentially growing cells that were either untreated or treated with 8 mM DTT to induce ER stress for the indicated amount of time. Mean values representing the percentage of the cell cortex covered by tubules (purple) or sheets (green), as well as the corresponding values of independent biological replicates are plotted ($n=3$). Error bars are standard error of the mean (s.e.m) of the total cell cortex area covered by ER (upper) or by sheets (lower). Asterisks indicate statistical significance compared with the corresponding wild-type, as judged by a two-tailed Student's t-test assuming equal variance. ** $P < 0.01$; * $P < 0.05$; n.s., not significant. **(B-E).** Relative GFP fluorescence as a measure for UPR activation assessed by flow cytometry. Wild-type and *ice2Δ* cells expressing the UPRE-GFP reported (B,D; SSY2306 and SSY2312) or the *HAC1* mRNA splicing reporter (C,E; SSY2309 and SSY2313) were left

untreated, treated with 8 mM DTT (B,C) or with 1µg/ml tunicamycin (D,E) for the for the indicated amount of time to induce ER stress. Mean values as well as the corresponding values of independent biological replicates are presented (n=3). Data were normalised to the corresponding untreated wild-type. Error bars are s.e.m and asterisks indicate statistical significance compared with the corresponding untreated condition, as judged by a two-tailed Student's t-test assuming equal variance, apart from the test against the normalised value for the wild-type where unequal variance was assumed. **P < 0.01; *P < 0.05; n.s., not significant.

Closer examination of the fluorescence microscopy images, however, revealed an unexpected phenotype. After prolonged DTT treatment, there was the appearance of unusual puncta positive for Rtn1p-mCherry but negative for Sec63p-mNeon (Figures 8A and 8B). These Rtn1-only puncta have not been described before and appeared earlier and in greater numbers in *ice2Δ* cells compared with the wild-type (Figure 8C). This observation suggests that ER stress-induced ER expansion in *ice2Δ* cells was not simply delayed but aberrant, supporting the notion that Ice2p is important for proper ER expansion also under conditions of ER stress. Experiments where the nature of these Rtn1-only puncta was further explored are presented in section 3.7.

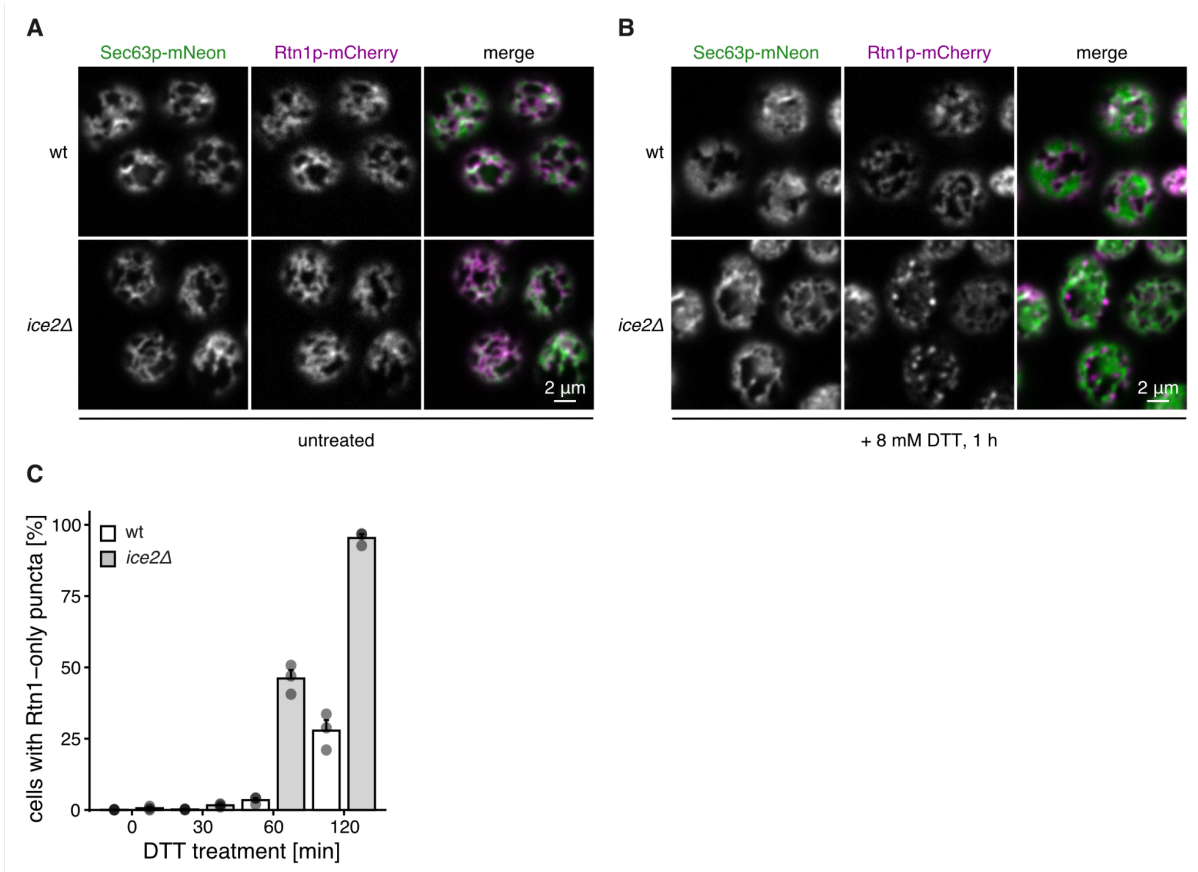


Figure 8. *ICE2* is required for ER stress-induced ER expansion

(A,B). Sec63p-mNeon and Rtn1p-mCherry fluorescence microscopy images of cortical sections of wild-type (wt; SSY1405) and *ice2Δ* (SSY1603) exponentially growing cells that were untreated (A) or treated with 8 mM DTT for 1 h to induce ER stress (B). **C.** Quantification of the percentage of wild-type (SSY1405) and *ice2Δ* (SSY1603) cells displaying the Rtn1-only puncta phenotype. Exponentially growing cells were either left untreated or were treated with 8 mM DTT for the indicated amount of time to induce ER stress. Mean values as well as the corresponding values of independent biological replicates are presented (n=3). Error bars are s.e.m and asterisks indicate statistical significance compared with the corresponding untreated condition, as judged by a two-tailed Student's t-test assuming equal variance. **P < 0.01; *P < 0.05; n.s., not significant.

3.2.3 *ICE2* overexpression and ER expansion

After establishing that *ICE2* deletion impairs ER expansion, the next logical step was to ask whether overexpression of *ICE2* has the opposite effect. Indeed, when I overexpressed *ICE2*, I observed ER expansion (Figure 9A), consistent with previous reports (Emmerstorfer et al., 2015). *ICE2* overexpression led to ER expansion without causing the activation of the UPR (Figure 9B), ruling this out as a potential explanation for the above observation. Moreover, *ICE2* overexpression led to ER expansion in *hac1Δ* cells (Figure 9A), which are unable to activate UPR signalling. These results show that *ICE2* promotes ER expansion both without activating, and independently of the UPR.

Taken together with the previous data, these results show that *ICE2* is required for and promotes ER expansion.

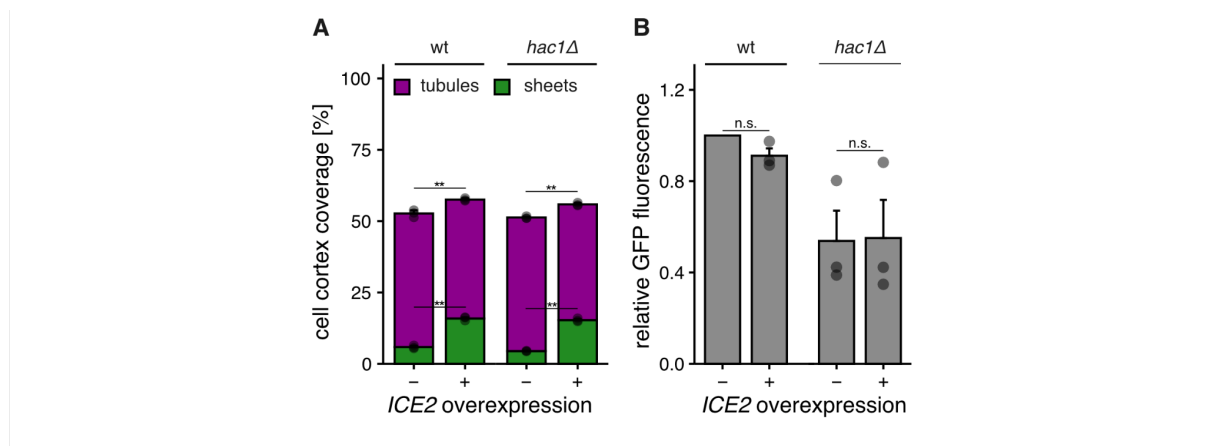


Figure 9. *ICE2* overexpression promotes ER expansion independently of and without activating the UPR

A. Quantification of cortical ER structures of wild-type (wt; SSY2228) and *hac1Δ* (SSY2231) exponentially growing cells that were transformed either with an empty vector (pRS315) or with a plasmid to overexpress *ICE2* (pSS761). Mean values representing the percentage of the cell cortex covered by tubules (purple) or sheets (green), as well as the corresponding values of independent biological replicates are plotted (n=3). Error bars are standard error of the mean (s.e.m) of the total cell cortex area covered by ER (upper) or by sheets (lower). Asterisks indicate statistical significance compared with the corresponding wild-type, as judged by a two-tailed Student's t-test assuming equal variance. **P < 0.01. **B.** Relative GFP fluorescence as measured by flow cytometry of cells expressing the UPR-GFP transcriptional UPR reporter. Wild-type (SSY2306) and *hac1Δ* (SSY2314) exponentially growing cells were transformed either with an empty vector (pRS315) or with a plasmid to overexpress *ICE2* (pSS761). Mean values as well as the corresponding values of independent biological replicates are presented (n=3). Data were normalised to untreated wild-type. Error bars are s.e.m and asterisks indicate statistical significance compared with the corresponding untreated condition, as judged by a two-tailed Student's t-test assuming equal variance, apart from the test against the normalised value for the wild-type where unequal variance was assumed. n.s., not significant.

3.3 Unravelling the molecular role of Ice2p

3.3.1 Ice2p acts independently of the reticulon proteins

An attractive hypothesis to test is that Ice2p could be acting by regulating the reticulons. To test whether *ICE2* acts in the same pathway as the reticulons, I collaborated with Peter Bircham to assess their genetic interactions. Genetic interactions are typically defined based on cellular fitness or growth and can be assessed by comparing the single and double mutant phenotypes. For genes acting in independent pathways, the growth phenotype of the double mutant is expected to be the product of the growth phenotypes associated with the corresponding single mutants (Costanzo et al., 2019). When the double mutant phenotype deviates from this expectation, then the two genes display a genetic interaction. A negative genetic interaction, i.e. when the double mutant has a synthetic growth defect, typically indicates that the two genes in question contribute independently to the same process. A positive genetic interaction, on the other hand, can argue towards the two genes being part of the same pathway. Two genes can display a positive genetic interaction also if they are part of independent pathways, provided that they have opposing functions.

Deletion of *ICE2* led to a mild growth phenotype, as previously reported (Markgraf et al., 2014), whereas deletion of all the known reticulons in yeast, namely *RTN1*, *YOP1* and *RTN2* (strain referred to as $\Delta rtns$) led to no growth phenotype (Figure 10A). The quadruple mutant displayed an intermediate phenotype, suggesting that *ICE2* displays a positive genetic interaction with the reticulons. To test if these genes act in the same or independent pathways, I performed fluorescence microscopy experiments to assess the morphology of the ER of different mutants. Deletion of the reticulons led to ER expansion, as reported previously (Voeltz et al., 2006) and additional deletion of *ICE2* partially reverted this phenotype (Figure 10B). This result suggests that *ICE2* and the reticulons act in independent pathways. It further suggests that there are additional proteins other than Rtn1p, Rtn2p and Yop1p that contribute to ER tubule formation.

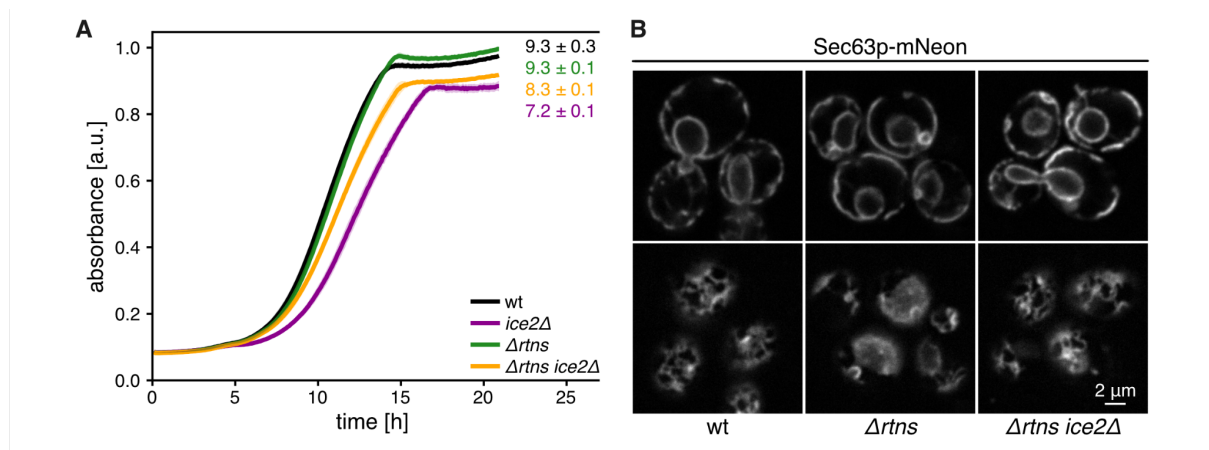


Figure 10. *ICE2* acts independently of the reticulons

A. Growth assay in liquid culture of wild-type (wt; SSY1034), *ice2Δ* (SSY2356), Δ *rtns* (SSY2235) and Δ *rtns ice2Δ* (SSY2236) cells. Cells were grown to saturation, diluted to an OD₆₀₀ of 0.05 and absorbance was measured every 5 min. Mean values of independent biological replicates \pm standard error of the mean (s.e.m) are plotted. Numbers represent the areas under the curves of independent biological replicates \pm s.e.m and are used as growth indices (n=3). Performed in collaboration with Peter Bircham. **B.** Sec63p-mNeon fluorescence microscopy images of mid and cortical sections of wild-type (SSY1034), Δ *rtns* (SSY2235) and Δ *rtns ice2Δ* (SSY2236) exponentially growing cells.

3.3.2 Ice2p acts independently of lipid droplets

Ice2p was previously linked to lipid droplet consumption after exit from stationary phase (Markgraf et al., 2014). Specifically, Ice2p was proposed to be important for the mobilisation of fatty acids from lipid droplets that could then be utilised for phospholipid synthesis. To test the hypothesis that this is how Ice2p promotes ER expansion, I used a strain lacking *DGA1*, *LRO1*, *ARE1* and *ARE2*, the absence of which renders these mutants unable to form lipid droplets (Petschnigg et al., 2009; Velázquez et al., 2016), hereafter referred to as Δ *LD* mutant. Δ *LD* cells grew like wild-type cells (Figure 11A) as previously reported (Velázquez et al., 2016) and deletion of *ICE2* led to a mild growth defect not only in the wild-type background, but also in the Δ *LD* background (Figure 11A). Moreover, the ER in Δ *LD* cells resembled the ER of wild-type cells at steady state, as expected (Petschnigg et al., 2009), and were able to expand their ER both upon *ino2** expression (Figure 11B) and DTT treatment (Figure 11C). Similar to wild-type cells, Δ *LD* cells no longer showed an expanded ER upon additional deletion of *ICE2*. These results show that Ice2p has functions that extend beyond lipid droplet consumption.

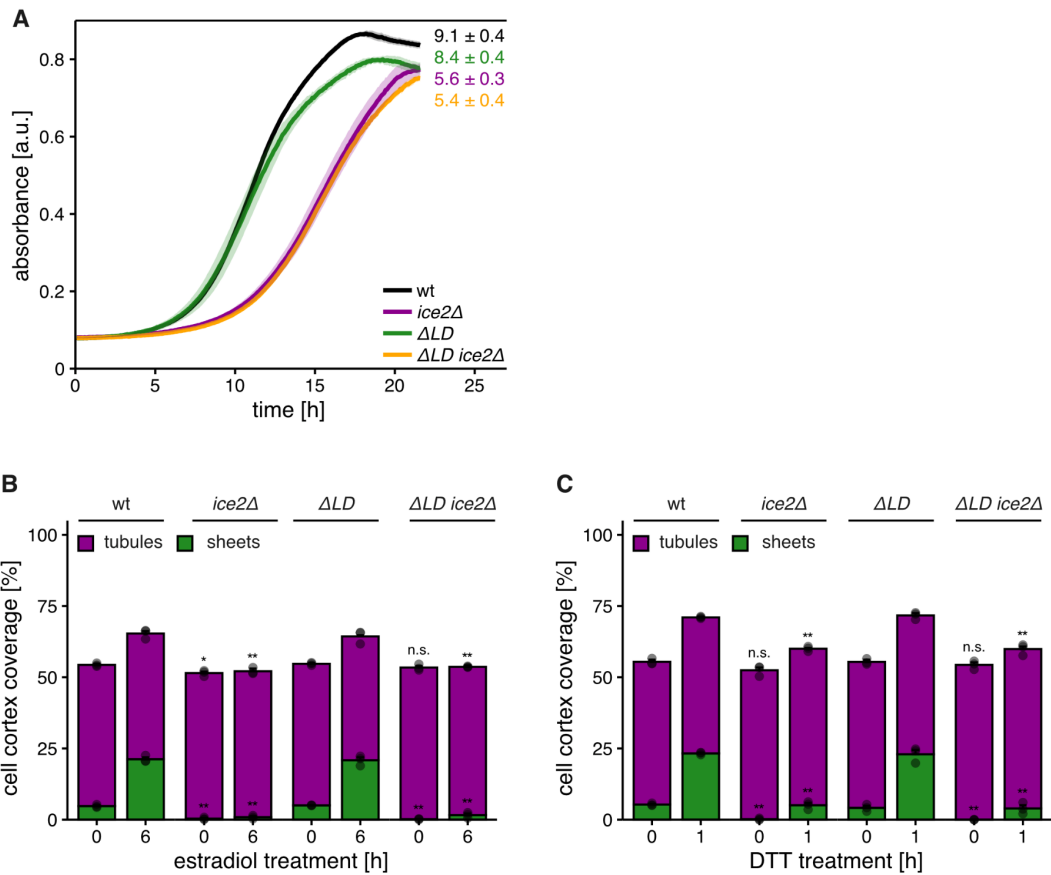


Figure 11. *ICE2* acts independently of lipid droplets

A. Growth assay in liquid culture of wild-type (SSY2228), *ice2Δ* (SSY2229), Δ LD (SSY2256) and Δ LD *ice2Δ* (SSY2230) cells. Cells were grown to saturation, diluted to an OD₆₀₀ of 0.05 and absorbance was measured every 5 min. Mean values of independent biological replicates \pm standard error of the mean (s.e.m) are plotted. Numbers represent the areas under the curves of independent biological replicates \pm s.e.m and are used as growth indices (n=3). Performed in collaboration with Peter Bircham. **(B-C).** Quantification of cortical ER structures of wild-type (SSY2598), *ice2Δ* (SSY2599), Δ LD (SSY2600) and Δ LD *ice2Δ* (SSY2601) exponentially growing cells that were untreated, treated with 800 nM estradiol for 6 h to induce *ino2** expression (C) or treated with 8 mM DTT for 1 h to induce ER stress (D). Mean values representing the percentage of the cell cortex covered by tubules (purple) or sheets (green), as well as the corresponding values of independent biological replicates are plotted (n=3). Error bars are standard error of the mean (s.e.m) of the total cell cortex area covered by ER (upper) or by sheets (lower). Asterisks indicate statistical significance compared with the corresponding wild-type, as judged by a two-tailed Student's t-test assuming equal variance. **P < 0.01; *P < 0.05; n.s., not significant.

3.3.3 *ICE2* is functionally linked to phospholipid synthesis

In order to gain insight into the molecular role of *ICE2*, I looked together with Peter Bircham and Sebastian Schuck at its reported genetic interactions. *ICE2* has been reported to genetically interact with genes involved in lipid synthesis (Schuldiner et al., 2005; Costanzo et al., 2010; Hoppins et al., 2011; Surma et al., 2013). While most of these interactions are

negative, *ICE2* displays positive genetic interactions with *SPO7*, *NEM1* and *PAH1* (Figure 12A). These three genes are part of a linear pathway promoting the dephosphorylation of phosphatidic acid (PA) to diacylglycerol (DAG) and thus play a central role in the regulation of lipid synthesis in yeast.

Since the information on the genetic interaction landscape of *ICE2* is mostly based on high throughput data, I designed and performed growth assays together with Peter Bircham to directly assess the genetic interactions of *ICE2* with *SPO7*, *NEM1* or *PAH1*. In line with the high throughput data, the growth defect displayed by the single *ICE2* mutant was completely rescued when *SPO7*, *NEM1* or *PAH1* were additionally deleted (Figures 12B, 12C and 12D). This is an extreme case of positive genetic interaction, called genetic suppression, and indicates that *ICE2* is part of the same pathway (Costanzo et al., 2019).

In order to assess whether this is relevant for the ER expansion-related function of Ice2p, I performed fluorescence microscopy experiments. Deletion of *SPO7*, *NEM1* or *PAH1* increases the availability of PA and directs lipid synthesis towards membrane phospholipid production, leading to ER expansion and characteristic nuclear envelope aberrations (Figure 12H), as reported previously (Siniosoglou et al., 1998; Santos-Rosa et al., 2005). Additional deletion of *ICE2* did not affect the peripheral or perinuclear ER morphology of these mutants (Figure 12H). If Ice2p was opposing Pah1p activity via a distinct pathway, combining the deletion of *ICE2* with deletions of *SPO7*, *NEM1* or *PAH1* would result in intermediate phenotypes. A case demonstrating this is the example of Dgk1p, which phosphorylates DAG to PA. The combination of *DGK1* deletion with *SPO7*, *NEM1* or *PAH1* led to an intermediate phenotype, both in cellular growth and ER morphology (Figures 12E-G and 12I). Therefore, the above results indicate that Ice2p acts on the same pathway as Spo7p, Nem1p and Pah1p. Moreover, the observation that the double mutants phenocopy the single *SPO7*, *NEM1* and *PAH1* mutants places Spo7p, Nem1p and Pah1p downstream of Ice2p in this pathway. Finally, since Ice2p functionally opposes Spo7p, Nem1p and Pah1p, these results suggest that Ice2p inhibits them.

Together, these results place Ice2p in the context of lipid synthesis and specifically in the Spo7p-Nem1p-Pah1p pathway.

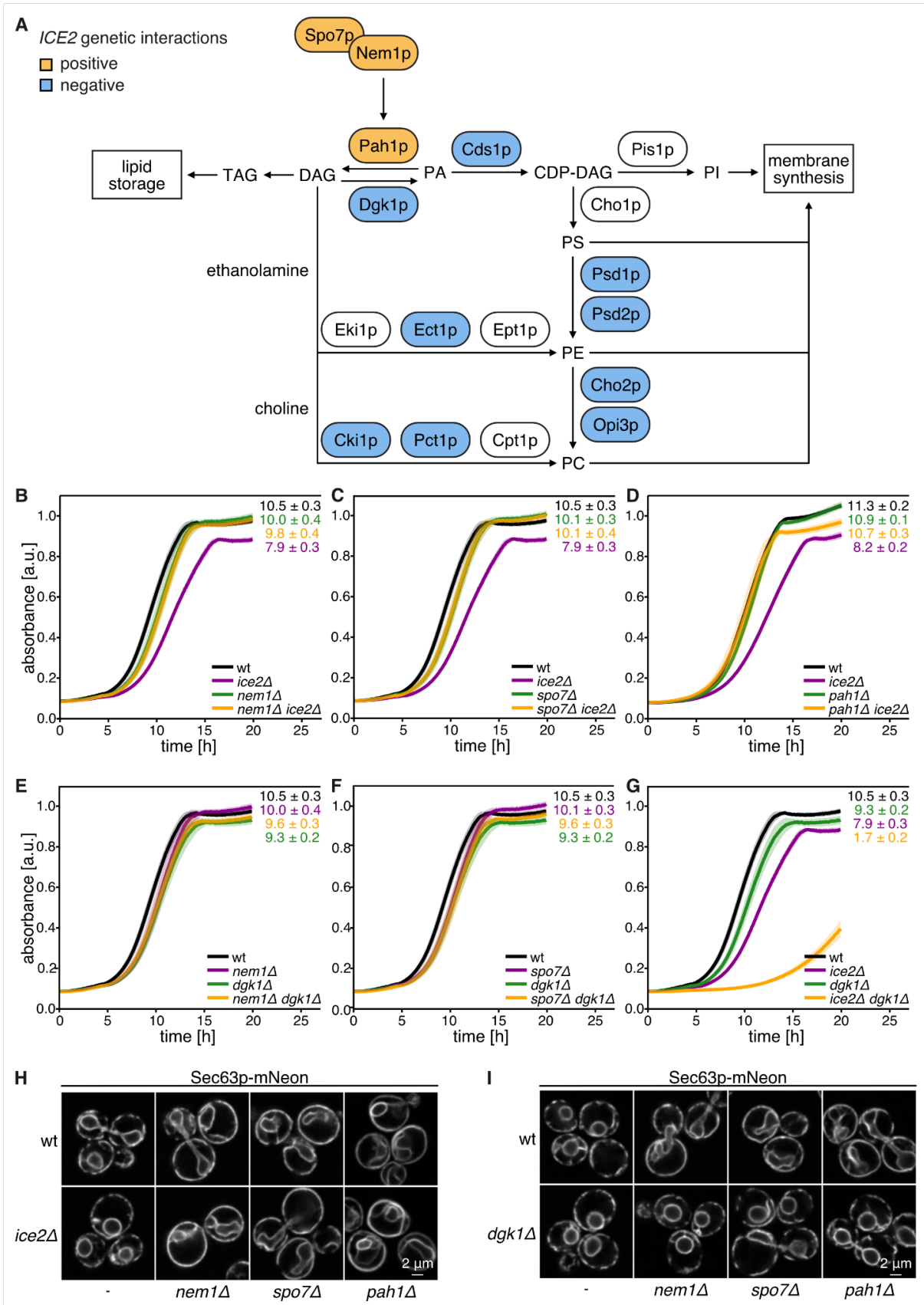


Figure 12. *ICE2* is functionally linked to *SPO7*, *NEM1* and *PAH1*

A. Reported genetic interactions of *ICE2* with lipid synthesis genes mapped on the schematic depicting phospholipid synthesis pathways in yeast that was presented in Figure 1. TAG: triacylglycerol, DAG: diacylglycerol, CDP-DAG: cytidine diphosphate diacylglycerol, PI: phosphatidylinositol, PS: phosphatidylserine, PE: phosphatidylethanolamine, PC: phosphatidylcholine. Modified from (Papagiannidis et al., 2021). **(B-E).** Growth assays in liquid culture of wild-type (wt; SSY1404), *ice2Δ* (SSY2356), *nem1Δ* (SSY2482), *nem1Δ ice2Δ* (SSY2484), *spo7Δ* (SSY2481), *spo7Δ ice2Δ* (SSY2483), *pah1Δ* (SSY2807), *pah1Δ ice2Δ* (SSY2808), *dgk1Δ* (SSY2480), *nem1Δ dgk1Δ* (SSY2485), *spo7Δ dgk1Δ* (SSY2486) and *ice2Δ dgk1Δ* (SSY2539) cells. Cells were grown to saturation, diluted to an OD₆₀₀ of 0.05 and absorbance was measured every 5 min. Mean values of independent biological replicates ± standard error of the mean (s.e.m) are plotted. Numbers represent the areas under the curves of independent biological replicates ± s.e.m and are used as growth indices (n=3). Data for wild-type are the same in panels (A-B, D-G), for *ice2Δ* in panels (B,C and D), for *nem1Δ* in panels (B and E), for *spo7Δ* in panels (C and F), and for *dgk1Δ* in panels (E-G). **(H,I).** Sec63p-mNeon fluorescence microscopy images of mid-sections of wild-type (SSY1404), *ice2Δ* (SSY2356), *nem1Δ* (SSY2482), *nem1Δ ice2Δ* (SSY2484), *spo7Δ* (SSY2481), *spo7Δ ice2Δ* (SSY2483), *pah1Δ* (SSY2807), *pah1Δ ice2Δ* (SSY2808), *dgk1Δ* (SSY2480), *nem1Δ dgk1Δ* (SSY2485), *spo7Δ dgk1Δ* (SSY2486) and *pah1Δ dgk1Δ* (SSY2822) exponentially growing cells. Experiments presented in panels B,C, E, F and G were performed in collaboration with Peter Bircham.

3.3.4 Ice2p controls the phosphorylation status of Pah1p

One way in which Ice2p could regulate the activity of Pah1p is by controlling its abundance. If Ice2p mediated the degradation of Pah1p, then deletion of *ICE2* would lead to higher Pah1p levels and, presumably, Pah1p activity whereas *ICE2* overexpression would have the opposite effect. To test that, I assessed the levels of Pah1p-HA by Western blotting in the presence and absence of *ICE2*. The levels of Pah1p-HA, however, followed the opposite trends than expected (Figure 13A), arguing against Ice2p mediating Pah1p degradation. Unexpectedly, deletion of *NEM1*, which leads to Pah1p hyper-phosphorylation and would be expected to increase Pah1p stability, also showed the opposite trend than expected. Pah1p stability is reported to decrease in conditions where Pah1p is active. I therefore reasoned that repeating the previous experiment with cells grown to stationary phase might provide a sensitised condition, allowing me to better assess the impact of *ICE2* overexpression or deletion on the levels of Pah1p. Regardless of the strain background, however, there was no Pah1p-HA protein detected in lysates from cells grown to stationary phase, rendering the experiment inconclusive.

The activity of Pah1p is subject to phosphoregulation. When inactive, Pah1p is cytosolic and heavily phosphorylated. Activation of Pah1p requires its recruitment to the ER membrane and dephosphorylation by the Spo7p-Nem1p complex. Since the phosphorylation status of Pah1p is commonly used as a readout for its activity (O'Hara et al., 2006), I next investigated the impact of *ICE2* deletion on Pah1p phosphorylation.

When run on regular SDS-PAGE gels, Pah1p from *ice2Δ* cells migrated faster than the wild-type whereas Pah1p from *nem1Δ* cells migrated slower (Figure 13A, 13B and 13C top). These differences were abolished after treatment of cell lysates with alkaline phosphatase (Figure 13B), suggesting that the differences in the running behaviour were due to differences in the phosphorylation status of Pah1p. Although reproducible, these differences were only marginal. To enhance differences in running behaviour of phosphorylated and dephosphorylated Pah1p, I performed PhosTag-PAGE. PhosTag is a compound which binds phosphorylated residues (Kinoshita et al., 2006; Nagy et al., 2018). When covalently linked to acrylamide and co-polymerised into polyacrylamide gels, PhosTag retains the phosphorylated proteins causing them to migrate slower. Pah1p-HA from wild-type cells ran as a smear (Figure 13C), which was expected due to the numerous phosphorylation sites of this protein (Carman and Han, 2019). *ICE2* deletion led to a smear of higher mobility,

supporting the notion that Ice2p controls the phosphorylation status of Pah1p. Importantly, the effect of *ICE2* deletion was dependent on *NEM1*; Pah1p-HA from *nem1Δ* and *nem1Δice2Δ* ran identically, as low mobility bands.

These results show that Ice2p promotes the phosphorylation of Pah1p. This could be achieved by Ice2p either promoting the phosphorylation of Pah1p or by inhibiting its dephosphorylation.

To address this, I reconstituted the dephosphorylation reaction of Pah1 by the Spo7p-Nem1p complex in vitro (Figure 13D). Hyper-phosphorylated Pah1p-FLAG was immuno-isolated from *nem1Δ* cells and was used as a substrate for the reaction. Spo7p, Nem1p and Ice2p are all ER transmembrane proteins. For this reason, obtaining them as purified proteins and reconstituting them into liposomes in their correct orientation is not easily possible. Therefore, I prepared ER microsomes from different mutants and used them as a source for these proteins. Of note, all ER microsome donor strains lacked *PAH1*, for two reasons. First, to avoid contamination of the assay by endogenous Pah1p. Second, *PAH1* deletion ensures identical ER morphologies between the strains tested, ensuring consistency between the different microsome preparations. After incubation of Pah1p-FLAG with the microsomes, samples were analysed by PhosTag-PAGE. The input sample ran as a low mobility band, and was dephosphorylated when treated with alkaline phosphatase (Figure 13E). After incubation with wild-type derived microsomes, Pah1p-FLAG was partially dephosphorylated. This was expected since the stable (Siniosoglou et al., 1998) ER transmembrane Spo7p-Nem1p complex is present in wild-type microsomes (Figure 13F). Incubation with *ice2Δ* derived microsomes led to a higher degree of Pah1p-FLAG dephosphorylation (Figure 13E), even though the Nem1p-HA levels were not higher than in the wild-type microsomes (Figure 13F). Presence or absence of Ice2p in microsomes derived from *nem1Δ* strains made no difference in Pah1p-FLAG dephosphorylation (Figure 13E). There was a small degree of dephosphorylation of Pah1p-FLAG from *nem1Δ* derived microsomes, which could be due to an unspecific or yet-to-be-defined phosphatase of Pah1p. To exclude the possibility of a kinase activity being present in the reconstituted assay, dephosphorylated Pah1p-FLAG was immuno-isolated from *ice2Δ* cells and incubated with *nem1Δ* derived microsomes. No kinase activity was observed (Figure 13G).

Together, these results show that Ice2p inhibits Pah1p dephosphorylation by opposing the activity of the Spo7p-Nem1p complex.

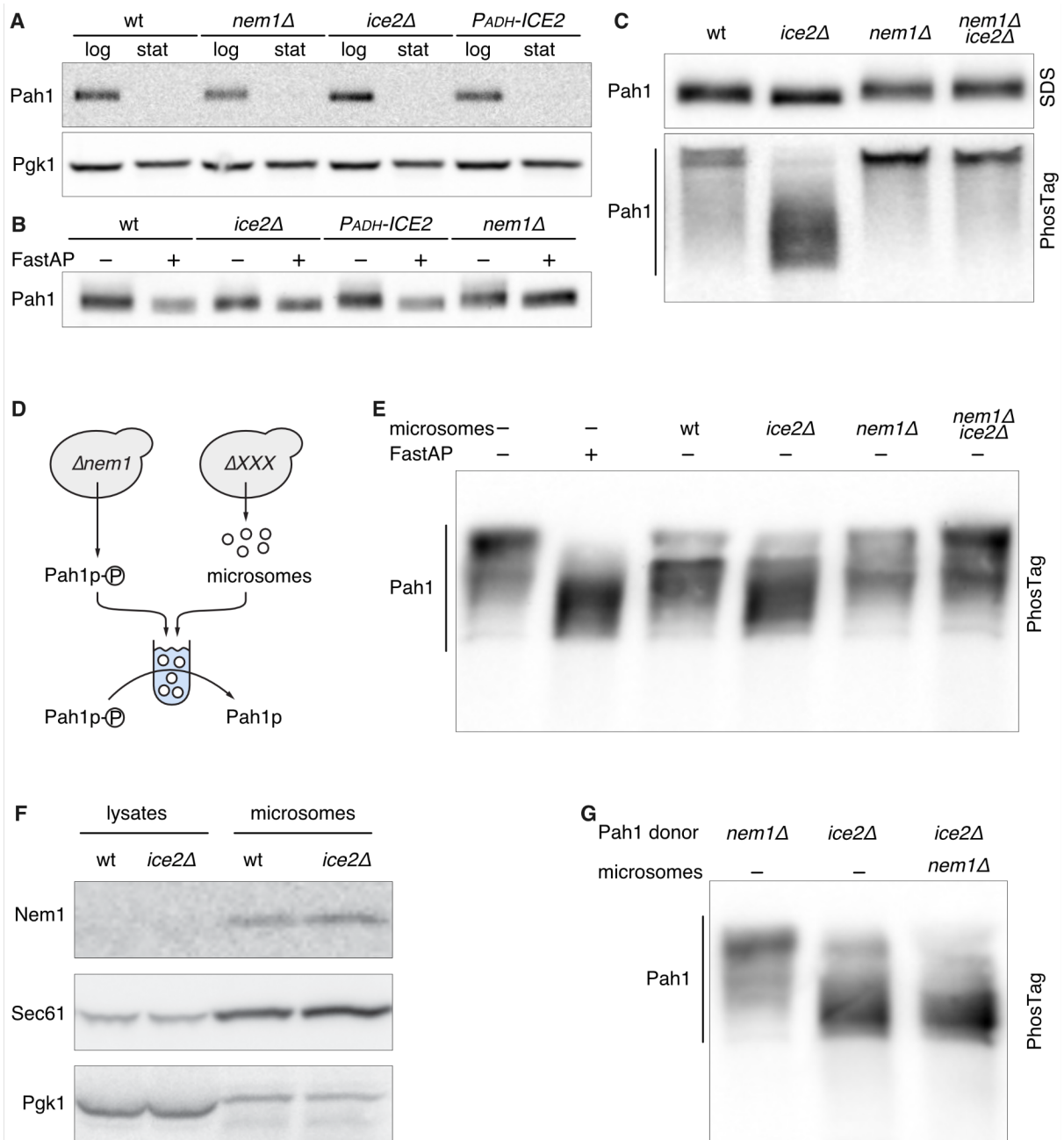


Figure 13. Ice2p opposes Pah1p dephosphorylation by inhibiting the Spo7p-Nem1p complex

A. Western blots of Pah1p-HA and Pgk1p of whole cell lysates of wild-type (wt; SSY2592), *nem1Δ* (SSY2593), *ice2Δ* (SSY2594) cells and cells constitutively overexpressing *ICE2* (*P_{ADH1}-ICE2*; SSY2602), which are all expressing Pah1p-HA. Cells were grown to exponential (log) or stationary (stat) phase. **B.** Western blot of Pah1p-HA of whole cell lysates of wild-type (SSY2592), *ice2Δ* (SSY2594), *P_{ADH1}-ICE2* (SSY2602) and *nem1Δ* (SSY2593) exponentially growing cells. Cell lysates were either untreated or treated with alkaline phosphatase (FastAP) for 1 h. **C.** Western blots of Pah1p-HA of whole cell lysates of wild-type (SSY2592), *ice2Δ* (SSY2594), *nem1Δ* (SSY2593) and *ice2Δ nem1Δ* (SSY2718) exponentially growing cells. Lysates were analysed by SDS-PAGE (top) and PhosTag-PAGE (bottom). **D.** Schematic depicting the in vitro reconstitution of the Pah1p dephosphorylation reaction. **E.** Western blot of immunoprecipitated Pah1p-FLAG from *nem1Δ* (SSY3065) that was untreated, treated with alkaline phosphatase or treated with microsomes purified from wild-type (SSY3053), *nem1Δ* (SSY3075), *ice2Δ* (SSY2074) or *nem1Δ ice2Δ* (SSY3095) exponentially growing cells. Reactions were analysed by PhosTag-PAGE. Microsome donor strains were *PEP4*, *PRB1* and *PAH1* deletion mutants. **F.** Western blots of Nem1p-HA, Sec61p and Pgk1p of whole cell lysates (left) and purified microsomes (right) from wild-type (SSY3140) and *ice2Δ*

(SSY3141) exponentially growing cells. Nem1p-HA was not detectable in whole cell lysates due to its low abundance. **G.** Western blot of immunoprecipitated Pah1p-FLAG from *nem1Δ* (SSY3065) or *ice2Δ* (SSY3096) that was untreated or treated with microsomes purified from *nem1Δ* (SSY3075) exponentially growing cells. Reactions were analysed by PhosTag-PAGE. Microsome donor strains were *PEP4*, *PRB1* and *PAH1* deletion mutants.

3.3.5 Ice2 interacts with and restricts the Spo7p-Nem1p complex

Ice2p could control the activity of the Spo7p-Nem1p complex in different ways. The first hypothesis that I tested was that Ice2p promotes the degradation of Spo7p or Nem1p. In this scenario, deletion of *ICE2* would increase their protein levels whereas *ICE2* overexpression would have the opposite effect. The levels of both Spo7p and Nem1p, however, followed the opposite trends than expected, arguing against this hypothesis (Figure 14A).

Next, I performed co-immunoprecipitation (coIP) experiments to test whether Ice2p interacts with the Spo7p-Nem1p complex. Indeed, Ice2p-HA precipitated with both Spo7p-FLAG (Figure 14B) and Nem1p-FLAG (Figure 14C) in wild-type cells, but not with Dpm1p, an abundant ER membrane protein which was used as a negative control. Moreover, Ice2p-HA still interacted with Spo7p-FLAG in *nem1Δ* cells (Figure 14D), suggesting that interaction with Spo7p does not depend on Nem1p. Interaction of Ice2p with Nem1p in the absence of *SPO7* could not be tested, since Nem1p is unstable in these mutants (Mirheydari et al., 2020; Figure 14E). Hence, Ice2p interacts with the Spo7p-Nem1p complex, although it cannot be ruled out that this interaction is indirect.

Interaction of Ice2p with the Spo7p-Nem1p complex predicts that Ice2p should be in the proximity of Pah1p. I tested this prediction using proximity biotinylation as an assay. I tagged Ice2p with TurboID (Branon et al 2018), and assessed biotinylation of Pah1p-HA. Biotinylation of Pah1p-HA was observed in wild-type cells and was greatly reduced in *spo7Δ* and *nem1Δ* cells (Figure 14F).

These results indicate that Ice2p forms a ternary complex with Spo7p-Nem1p. This notion was further supported by comparison of the relative abundances of these proteins (Figure 14G). Ice2p-HA levels were similar to the ones of Spo7p-HA, and both proteins were more abundant than Nem1p-HA, consistent with high throughput data (Ho et al., 2018).

Next, I assessed the relative localisation of Ice2p, Spo7p and Nem1p by fluorescence microscopy. All three proteins displayed a general ER localisation, forming occasional puncta (Figure 14H). Specifically, Ice2p foci have been suggested to form at sites of lipid droplet

consumption (Estrada de Martin et al., 2005; Markgraf et al., 2014) whereas the Spo7p-Nem1p complex has been suggested to form foci at sites of lipid droplet synthesis (Siniossoglou et al., 1998; Adeyo et al., 2011). Ice2p colocalized with both Spo7p and Nem1p, a phenotype which is best appreciated in distinct foci as well as around the nuclear envelope (Figure 14H). A model consistent with my biochemical and imaging data would be that Ice2p restricts the Spo7p-Nem1p complex to distinct foci, limiting their activity. If that were true, then Spo7p and Nem1p would no longer form foci in *ice2Δ* mutants, leading to their unrestricted activity. In line with this, imaging experiments that were designed and initially performed by me and repeated and quantified by Oliver Pajonk showed that no Spo7p or Nem1p foci were observed in *ice2Δ* cells (Figure 14I).

Interestingly, the Ice2p foci colocalized neither with Sei1p, a lipid droplet biogenesis factor (Adeyo et al., 2011), nor with lipid droplets, as visualised with monodansylpentane (MDH; Figure 14J).

These results show that Ice2p contributes to the localisation of the Spo7p-Nem1p complex. This, in combination with the results indicating that Ice2p regulates the activity of the Spo7p-Nem1p complex, suggests the following hypothesis: In steady state, Ice2p interacts with and restricts the localisation and activity of Spo7p-Nem1p complex. In the absence of *ICE2*, the Spo7p-Nem1p complex can redistribute and exhibit its activity all over the ER.

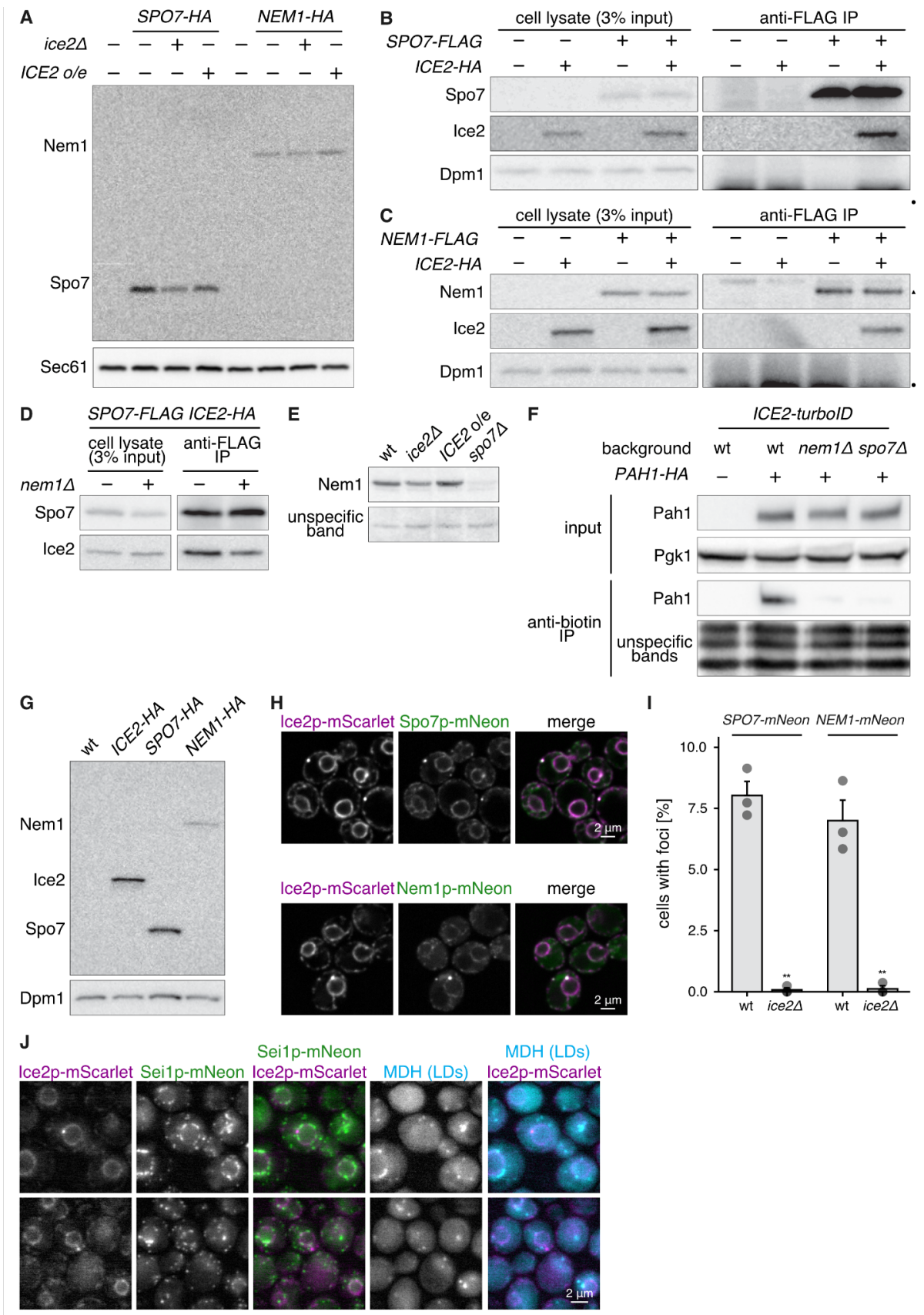


Figure 14. Ice2p interacts with and spatially restricts the Spo7p-Nem1p complex

A. Western blots of Nem1p-HA, Spo7p-HA and Sec61p of total cell membranes of wild-type cells (SSY122), wild-type, *ice2Δ* and *ICE2*-overexpressing cells (*ICE2* o/e) expressing Spo7p-HA (SSY2910, SSY2911 and SSY2912, respectively), and wild-type, *ice2Δ* and *ICE2* o/e cells expressing Nem1p-HA (SSY2913, SSY2915 and SSY2915, respectively). **B.** Western blots of Spo7p-FLAG, Ice2p-HA and Dpm1 of whole cell lysates (left) or anti-FLAG immunoprecipitates (IPs). Wild-type (SSY122), cells expressing Ice2p-HA (SSY2421), cells expressing Spo7p-FLAG (SSY3183) and cells expressing Ice2p-HA and Spo7p-FLAG (SSY3184) were analysed. The circle indicates bands of the light chain from the antibody used for the immunoprecipitation. **C.** Western blots of Nem1p-FLAG, Ice2p-HA and Dpm1p of whole cell lysates (left) or anti-FLAG IPs. Wild-type (SSY122), cells expressing Ice2p-HA (SSY2421), cells expressing Nem1p-FLAG (SSY3195) and cells expressing Ice2p-HA and Nem1p-FLAG (SSY3196) were analysed. The circle indicates bands of the light chain from the antibody used for the immunoprecipitation and the triangle bands of proteins that were non-specifically immunoprecipitated with the anti-FLAG antibody. **D.** Western blots of Spo7p-FLAG and Ice2p-HA of whole cell lysates (left) or anti-FLAG IPs. Wild-type (SSY3184) and *nem1Δ* (SSY3197) cells expressing Ice2p-HA and Spo7p-FLAG were analysed. **E.** Western blots of Nem1p-HA of total cell membranes of wild-type (SSY2913), *ice2Δ* (SSY2914), *ICE2* o/e (SSY2915) and *spo7Δ* (SSY2945) cells. Unspecific band served as a loading control. **F.** Western blots of Pah1p-HA, Pgc1p and biotinylated proteins of whole cell lysates (top) and anti-biotin IPs (bottom). Wild-type cells (wt; SSY2978), wild-type, *nem1Δ* and *spo7Δ* cells expressing Pah1p-HA (SSY2979, SSY3117 and SSY3118, respectively) were analysed. All strains were expressing Ice2p-TurboID. Unspecific biotinylated proteins were used as a loading control. **G.** Western blots of Ice2p-HA, Spo7p-HA, Nem1p-HA and Dpm1p of total cell membranes of wild-type (SSY122) cells and cells expressing Ice2p-HA (SSY2421), Spo7p-HA (SSY2910) and cells expressing Nem1p-HA (SSY2915). **H.** Fluorescence microscopy images of mid-sections of exponentially growing cells expressing Ice2p-mScarlet and Spo7p-mNeon (SSY3244), and Ice2p-mScarlet and Nem1p-mNeon (SSY3245). **I.** Quantification of the percentage of wild-type (SSY2916, SSY2917) and *ice2Δ* (SSY3238, SSY3239) exponentially growing cells displaying Spo7p-mNeon and Nem1p-mNeon foci. Mean values as well as the corresponding values of independent biological replicates are presented (n=3). Error bars are s.e.m and asterisks indicate statistical significance compared with the corresponding wild-type, as judged by a two-tailed Student's t-test assuming equal variance. **P < 0.01. Experiment repetitions and quantification were performed by Oliver Pajonk. **J.** Fluorescence microscopy images of mid-sections of exponentially growing cells expressing Ice2p-mScarlet and Sei1p-mNeon. Lipid droplets (LDs) were visualised with monodansylpentane (MDH).

3.4 Inhibition of Spo7p-Nem1p by Ice2p promotes phospholipid synthesis and ER expansion

After establishing that Ice2p promotes Pah1p dephosphorylation by interacting with and inhibiting the activity of the Spo7p-Nem1p complex, the next step was to assess whether this regulation has a functional output.

3.4.1 *ICE2* deletion promotes phospholipid synthesis

Pah1p plays a central role in lipid metabolism in yeast by controlling the conversion of PA to DAG. The availability of PA and DAG define, to a large extent, whether cells produce membrane phospholipids or store lipids in lipid droplets for future use. Overactive Pah1p

pushes this balance towards lipid storage by decreasing the PA availability while increasing the availability of DAG. Inactive Pah1p, on the other hand, has the opposite effect.

In order to assess if the regulation of Pah1p by Ice2p has a functional output, the lipidomes of cells were measured in collaboration with Christian Luchtenborg and Britta Bruegger at the Biochemistry Center Heidelberg (BZH). Deletion of *ICE2* led to an increase in triacylglycerol (TAG) and ergosterol ester (EE) levels and a decrease in the levels of the main membrane phospholipids phosphatidylethanolamine (PE) and phosphatidylcholine (PC) (Figure 15), in agreement with previous reports (Markgraf et al., 2014). These changes did not only reflect relative changes (Figure 15A); *ICE2* deletion had an impact on the total lipid levels normalised to total protein content (Figure 15C). Deletion of *SPO7* or *NEM1* had the opposite effect, namely decrease of storage lipids at the expense of membrane phospholipids (Figure 15). Additional deletion of *ICE2* did not affect the lipidome of the *SPO7* or *NEM1* single mutants.

These results are in line with the growth, imaging and biochemical data in terms of epistasis, and support the idea that Ice2p regulates lipid metabolism by controlling the phosphorylation status and hence activity of Pah1p.

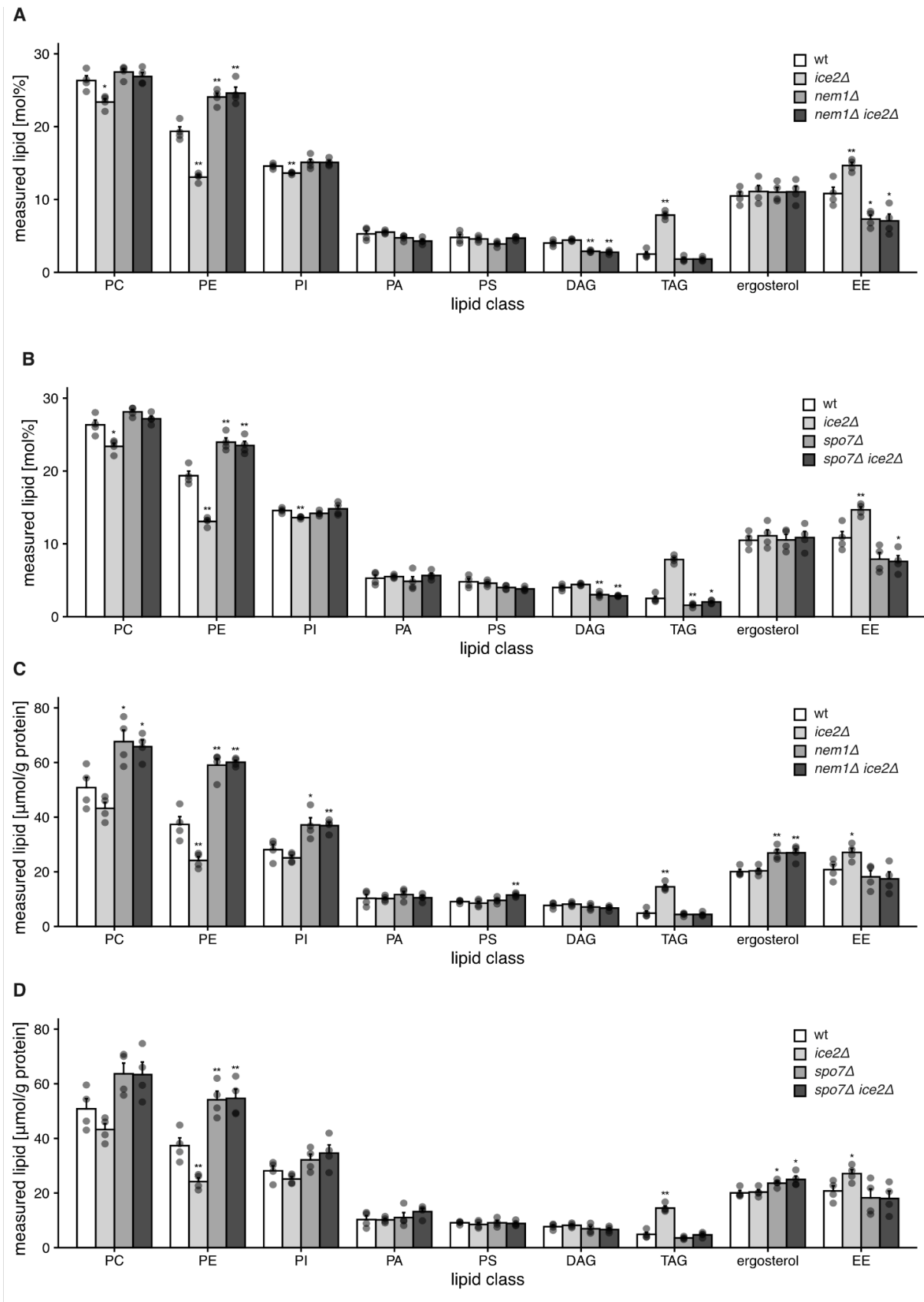


Figure 15. Inhibition of the Spo7p-Nem1p complex by Ice2p promotes phospholipid synthesis

(A-D). Whole cell lipidomic analysis of wild-type (SSY1404), *ice2Δ* (SSY2356), *nem1Δ* (SSY2482), *nem1Δ ice2Δ* (SSY2484), *spo7Δ* (SSY2481) and *spo7Δ ice2Δ* (SSY2483) exponentially growing cells. Mean values representing the mol % of each measured lipid (A,B) or the μmol of each measured lipid normalised to g of total protein (C,D), as well as the corresponding values of independent biological replicates are presented (n=4). Error bars are s.e.m and asterisks indicate statistical significance compared with the corresponding untreated condition, as judged by a two-tailed Student's t-test assuming equal variance. **P < 0.01; *P < 0.05. PC: phosphatidylcholine, PE: phosphatidylethanolamine, PI: phosphatidylinositol, PA: phosphatidic acid, PS: phosphatidylserine, DAG: diacylglycerol, TAG: triacylglycerol, EE: ergosterol esters. Data for wild-type and *ice2Δ* are the same in panels (A,B) and (C,D). Lipidomic analysis (all steps after cell lysis) was performed by Christian Luchtenborg and Britta Brügger.

3.4.2 Ice2p promotes ER expansion by inhibiting Pah1p

The next step was to test whether Ice2p can promote ER expansion by regulating the phosphorylation status of Pah1p. To this end, I replaced wild-type *PAH1* with a mutant version in which seven phosphorylation sites were mutated to alanines, *pah1(7A)*. The phospho-deficient *pah1(7A)p* is constitutively active, although some Spo7p-Nem1p regulation still remains (Su et al., 2014). *ICE2* overexpression in wild-type cells led to ER expansion, as before (Figure 16A). Cells in which the wild-type *PAH1* was replaced by *pah1(7A)* displayed an underexpanded ER already in steady state, and additional overexpression of *ICE2* led to only partial ER expansion.

This result suggests that Ice2p manifests its role in ER expansion, at least in part, by inhibiting the dephosphorylation of Pah1p. It also suggests that regulation of Pah1p by Ice2p extends beyond these seven phosphorylation sites. This was additionally supported by the following observations: First, cells expressing *pah1(7A)* displayed an ER expansion and morphology phenotype which is between the wild-type and *ice2Δ* after treatment with DTT (Figures 16B and 16C). Second, the *pah1(7A)* mutant was still subject to Spo7p-Nem1p regulation in the absence of *ICE2* (Figure 16D). Finally, the lipidome changes caused by the *pah1(7A)* mutant were, like in the case of ER phenotypes, between the wild-type and *ice2Δ* phenotypes (Figure 16E).

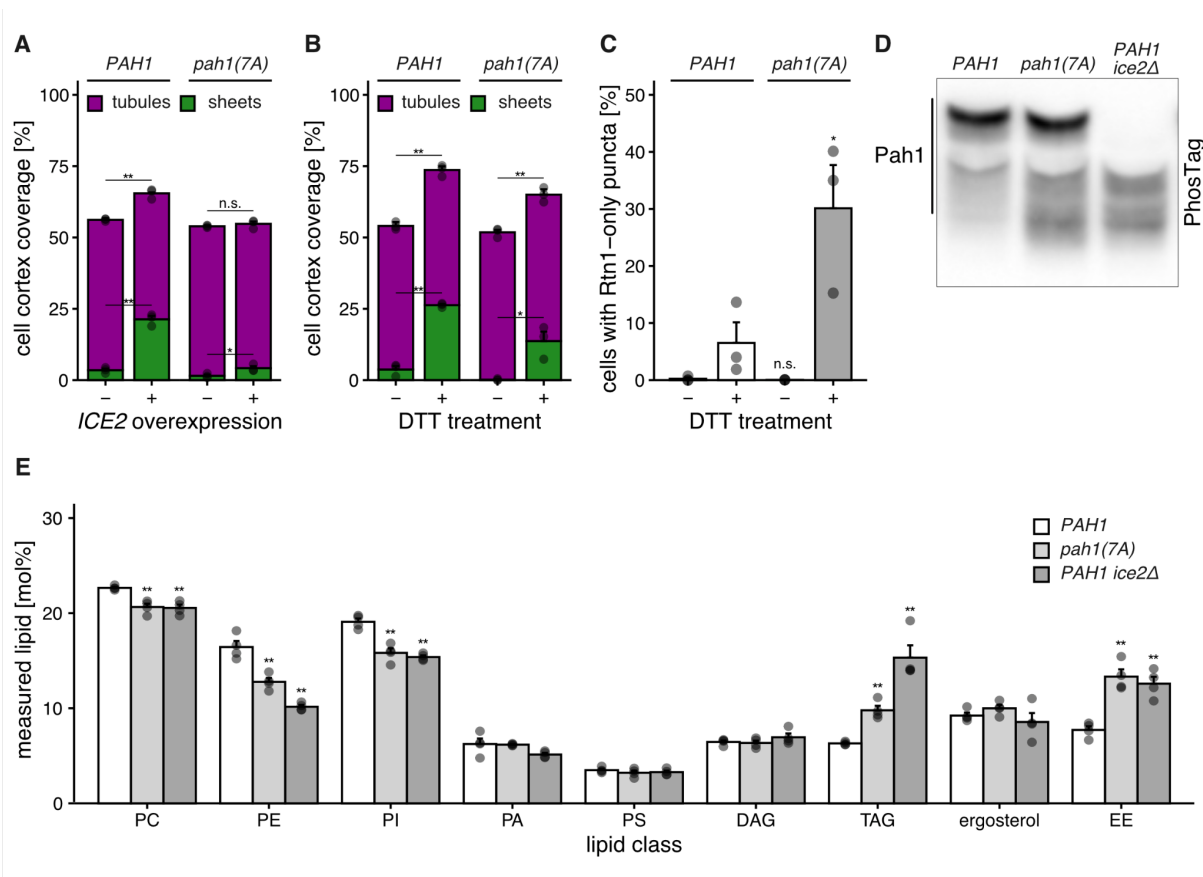


Figure 16. Ice2p promotes ER expansion by regulating the phosphorylation status of Pah1p

A. Quantification of cortical ER structures of wild-type and *ICE2*-overexpressing cells in which *PAH1* was replaced with *PAH1-HA* or *pah1(7A)-HA* (SSY2841, SSY2842, SSY2843, SSY2844). Mean values representing the percentage of the cell cortex covered by tubules (purple) or sheets (green), as well as the corresponding values of independent biological replicates are plotted ($n=3$). Error bars are standard error of the mean (s.e.m) of the total cell cortex area covered by ER (upper) or by sheets (lower). Asterisks indicate statistical significance compared with the corresponding wild-type, as judged by a two-tailed Student's t-test assuming equal variance. $**P < 0.01$; $*P < 0.05$; n.s., not significant. **B.** Quantification of cortical ER structures of cells in which *PAH1* was replaced with *PAH1-HA* (SSY2841) or *pah1(7A)-HA* (SSY2842) that were either untreated or treated with 8 mM DTT for 1 h to induce ER stress. Mean values representing the percentage of the cell cortex covered by tubules (purple) or sheets (green), as well as the corresponding values of independent biological replicates are plotted ($n=3$). Error bars are standard error of the mean (s.e.m) of the total cell cortex area covered by ER (upper) or by sheets (lower). Asterisks indicate statistical significance compared with the corresponding wild-type, as judged by a two-tailed Student's t-test assuming equal variance. $**P < 0.01$; $*P < 0.05$. **C.** Quantification of the percentage of cells displaying the Rtn1-only puncta phenotype. Wild-type (SSY1405) and *ice2Δ* (SSY1603) cells displaying the Rtn1-only puncta phenotype. Cells in which *PAH1* was replaced with *PAH1-HA* (SSY2841) or *pah1(7A)-HA* (SSY2842) were either untreated or treated with 8 mM DTT for 1 h to induce ER stress. Mean values as well as the corresponding values of independent biological replicates are presented ($n=3$). Error bars are s.e.m and asterisks indicate statistical significance compared with the corresponding untreated condition, as judged by a two-tailed Student's t-test assuming equal variance. $*P < 0.05$; n.s., not significant. **D.** Western blot of Pah1p-HA of total cell lysates of cells in which *PAH1* was replaced with *PAH1-HA* (SSY2841), cells in which *PAH1* was replaced with *pah1(7A)-HA* (SSY2842) and *ice2Δ* cells in which *PAH1* was replaced with *PAH1-HA* (SSY2970). **E.** Whole cell lipidomic analysis of cells in which *PAH1* was replaced with *PAH1-HA* (SSY2841), cells in which *PAH1* was replaced with *pah1(7A)-HA* (SSY2842) and *ice2Δ* cells in which *PAH1* was replaced with *PAH1-HA* (SSY2970). Mean values representing the mol % of each measured lipid as well as the corresponding values of independent biological replicates are presented ($n=4$). Error bars are s.e.m and asterisks indicate statistical significance compared with the corresponding untreated condition, as judged by a two-tailed Student's t-test assuming equal variance. $**P < 0.01$; PC: phosphatidylcholine, PE: phosphatidylethanolamine, PI: phosphatidylinositol, PA:

phosphatidic acid, PS: phosphatidylserine, DAG: diacylglycerol, TAG: triacylglycerol, EE: ergosterol esters. Lipidomic analysis (all steps after cell lysis) was performed by Christian Luchtenborg and Britta Brügger.

3.5 How does *ICE2* coordinate with other pathways regulating ER homeostasis?

In the following section, I set out to assess the role of the Ice2p-mediated regulation of Pah1p activity in a broader cellular context.

3.5.1 *ICE2* cooperates with *OPI1* to promote ER expansion

Both deletion of *OPI1* and overexpression of *ICE2* lead to ER expansion. I therefore wondered if these two pathways are linked or independent of each other. To address this question, I overexpressed *ICE2* in cells lacking *OPI1*. The ER of these cells was remarkably expanded (Figures 17A and 17B), suggesting that these two pathways contribute independently to ER membrane biogenesis.

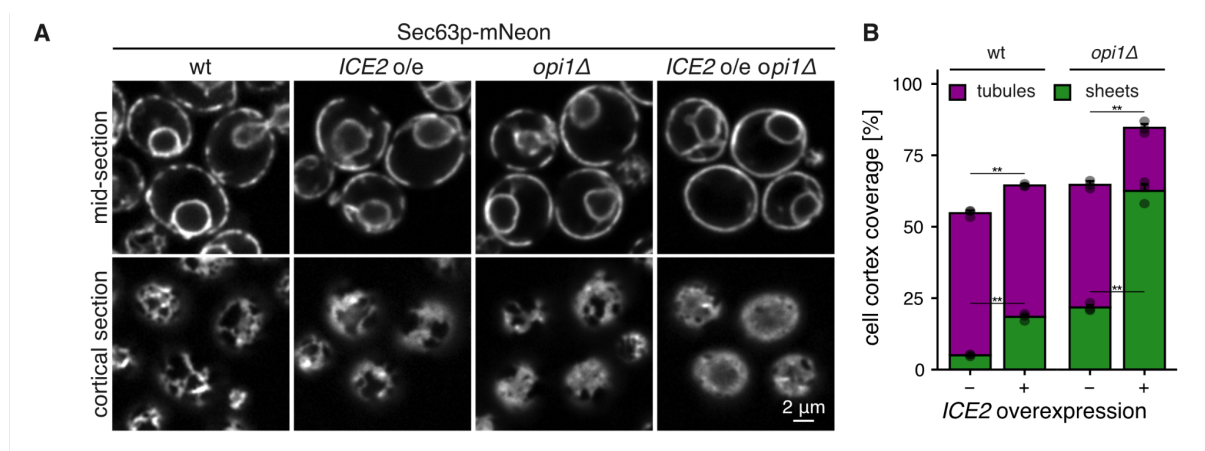


Figure 17. *ICE2* cooperates with *OPI1* to promote ER expansion

A. Sec63p-mNeon fluorescence microscopy images of mid- and cortical sections of wild-type (wt; SSY1404), *ICE2* overexpressing (*ICE2* o/e; SSY2588), *opi1Δ* (SSY2595) and *ICE2* o/e *opi1Δ* (SSY2596) exponentially growing cells. **B.** Quantification of cortical ER structures of wild-type (SSY1404), *ICE2* o/e (SSY2588), *opi1Δ* (SSY2595) and *ICE2* o/e *opi1Δ* (SSY2596) exponentially growing cells. Mean values representing the percentage of the cell cortex covered by tubules (purple) or sheets (green), as well as the corresponding values of independent biological replicates are plotted (n=3). Error bars are standard error of the mean (s.e.m) of the total cell cortex area covered by ER (upper) or by sheets (lower). Asterisks indicate statistical significance compared with the corresponding wild-type, as judged by a two-tailed Student's t-test assuming equal variance. **P < 0.01.

3.5.2 *ICE2* helps maintain cell homeostasis

ICE2 overexpression leads to ER expansion without activating and independently of the UPR (Figure 9). *Ice2p* could, thus, either function independently of the UPR, or be a downstream target of it. *ICE2* displayed a negative genetic interaction with *HAC1*, as observed by growth assays both in liquid media (Figure 18A, experiment designed and initially performed by me and repeated by Giulia Ruffini) and on plates (Figures 18A and 18B), consistent with high throughput data (Schuldiner et al., 2005; Costanzo et al., 2010; Bircham et al., 2011; Surma et al., 2013, Costanzo et al., 2016). Moreover, this phenotype was enhanced in conditions of ER stress (Figure 18B).

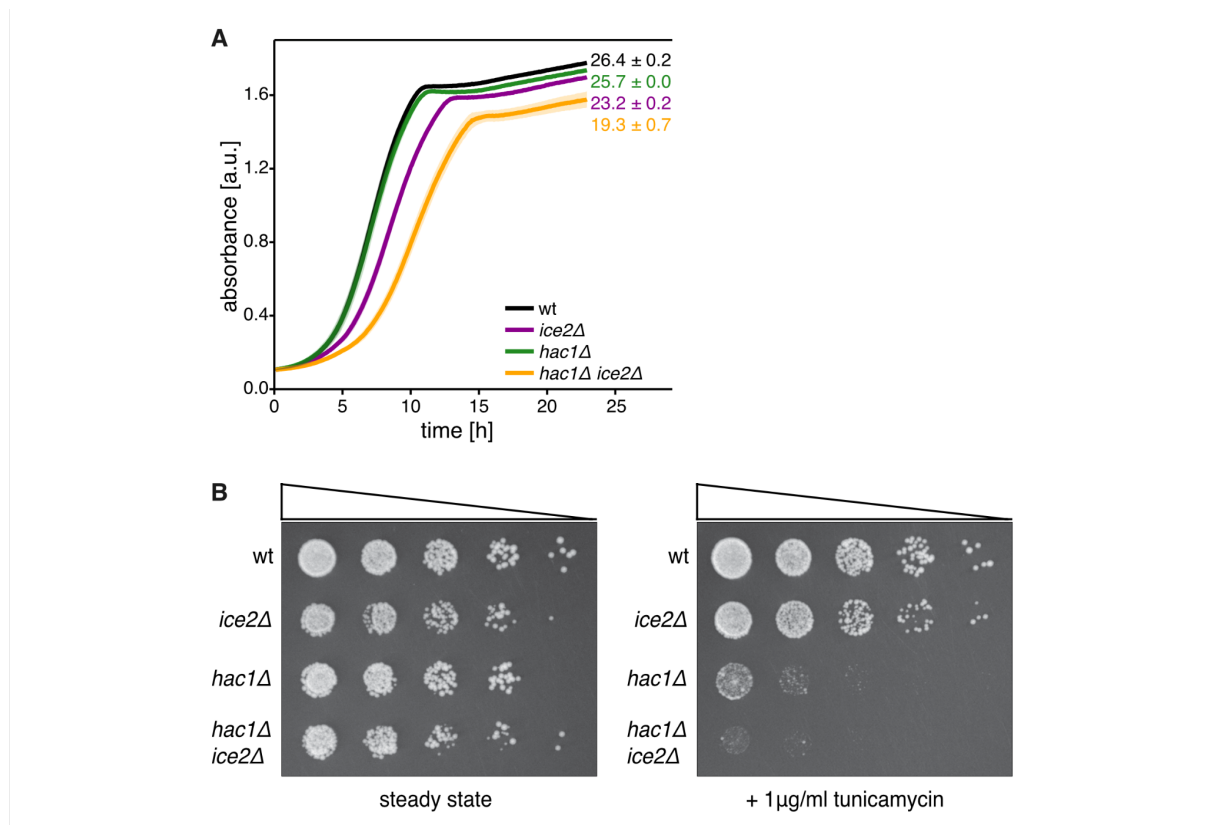


Figure 18. *ICE2* cooperates with the UPR to maintain cell homeostasis

A. Growth assay in liquid culture of wild-type (SSY1404), *ice2Δ* (SSY2356), *hac1Δ* (SSY2805) and *hac1Δ ice2Δ* (SSY2806) cells. Cells were grown to exponential phase, diluted to an OD_{600} of 0.05 and absorbance was measured every 5 min. Mean values of independent biological replicates \pm s.e.m are plotted. Numbers represent the areas under the curves of independent biological replicates \pm s.e.m and are used as growth indices ($n=3$). Experiment repetitions were performed by Giulia Ruffini. **B.** Growth assay on agar plates of wild-type (SSY1404), *ice2Δ* (SSY2356), *hac1Δ* (SSY2805) and *hac1Δ ice2Δ* (SSY2806) cells. Cells were grown to saturation, diluted to an OD_{600} of 0.2 and 5-fold serial dilutions were spotted on SCD (left) or SCD + 1 μ g/ml tunicamycin plates.

3.6 Preliminary observations on the physiological role of the regulation of Pah1p

The results so far have placed Ice2p in the midst of lipid synthesis in yeast, and have indicated that Ice2p promotes ER membrane biogenesis by inhibiting the dephosphorylation of Pah1p. Physiological conditions, however, where this regulation is relevant have not yet been addressed.

3.6.1 Stress-induced and lipid synthesis-induced ER expansion

If cells use the regulation of Pah1p to achieve ER expansion, one would expect an increase in the phosphorylation status in such conditions. To address this, I treated cells with the ER stressors DTT and tunicamycin and monitored the phosphorylation status of Pah1p-HA using PhosTag gels. These experiments have an inherent limitation. That is, that Pah1p is mostly phosphorylated at steady state and further phosphorylation, for example in the absence of *NEM1*, is only marginally resolved (Figure 13 C). Slight changes in that direction would therefore be hard to assess. Nevertheless, there was a slight but reproducible increase in the phosphorylation status of Pah1p-HA appearing 30 min after treatment with 8 mM DTT or 2 µg/ml tunicamycin (Figures 19A and 19B), which was not observed when the catalytically inactive *pah1(D398A D400A)p-HA* (Karanasios et al., 2010) or *pah1(7A)p-HA* were tested. These results suggest that the phosphorylation status of Pah1p is regulated in the context of stress-induced ER expansion. Whether this occurs in an Ice2p-dependent manner, by the activity of one or more Pah1p kinases or a combination of both is yet to be determined. Closer examination of these data revealed an unexpected observation. Already 1 h after each treatment the running behaviour of Pah1p-HA resembled the untreated condition, evident by the reappearance of the higher-mobility smear. Moreover, after 2 h of each treatment there seemed to be Pah1p-HA dephosphorylation, despite the fact that ER keeps expanding in these conditions (see for example Figure 7A). This could depend on the growth phase of the cell population or be a homeostatic mechanism counteracting ER expansion. Further experiments provided indications that both of the above-mentioned factors contribute to the observed phenotypes (Figure 19C). When I treated wild-type cells with estradiol, which does

not have an effect on the expansion state of the ER (Papagiannidis et al., 2021), there was a slight decrease in the phosphorylation status of Pah1p-HA after 6 h, when cells reached an OD_{600} of 1.3. Moreover, when I used estradiol to induce the expression of *ino2**p, which leads to ER expansion, there was a clear trend towards Pah1p-HA dephosphorylation – exceeding the effect of the cell growth state. This result suggests that cells dephosphorylate Pah1p as a response to Ino2p-Ino4p-driven ER expansion. Inducible expression of *hac1ⁱ*, an intron-less version of the *HAC1* mRNA (Pincus et al., 2014), phenocopied the untreated condition, suggesting that the observed dephosphorylation of Pah1p-HA is unlikely to be UPR-mediated. This is in line with data showing that *ino2**p-mediated ER expansion does not activate the UPR (Papagiannidis et al., 2021).

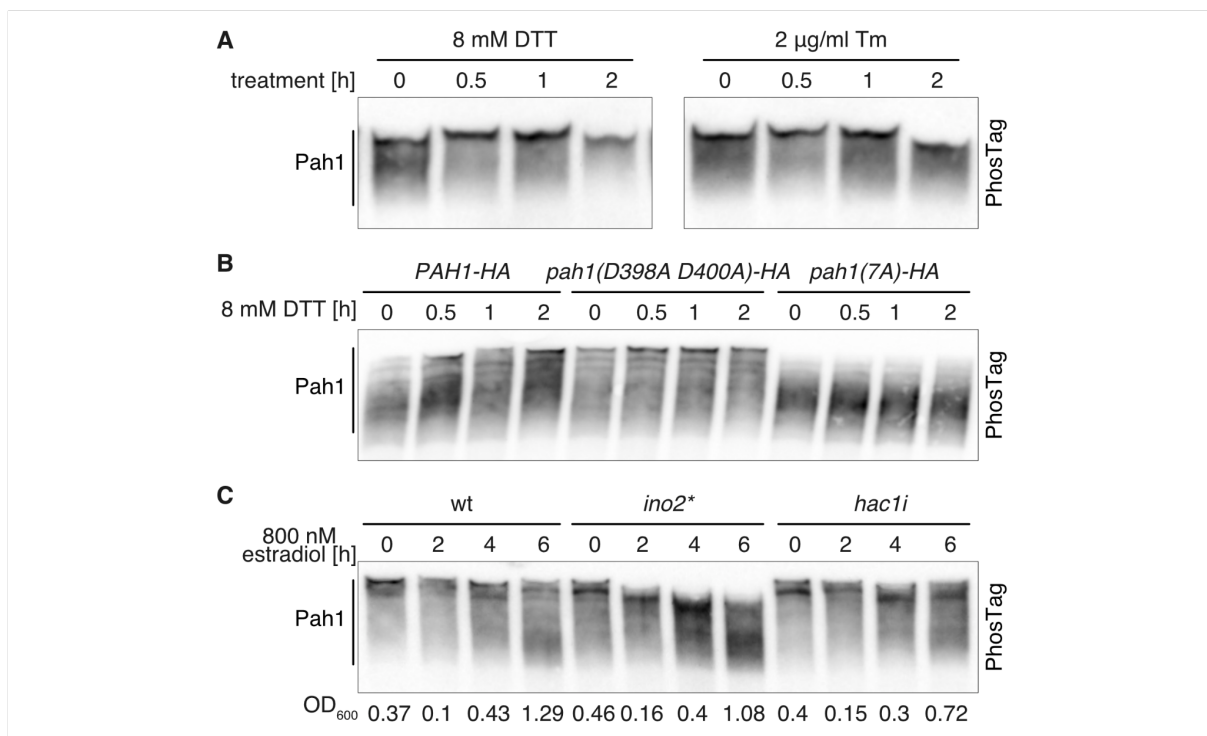


Figure 19. Preliminary data on role of the regulation of Pah1p during ER stress

A. Western blots of Pah1p-HA of whole cell lysates of exponentially growing cells (SSY2592) that were either untreated or treated with 8 mM DTT (left) or 1 µg/ml tunicamycin (Tm; right) for the indicated amounts of time to induce ER stress. Samples were analysed with PhosTag-PAGE. **B.** Western blot of Pah1p-HA of whole cell lysates of cells transformed with a plasmid to express wild-type *PAH1-HA* (pSS1045), the catalytically inactive *pah1(D398A D400A)-HA* (pSS1046) or *pah1(7A)-HA* (pSS1047). Exponentially growing cells were either left untreated or were treated with 8 mM DTT for the indicated amounts of time to induce ER stress. Samples were analysed with PhosTag-PAGE. **C.** Western blots of Pah1p-HA of whole cell lysates of wild-type (wt; SSY2804) cells, cells harbouring the estradiol-inducible *ino2** system (SSY 2840) and cells harbouring an estradiol-inducible *hac1ⁱ*. Exponentially growing cells were either untreated or 800 nM estradiol for the indicated amounts of time. OD_{600} are also displayed. Samples were analysed with PhosTag-PAGE.

3.6.2 ER expansion upon exit from stationary phase

Pah1p activity is increased in stationary phase, where cells produce lipid droplets. I therefore wondered whether, as an extension, the morphology of the ER changes. Indeed, the ER of wild-type cells in stationary phase was almost exclusively tubular, a phenotype which was also observed in *ice2Δ* cells (Figure 20A). Given the fact that exponentially growing wild-type cells have a proportion of ER sheets (see for example Figure 6A), this means that when cells resume growth there are mechanisms that ensure some ER expansion. Exploring the expansion of the ER during exit of cells from stationary phase with analysis of fluorescence microscopy images using the tool developed by Peter Bircham was not possible due to technical limitations. Specifically, during the first 4 hours after exit from stationary phase there was a high degree of population heterogeneity in terms of ER expansion state, making the semi-automated tool not suitable for the analysis of these images (data not shown).

Testing the phosphorylation status and levels of Pah1p in these conditions was only partially informative. As observed before (Figure 13A), Pah1p-HA was not detectable in cells grown to stationary phase, a phenotype which persisted at least until 1 h after cells were diluted in fresh medium (Figure 20 B). Three hours after dilution to fresh medium Pah1p-HA was detectable and Pah1p-HA levels kept increasing for another 4.5 h before starting to decrease again. Pah1p-HA appeared mostly phosphorylated during this time frame. There appeared to be a slight increase in the phosphorylation status of Pah1p-HA between 4 h and 6 h after dilution, but that might reflect the higher signal intensity of the increased Pah1p-HA levels. Curiously, Pah1p-HA in *ice2Δ* cells phenocopied the wild-type up until 4 h after dilution, appearing mostly phosphorylated. Only at later time points did it appear to be dephosphorylated. Measuring of the UPR activity by means of the transcriptional reporter indicated that the ER expansion upon exit from stationary phase is not mediated by the UPR (Figure 20C). This notion is further supported by the observation that cells that cannot activate the UPR still have a wild-type looking ER in exponential phase (Figure 9A).

These data suggest that *ICE2* could promote ER expansion during exit from stationary phase. If and to which extent this is by regulation of Pah1p remains to be determined.

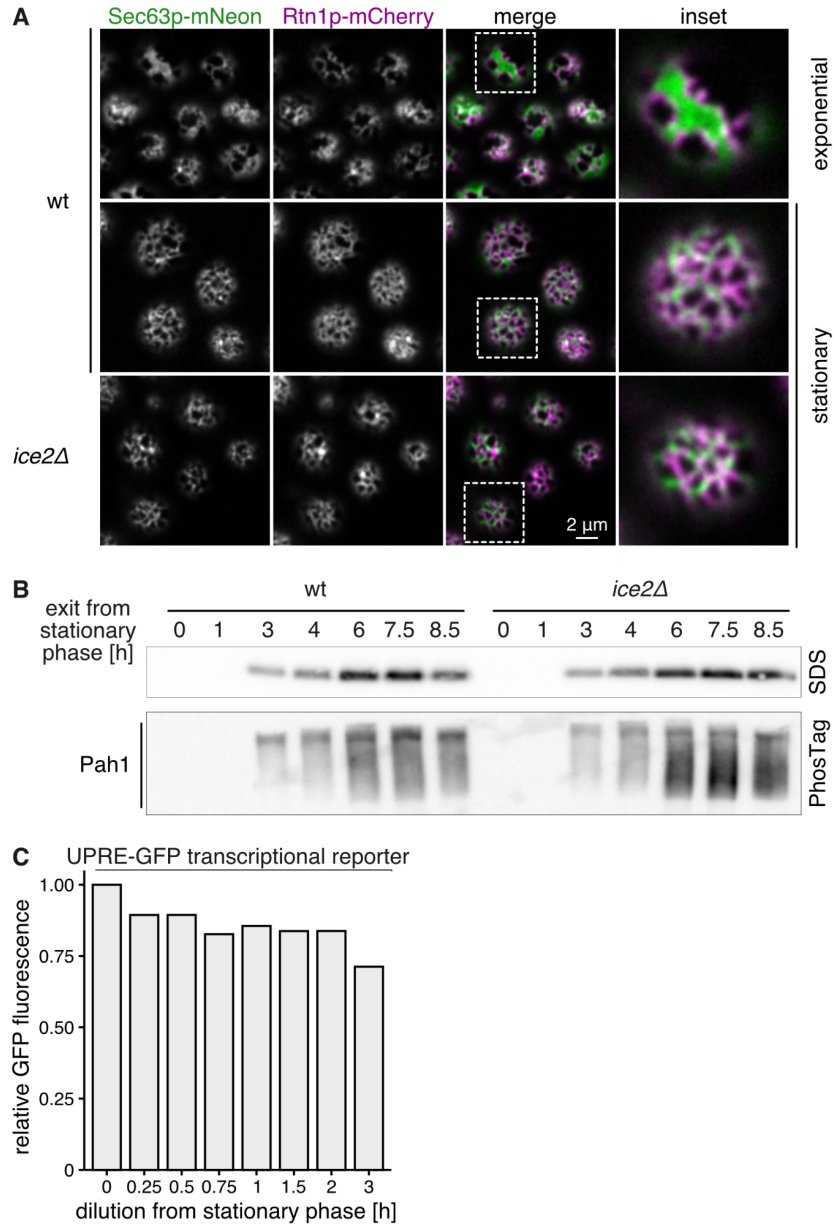


Figure 20. Preliminary data on role of the regulation of Pah1p during exit from stationary phase

A. Sec63p-mNeon and Rtn1p-mCherry fluorescence microscopy images of cortical sections of wild-type (wt; SSY1404) and *ice2Δ* (SSY2356) cells that were grown to exponential or stationary phase as indicated. The boxed areas are shown at higher magnification in the lower panel. Experiment designed and initially performed by me and repeated by Oliver Pajonk under my supervision. **B.** Western blots of Pah1p-HA of whole cell lysates of wild-type (SSY2592) and *ice2Δ* (SSY2593) cells. Samples were taken at the indicated amounts of time after dilution of cells grown to stationary phase in fresh medium and were analysed by PhosTag-PAGE. **C.** Relative GFP fluorescence as measured by flow cytometry of cells expressing the UPRE-GFP transcriptional UPR reporter (SSY2487). Cells were grown to stationary phase before being diluted in fresh medium. Fluorescence was measured at the indicated time points ($n=1$).

3.7 ER expansion by regulation of ER-tubulating proteins

Upon DTT treatment, Rtn1-only puncta accumulated over time in the wild-type and appeared in even greater numbers in *ICE2* deletion mutants (Figure 8C). As this was an unexpected phenotype, I wanted to further investigate whether this phenotype is *ICE2*-specific. To this end, I examined the formation of Rtn1-only puncta in cells lacking *DGK1*, which is another underexpansion hit from the ER biogenesis screen (Papagiannidis et al., 2021). *DGK1* mutants displayed the Rtn1-only puncta phenotype to the same extent as *ICE2* mutants (Figure 21A). Although Rtn1-only puncta formed in lower numbers in wild-type cells (Figure 8C), this observation suggests that this is a general phenotype and not specific to *ICE2* mutants.

Next, I designed experiments to test whether these puncta were specific to the fluorescent protein or the ER stressor used. Rtn1-only puncta also formed after tunicamycin treatment (Figure 21B) and also when mNeon was used to tag Rtn1p instead of mCherry (Figures 21C and 21D), suggesting that this phenotype is not a DTT or Rtn1p-mCherry specific artefact. Taken together, these results suggest that the observed phenotype is unlikely to be an artificial one and might thus have a physiological explanation.

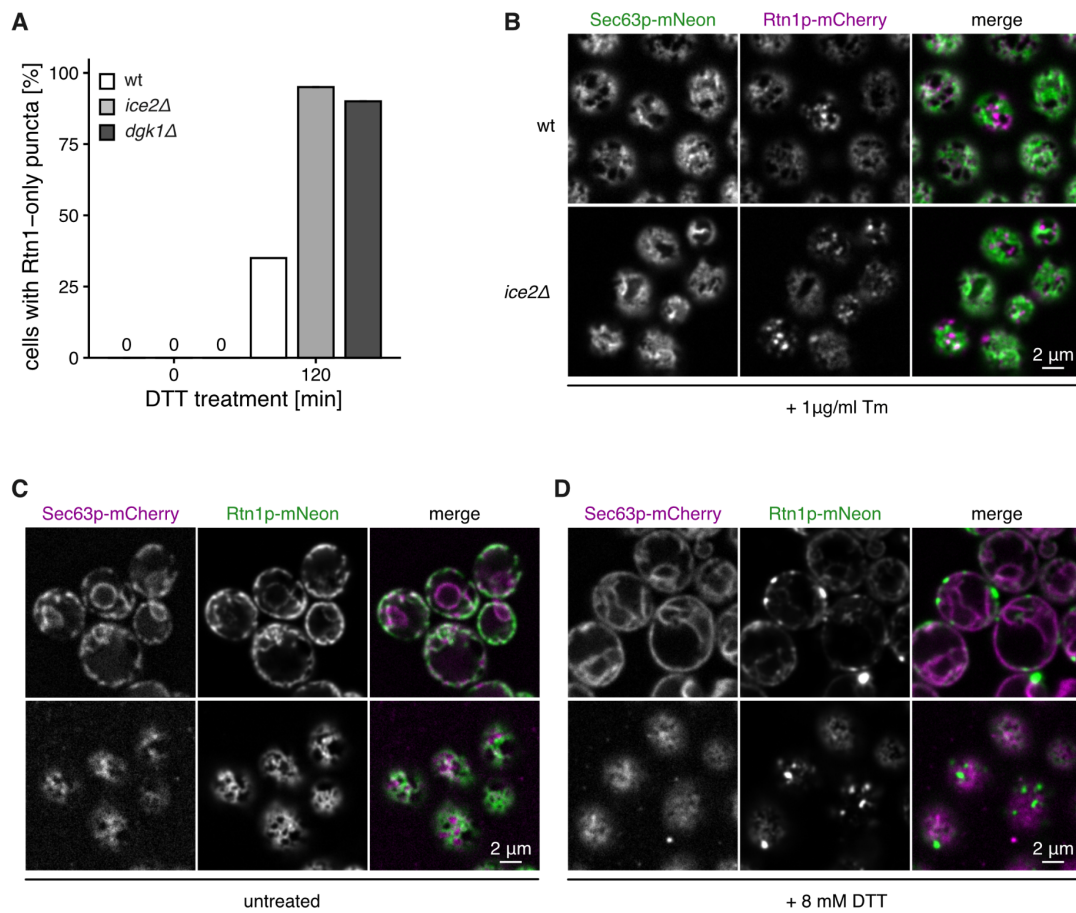


Figure 21. Rtn1-only puncta are not specific to the ER stressor or fluorescent protein used

A. Quantification of the percentage of wild-type (wt; SSY1404) and *ice2Δ* (SSY2356) and *dgk1Δ* (SSY480) cells displaying the Rtn1-only puncta phenotype. Exponentially growing cells were either left untreated or were treated with 8 mM DTT for the indicated amount of time to induce ER stress. $n=1$. **B.** Sec63p-mNeon and Rtn1p-mCherry fluorescence microscopy images of cortical sections of wild-type (SSY1404) and *ice2Δ* (SSY2356) cells. Exponentially growing cells were either left untreated or were treated with 1 μg/ml tunicamycin (Tm) for 2 h to induce ER stress. **(C,D).** Sec63p-mCherry and Rtn1p-mNeon fluorescence microscopy images of mid- and cortical sections of exponentially growing cells (SSY2711) that were either untreated (C) or treated with 8 mM DTT for 2 h to induce ER stress (D).

I next asked whether Yop1p, the reticulon-like protein in yeast, also forms puncta in conditions of ER stress. Indeed, Yop1p formed Sec63p-negative puncta after prolonged DTT treatment (Figure 22A), and these puncta colocalized with the Rtn1p puncta (Figures 22B and 22C). These results suggest that the reticulon-only puncta might reflect a general mechanism regulating the activity of ER tubulating proteins.

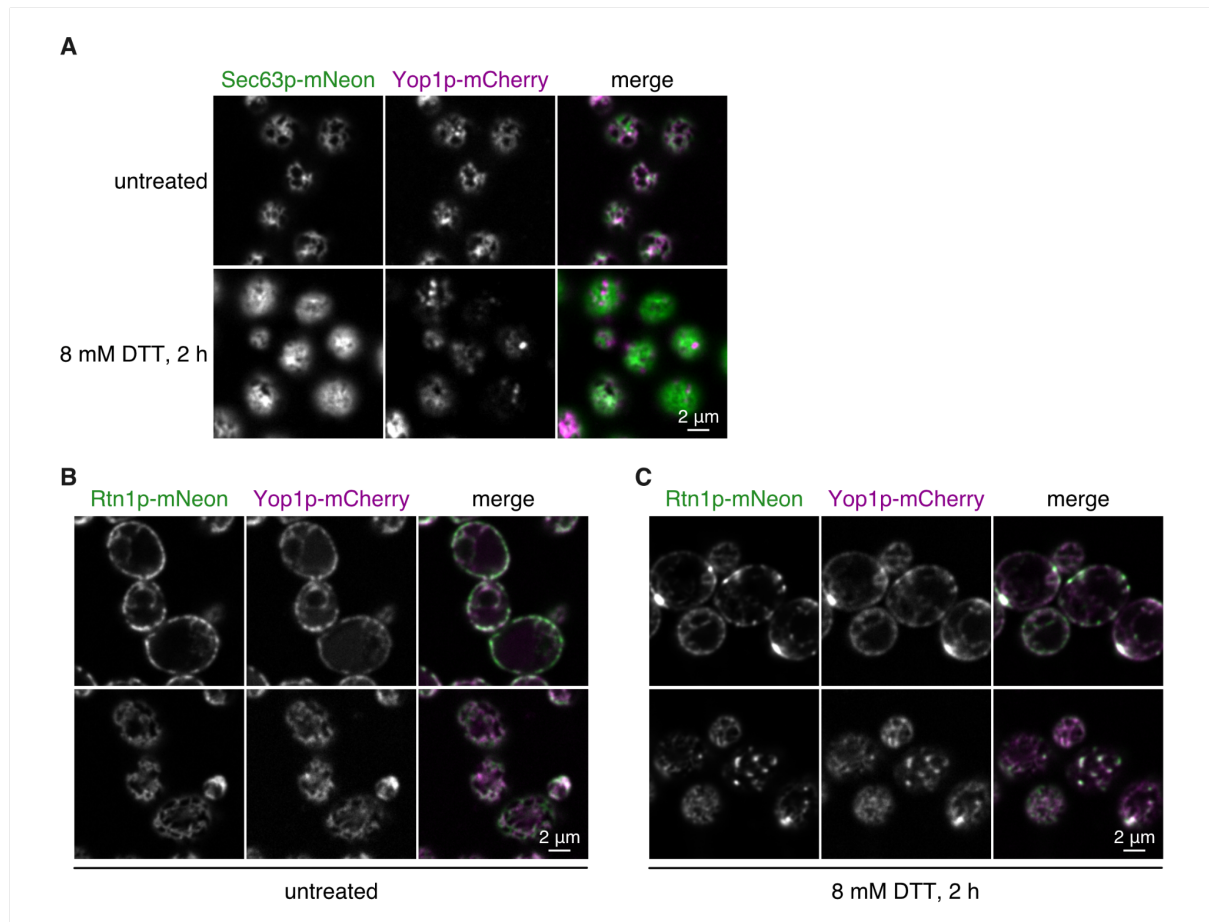


Figure 22. Yop1p also forms Sec63-negative puncta after prolonged ER stress

A. Sec63p-mNeon and Yop1p-mCherry fluorescence microscopy images of cortical sections of exponentially grown cells (SSY2648) that were either left untreated or were treated with 8 mM DTT 2 h to induce ER stress. **(B,C).** Rtn1p-mNeon and Yop1p-mCherry fluorescence microscopy images of mid and cortical sections of exponentially grown cells (SSY2713) that were either untreated (B), or treated with 8 mM DTT 2 h to induce ER stress (C).

The observation that reticulon-only puncta do not colocalize with the general ER marker Sec63p raised the possibility that these puncta are no longer ER membrane bound but cytosolic. To test for this possibility, two complementary approaches were used. First, I tested the membrane association of Rtn1p by subcellular fractionation. In untreated cells, most of Rtn1p was observed in the membrane fraction (Figure 23A), as expected. After treatment with DTT around 50% of Rtn1p was observed in the supernatant, suggesting that the reticulon-only puncta are not associated with the ER membrane. This phenotype was more pronounced in *ice2Δ* cells, in line with the fluorescence microscopy data. The second approach to determine whether Rtn1p puncta are associated with the ER was correlative light and electron microscopy (CLEM), which provides the necessary resolution to visualise membrane compartments while enabling the identification of areas of interest by fluorescence microscopy. This experiment was conceptualised, designed and performed together with Ayelen Valko with the help of Charlotta Funaya from the electron microscopy core facility in Heidelberg. For this experiment *ice2Δ* cells expressing Rtn1p-mNeon and the transmembrane ER marker mCherry-Ubc6p were used. *ICE2* deletion mutants were selected due to the higher occurrence of the Rtn1-only puncta phenotype. The selection of fluorescent proteins was based on the fact that they were previously successfully used for CLEM by Jasmin Schäfer (data not shown). Resulting images showed that Rtn1p-mNeon puncta which were mCherry-Ubc6p negative did not colocalize with ER membrane structures (Figure 23B, arrows). On the other hand, Rtn1p-mNeon puncta which colocalized with mCherry-Ubc6p also colocalized with ER membrane structures (Figure 23B, arrowhead). This result further supports the notion that the reticulon-only puncta are not associated with the ER membrane.

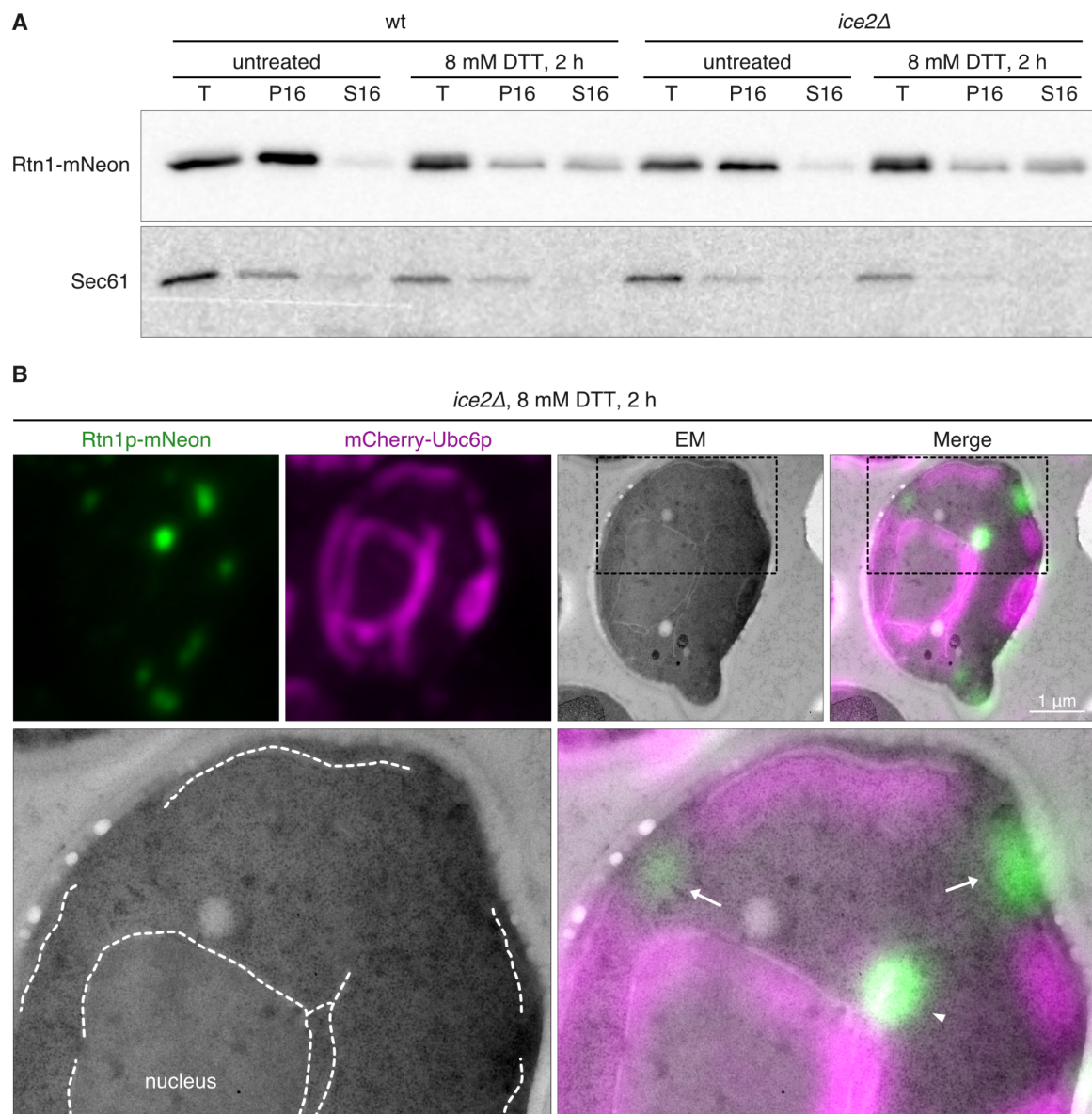


Figure 23. Rtn1-only puncta are not membrane bound

A. Western blots of Rtn1p-mNeon and Sec61p subcellular fractions of wild-type (SSY2713) and *ice2Δ* (SSY2714) cells. Exponentially growing cells were either left untreated or were treated with 8 mM DTT for 2 h to induce ER stress. T: total cell lysate; P16: 16.000 x g pellet; S16: 16,000 xg supernatant. **B.** Correlative light and electron microscopy images of 90 nm thin sections of an *ice2Δ* (SSY3198) cell expressing Rtn1p-mNeon and mCherry-Ubc6 that was treated with 8 mM DTT for 2 h to induce ER stress. The boxed areas are shown at higher magnification in the lower panel. The ER membrane is traced in white. Rtn1-only puncta (arrows) do not colocalize with the ER membrane whereas Rtn1p-and-Ubc6p-positive puncta (arrowhead) do. Experiment was designed and performed in collaboration with Ayelen Valko. High-pressure freezing, freeze substitution, sectioning and post-staining was performed by Charlotta Funaya.

Next, I asked whether the observed puncta are formed by protein molecules that had initially been inserted in the ER membrane and redistributed upon ER stress. To address this an imaging pulse-chase experiment was conducted. This experiment was conceptualised and designed together with Ayelen Valko and performed by Artur Astapenka under my supervision. Specifically, Rtn1p-mNeon was placed under the control of the inducible *GAL1* promoter in strains where Sec63p was tagged with mCherry. After induction of Rtn1p-mNeon expression for 45 min by switching the carbon source in the growth medium from glucose to galactose, cells were let to recover for 2 h in the presence of glucose, which inhibits the *GAL1* promoter (Johnston, 1987), and were then treated with 8 mM DTT for 2 h. If only newly synthesised molecules localised at the puncta, then no Rtn1-only puncta would be observed. Induced Rtn1p-mNeon showed no punctate localisation in untreated cells (Figure 24A). After treatment with DTT, however, Rtn1p-mNeon formed puncta which were negative Sec63p-mCherry (Figure 24B). This result supports the hypothesis that the Rtn1p molecules forming these puncta were previously inserted in the ER membrane.

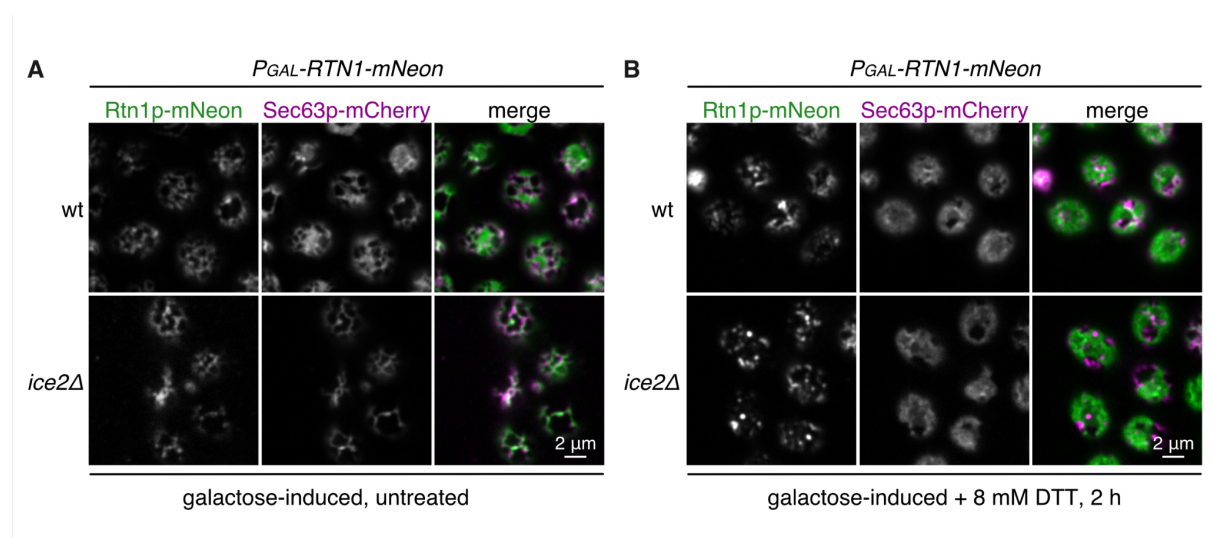


Figure 24. Cytosolic Rtn1-only puncta are formed by molecules that were initially membrane inserted

(A,B). Rtn1p-mNeon and Sec63p-mCherry fluorescence microscopy images of cortical sections of wild-type (wt; SSY3399) and *ice2Δ* (SSY3400) cells. Cells were grown to exponential phase in SC raffinose and Rtn1p-mNeon expression was induced with galactose for 45 min. Cells were then recovered in SCD for 2 h and were either untreated (A) or treated with 8 mM DTT for 2 h (B) before being imaged.

4. Discussion and outlook

In this work I uncovered the molecular role of Ice2p in the context of ER membrane biogenesis. Building up on the ER biogenesis screen performed by Peter Bircham I could show that Ice2p is required for and promotes ER expansion. I placed *ICE2* in the context of phospholipid synthesis regulation in yeast and specifically showed that it acts on the same pathway and upstream of *SPO7*, *NEM1* and *PAH1*. I then showed that Ice2p promotes the phosphorylation of Pah1p, by interacting with and inhibiting the Spo7p-Nem1p complex. I subsequently showed that the regulation of the Spo7p-Nem1p complex may be linked to its localisation and that it has a functional output. Specifically, I showed that inhibition of the Spo7p-Nem1p complex by Ice2p promotes phospholipid synthesis at the expense of storage lipid synthesis and also promotes ER expansion. Additionally, I showed that Ice2p acts in parallel to the transcriptional regulator Opi1p and coordinates with the UPR to maintain cell homeostasis. Moreover, I obtained preliminary data regarding the physiological conditions in which cells use this pathway to promote ER membrane biogenesis. Finally, while characterising the function of Ice2p, I discovered a new process involving the differential localisation of ER-tubulating proteins in the context of ER sheet formation and ER stress.

4.1 An updated model connecting lipid synthesis to ER membrane biogenesis

The results presented here uncover an additional layer of regulation within the network controlling ER membrane biogenesis in yeast and highlight the interplay between its two main branches, the regulation of phospholipid precursor abundance and the transcriptional regulation of phospholipid synthesis enzymes (Figure 25). The central molecule for this regulatory network remains PA, which serves as a precursor for both membrane phospholipids and the storage lipid TAG, and is also involved in the transcriptional regulation of phospholipid synthesis enzymes. The levels of PA, as well as its downstream use, are determined by Pah1p and Dgk1p (Klug and Daum, 2014). Ice2p promotes ER membrane biogenesis by inhibiting the Spo7p-Nem1p complex and thus opposing the activation of Pah1p (Figure 25A). When Pah1p is inactive, PA is not dephosphorylated to DAG and is thus channelled towards the production of membrane phospholipids. In addition to that, elevated

PA levels help retain Opi1p at the ER membrane, which results in the derepression of the Ino2p-Ino4p complex and consequently leads to the transcriptional activation of phospholipid synthesis enzymes (Loewen et al., 2004; Hofbauer et al., 2018). On the other hand, in the absence of Ice2p, active Pah1p promotes the synthesis of the storage lipid TAG (Figure 25B). It does so in three different ways. First, Pah1p dephosphorylates PA to DAG, which is the substrate for the TAG synthesis enzymes Lro1p and Dga1p. Second, by limiting the PA availability, Pah1p contributes to the translocation of Opi1p to the nucleus, which leads to repression of the Ino2p-Ino4p complex. Lastly, active Pah1p can translocate to the nucleus and associate with UAS_{INO} containing promoters further repressing the expression of phospholipid synthesis enzymes (Santos-Rosa et al., 2005).

Several observations highlight why it is important to coordinate the availability of phospholipid precursors with the production of lipid synthesis enzymes. As shown in Figure 6, deletion of *ICE2* impairs *ino2**p-driven ER expansion despite the transcriptional upregulation of UAS_{INO} containing genes, as exemplified by *INO1*. This suggests that in the absence of phospholipid precursors, upregulation of lipid synthesis enzymes cannot achieve ER membrane expansion. It also shows that active Pah1p is not sufficient to repress the transcriptional activation of *INO1* in the presence of an active *ino2**p-Ino4p complex. The opposite effect also holds true: increased availability of phospholipid precursors or lipid synthesis enzymes can alone promote ER expansion and in combination these effects are magnified (Figure 17).

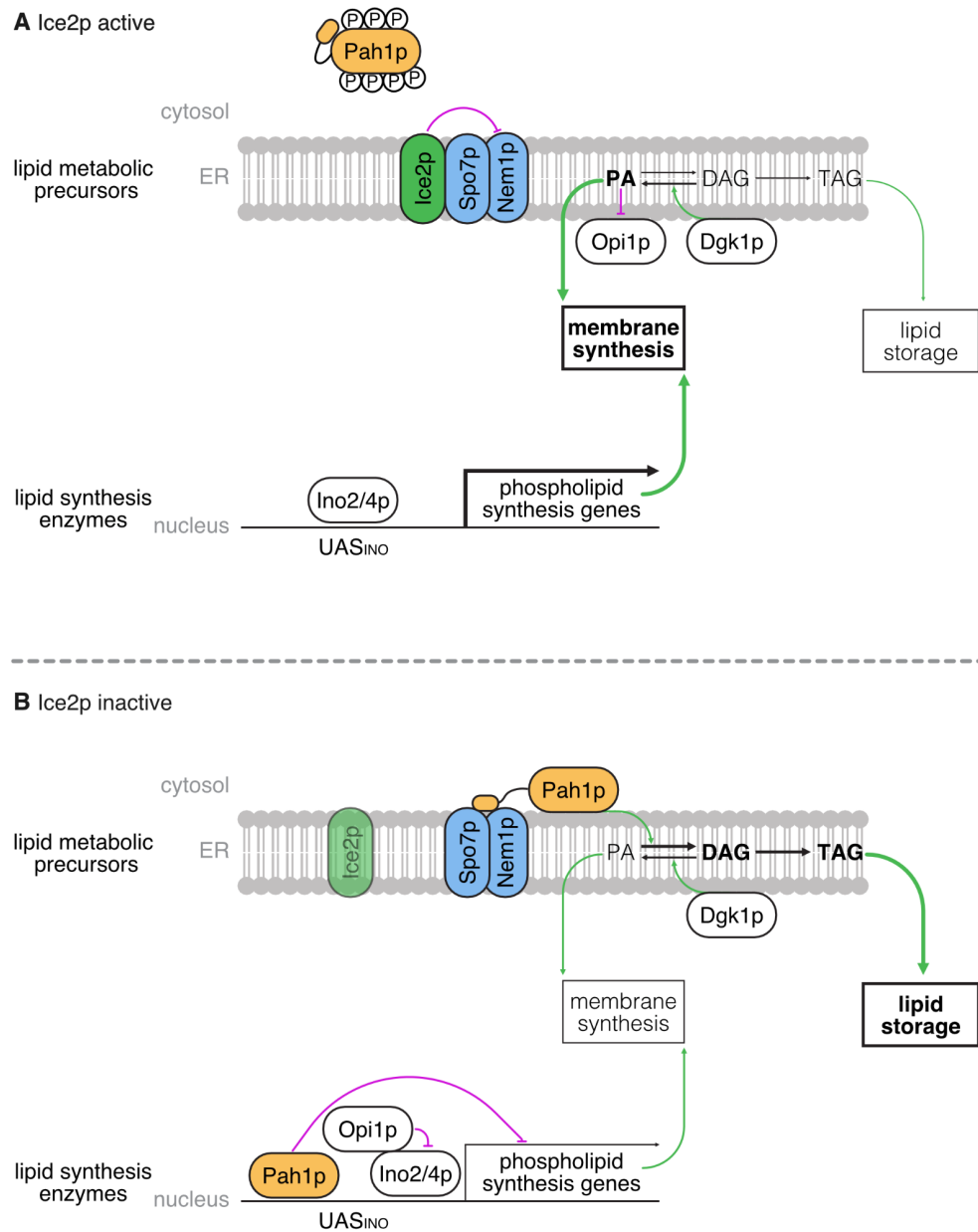


Figure 25. Model for pathways controlling ER membrane biogenesis

Schematic depicting a model for the control of ER membrane biogenesis in yeast, highlighting the interplay between the production of lipid precursors with the production of lipid synthesis enzymes. Modified from (Papagiannidis et al., 2021).

4.2 Revisiting existing literature on *ICE2*

4.2.1 Reported genetic interactions

The above model explains some of the reported genetic interactions of *ICE2*, extending beyond what has previously been published. For example, the negative genetic interaction between *ICE2* and *INO2* (Costanzo et al., 2010, 2016) and *INO4* (Costanzo et al., 2010; Hoppins et al., 2011; Costanzo et al., 2016) could be explained by the enhanced suppression of the phospholipid synthesis pathways, as could the one between *ICE2* and *SCS2* (Schuldiner et al., 2005; Loewen et al., 2007; Costanzo et al., 2010; Hoppins et al., 2011; Surma et al., 2013; Tavassoli et al., 2013; Costanzo et al., 2016). The negative genetic interactions of *ICE2* with the storage lipid synthetases *DGA1* (Schuldiner et al., 2005; Garbarino et al., 2009; Markgraf et al., 2014), *ARE1* (Surma et al., 2013) and *ARE2* (Costanzo et al., 2010) could be explained by the enhanced accumulation of DAG. The same holds true for the negative genetic interaction between *ICE2* and *DGK1* (Schuldiner et al., 2005; Loewen et al., 2007; Jonikas et al., 2009; Costanzo et al., 2010; Hoppins et al., 2011; Surma et al., 2013; Tavassoli et al., 2013; Costanzo et al., 2016). Similarly, the negative genetic interactions of *ICE2* genes involved in the synthesis of fatty acids like *FAT1* and *FAS2* (Costanzo et al., 2016), and PA, like *SCT1* (Costanzo et al., 2010, 2016), could be explained by the enhanced depletion of PA. Finally, the positive genetic interactions *ICE2* displays with the reticulons (Figure 10; Schuldiner et al., 2005; Loewen et al., 2007; Costanzo et al., 2010; Surma et al., 2013) could be explained by these proteins acting independently in the same process, ER expansion/ER sheet formation, but with opposing effects.

4.2.2 *ICE2* and protein quality control

The results presented here show that *ICE2* cooperates with the UPR to maintain homeostasis, which also provides an explanation for the observed negative genetic interaction between *ICE2* and *HAC1* (Figure 18; Schuldiner et al., 2005; Costanzo et al., 2010; Bircham et al., 2011; Surma et al., 2013; Costanzo et al., 2016) as well as *IRE1* (Schuldiner et al., 2005; Costanzo et al., 2010; Surma et al., 2013; Costanzo et al., 2016). *ICE2* has been

previously linked to ER protein quality control. Specifically, deletion of *ICE2* leads to reduced Ire1p clustering (Cohen et al., 2017) and reduced ERAD activity, as evident from to stabilisation of ERAD substrate CPY* (Schuldiner et al., 2005). *ICE2* deletion represses the Ino2p-Ino4p target *INO1* at steady state (Figure 6B), which could be an effect of increased Pah1p activity, both enzymatic and transcriptional. Several proteins involved in ER protein folding and quality control have the capacity to be transcriptionally regulated by Ino2p-Ino4p: Emc5p and Emc6p (Venters et al., 2011), which are both involved in the insertion of ER transmembrane domains into the ER (Guna et al., 2018), Wbp1p (Venters et al., 2011), which is involved in protein glycosylation (te Heesen et al., 1992), Ubx6p (Maclsaac et al., 2006), which has been described to be an interactor of Cdc48p and Doa10p (Decottignies et al., 2004), and Rpn3p (Venters et al., 2011), a proteasome subunit. Downregulation of these proteins, together with the ER underexpansion caused by *ICE2* deletion (Figure 7A), is expected to reduce the folding capacity of the ER and increase the load of the protein quality control pathways.

4.2.3 *ICE2* and its link to lipid droplets, ER inheritance and zinc homeostasis

Although a role of Ice2p in the channelling of DAG from lipid droplets to the ER during exit from stationary phase cannot not be excluded (Markgraf et al., 2014), Ice2p could promote lipid droplet consumption indirectly by inhibiting Pah1p, i.e TAG synthesis. The phenotypes that have been used to link *ICE2* to maintenance of cortical ER (Estrada de Martin et al., 2005) and ER-plasma membrane contact sites (Loewen et al., 2007; Quon et al., 2018) could also be a consequence of the ER underexpansion caused by *ICE2* deletion. Finally, the reported growth defect of *ICE2* mutants in the absence of zinc (Ruotolo et al., 2008; North et al., 2012) could be a consequence of overexpressed *PAH1* (Soto-Cardalda et al., 2012) in combination with Ino2p-Ino4p repression (Iwanyshyn et al., 2004).

4.3 The Pah1p/Lipin switch and ER expansion

In this work I showed that hyperactive Pah1p, as caused either by deletion of *ICE2* or by mutating seven of its key residues that are subject to phosphoregulation to alanine (*pah1(7A)p*), renders cells unable to properly expand their ER, both after activation of Ino2p-Ino4p and in conditions of ER stress (Figure 6, Figure 7 and Figure 16). On the other hand, inactive Pah1p, as presumably caused by *ICE2* overexpression, is sufficient to drive ER expansion independently of and without activating the UPR (Figure 9) and can lead to ER hyperexpansion when combined with activation of Ino2p-Ino4p (Figure 17). Therefore, by regulating Pah1p, cells have the capacity to channel their lipids either towards lipid storage or membrane biogenesis. Since Pah1p is central in defining the fate of lipids during lipid metabolism, this regulation is referred to as “Lipin switch”, named after the mammalian Pah1p homologue Lipin. While these observations provide insights into the molecular role of Ice2p as well as into the interconnection of lipid synthesis pathways with ER expansion, a main question remains unanswered. Do cells use the Pah1p/Lipin switch in order to achieve ER expansion?

4.3.1 The Pah1p/Lipin switch and ER stress

I addressed this question by monitoring the phosphorylation status of Pah1p under different conditions that promote ER expansion. This was technically difficult, since one would expect an increase of Pah1p phosphorylation in such instances, and the dynamic range of the PhosTag gels was limiting. Nevertheless, after treatment with the ER stressors DTT and tunicamycin I observed a subtle but reproducible increase in the phosphorylation status of Pah1p, followed by Pah1p dephosphorylation. Interestingly, I also observed Pah1p dephosphorylation after expression of *ino2^{*}p*, but no Pah1p phosphorylation, although such an event could have been missed given the time frame of the experiment. The initial phosphorylation of Pah1p is in line with the Pah1p/Lipin switch being used to promote ER expansion, and should be further examined. Since other studies have achieved higher resolution of Pah1p phospho-forms using the PhosTag system (Dubots et al., 2014), optimising this assay should be a starting point. The dephosphorylation of Pah1p after both stress-induced and lipid synthesis-induced ER expansion brings up an interesting point.

There is the possibility that after an initial pulse of ER expansion, cells homeostatically respond to it and try to counteract it to avoid uncontrolled ER expansion. It would not be the first time that cells counteract the overactivation of stress response pathways, as such is the case for the UPR, in both yeast and mammals (Rutkowski and Hegde, 2010; Walter and Ron, 2011; Chawla et al., 2011). Although an elegant way to avoid an overactivation of a stress response mechanism, this potential Pah1p activation will make it difficult to differentiate between the use of the Pah1p/Lipin switch to achieve ER expansion and the use of it to counteract it. It could, on the other hand, provide an explanation for the confusing observation that TAG levels and lipid droplet number increase during ER stress, at least after treatment with tunicamycin (Fei et al., 2009; Yamamoto et al., 2010). The fact that UPR induction by *hac1ⁱ* expression phenocopied the wild-type condition suggests that Pah1p phosphoregulation is unlikely to be mediated by the UPR, although this experiment should be repeated to match the time resolution of ER stress-mediated UPR activation. Finally, the observation that Δ LD cells were able to expand their ER both after induced activation of phospholipid synthesis and upon ER stress similar to wild-type cells suggests that cells do not rely on lipid mobilisation from lipid droplets to achieve ER expansion, but rather on de novo lipid synthesis. This is consistent with data showing that Δ LD cells show no growth defect on tunicamycin plates (Fei et al., 2009) and further highlights the importance of the Pah1p/Lipin switch for ER expansion and cell homeostasis in conditions of ER stress.

4.3.2 The Pah1p/Lipin switch and exit from stationary phase

In contrast to exponentially growing cells, cells grown to stationary phase displayed an underexpanded ER which was almost exclusively tubular. The transition of cells between stationary and exponential phase is therefore one condition in which physiological ER expansion occurs. Although preliminary data presented here are to a part inconclusive, this transition is promising in terms of the inverse regulation of lipid droplet synthesis and ER expansion by the Pah1p/Lipin switch. *ICE2* (Markgraf et al., 2014) and *DGK1* (Fakas et al., 2011) deletion mutants, both of which display unopposed Pah1p activity, have been reported to be relevant for exit of cells from stationary phase, highlighting the importance of Pah1p activity regulation during this time frame. The unexpected result that up to 3 h after dilution from stationary phase Pah1p from *ice2 Δ* cells appears to be phosphorylated should be further

investigated and importance of Ice2p and the Spo7p-Nem1p complex as well as different Pah1p kinases in these conditions should be assessed. Moreover, to dissect the contributions of lipid droplet consumption and de novo phospholipid synthesis, cerulenin, which inhibits fatty acid synthesis, and the ΔLD strain could be used. Cells treated with cerulenin will rely on lipid droplet consumption (Markgraf et al., 2014) whereas the ΔLD cells will rely on de novo lipid synthesis. Like in the case of Pah1p regulation during ER stress, the UPR does not appear to regulate exit of cells from stationary phase, at least not on the transcriptional level (Figure 20).

4.4 How could Ice2p be regulated?

How could the activity of Ice2p be regulated? Neither the *ICE2* mRNA levels (Pincus et al., 2014) nor the Ice2p protein levels (data not shown) increase in conditions of ER stress. The localisation of Ice2p can change, for example upon cell entry to stationary phase where the number of Ice2p foci increases (Markgraf et al., 2014), but how this is regulated is not clear. A part of Ice2p has been proposed to interact with lipids in lipid droplets (Markgraf et al., 2014) and a recent study proposed that Ice2p contains an intramembrane lipid binding site (Alli-Balogun and Levine, 2021). An attractive model, though speculative, is that Ice2p can sense changes in the lipid composition of the ER membrane. Another potential regulatory step could be the interaction between Ice2p and the Spo7p-Nem1p complex (Figure 10B,C,D), which could be regulated by posttranslational modifications. A recent study predicted the Ice2p-Spo7p interaction using AlphaFold (Humphreys et al., 2021), which not only supports the results presented here but also provides a potential interaction interface which could be studied in molecular terms. The identification of mechanisms that control Ice2p is interconnected with the physiological conditions where cells use the regulation of Pah1p by Ice2p.

4.5 Conservation

Pah1p, Spo7p and Nem1p are all conserved from yeast to humans (Han et al., 2012). Lipins, the mammalian Pah1p homologs, promote TAG synthesis and are subject to phosphoregulation by the NEP1R1-CTDNEP1 complex, the mammalian Spo7p-Nem1p homologs. Moreover, depletion of CTDNEP1 was recently shown to cause peripheral ER expansion in mammalian cells (Merta et al., 2021). Extending the model derived from yeast, where regulation of Pah1p activity dictates whether lipids are used to make membranes or stored in lipid droplets is, however, not straightforward. The reason for that is the fact that mammalian cells do not use the CDP-DAG pathway, but the Kennedy pathway to produce membrane phospholipids. In the Kennedy pathway, DAG serves as a precursor for both TAG and membrane phospholipids. Activation of Lipin, thus, would at the same time promote storage and membrane phospholipid synthesis and inactivation of Lipin would have the exact opposite effect. Under these circumstances, regulation of Lipin activity could not determine the way cells utilise their lipids. A way by which this could still be possible is based on the observation that, at least in *Arabidopsis thaliana* (Craddock et al., 2015) and mice (Zhang et al., 2019), PA can act as an allosteric activator of CCT α , an enzyme of the Kennedy pathway catalysing the rate limiting reaction of PC synthesis. If that is the case, then inhibition of Lipin would lead to an increase of PA levels, and preferential channelling of DAG towards membrane phospholipid synthesis (Jacquemyn et al., 2017).

In contrast to *SPO7*, *NEM1*, and *PAH1*, *ICE2* does not have a mammalian sequence homologue. A recent study identified the SERINC family of proteins to be structurally homologous to Ice2p (Alli-Balogun and Levine, 2021). SERINC proteins were first proposed to be involved in lipid metabolism (Inuzuka et al., 2005) but are currently mostly studied in virology, as factors restricting infection by HIV (Rosa et al., 2015; Gonzalez-Enriquez et al., 2017). Whether SERINC proteins can control the phosphorylation status of Lipin via inhibition of NEP1R1-CTDNEP1 or some other mammalian protein has assumed this role remains unclear.

4.6 ER morphogenesis factors and ER sheet formation

As mentioned in the introduction, ER sheets in yeast are thought to form when the tubulating capacity of the cells, as exhibited by the reticulons, is exceeded by the amount of ER membrane (Schuck et al., 2009). The fact that deletion of *ICE2* in the *Δrtns* mutant leads to ER tubule formation (Figure 10) suggests that there are more tubulating factors in yeast. This could include proteins that contain the reticulon homology domain, such as Atg40p (Mochida et al., 2015) or members of the Pex30 protein family (Ferreira and Carvalho, 2021).

In this work I presented data suggesting that, after prolonged ER stress, reticulon and reticulon-like proteins are extracted from the ER membrane. This phenotype has not been observed before and raises an attractive model. In conditions when cells cannot achieve sufficient ER sheet formation through lipid synthesis alone, they may actively remove reticulons from the ER membrane to do so. Rtn1p, Rtn2p and Yop1p have all been reported in high throughput studies to be subject to phosphorylation (Albuquerque et al., 2008; Holt et al., 2009; Weinert et al., 2013; Swaney et al., 2013; Rødkær et al., 2014; Chen et al., 2018; MacGilvray et al., 2020; Lanz et al., 2021). Whether the removal of reticulon proteins from the ER membrane is controlled by phosphorylation or another posttranslational modification is still to be determined. Considering that reticulons are the major ER shaping proteins across different species, this raises many questions. Is this process physiologically relevant and if so, is it conserved? How are these proteins extracted from the ER? What happens to these structures after resolution of stress?

4.7 Control of ER size and shape – future directions

In this work, different pathways contributing to ER homeostasis have been discussed, namely; the UPR, the pathways controlling lipid precursor availability and expression of lipid synthesis enzymes, and the pathways leading to ER tubule formation. The extent to which these pathways coordinate with each other in regulating of ER size and shape is to a large extent unexplored.

Various aspects of lipid synthesis pathways are regulated by the UPR in yeast. For example, *DGK1* is a UPR target gene (Pincus et al., 2014) and activation of the UPR promotes Opi1p dissociation from Ino2p (Brickner and Walter, 2004) but how this is achieved remains unclear.

Although *ICE2* is not a UPR target gene, it cannot be excluded that Ice2p and the Pah1p/Lipin switch is post-transcriptionally regulated by mechanisms that involve the UPR. Thus, studying the effects of the UPR that extend beyond transcriptional regulation might provide insights in different aspects of ER biology.

Furthermore, both inactivation of the Lipin switch (Merta et al., 2021) and activation of the UPR (Shaffer et al., 2004) promote ER expansion in mammalian cells. The UPR plays a central role in the differentiation of exocrine cells, such as pancreatic acinar, salivary gland acinar and plasma cells (Lee et al., 2005; Hu et al., 2009a). Importantly, activation of the UPR in plasma cells precedes the accumulation of antibodies (Lee et al., 2005; Hu et al., 2009a), which argues against the UPR being important merely to buffer the increased protein load. An attractive hypothesis to test is that the Lipin switch and the UPR are coordinated in physiological conditions. Indications pointing towards the coordination of both pathways come from studies showing the relevance of each pathway in the regeneration of axons (Oñate et al., 2016; Ohtake et al., 2018; Yang et al., 2020).

ER expansion can occur without the formation of ER sheets. For example, lipid-hormone producing cells, such as Leyding cells, display an expanded, tubular ER (Fawcett, 1981; Benton et al., 1995; Li et al., 2019). It is not known whether the UPR, the Lipin switch or other pathways mediate this expansion. Although overexpression of reticulon proteins can lead to the tubulation of expanded ER (Schuck et al., 2009), it is not clear whether Leydig cells achieve their characteristic tubular ER by the same mechanism. The data presented in this thesis suggest that the regulation of activity of reticulons might extend beyond the control of their levels to their localization and possibly posttranslational modification.

Uncovering how cells integrate these different pathways to govern ER size and shape will not only provide insights into ER homeostasis, but on a broader scale, into cell differentiation and the molecular basis underlying ER-associated diseases, paving the way to develop targeted therapeutics.

“In order for science to go on, it has to have mysteries”

Freeman Dyson

5. Bibliography

- Adeyo, O., P.J. Horn, S. Lee, D.D. Binns, A. Chandrabhas, K.D. Chapman, and J.M. Goodman. 2011. The yeast lipin orthologue Pah1p is important for biogenesis of lipid droplets. *J. Cell Biol.* 192:1043–1055. doi:10.1083/jcb.201010111.
- Albuquerque, C.P., M.B. Smolka, S.H. Payne, V. Bafna, J. Eng, and H. Zhou. 2008. A multidimensional chromatography technology for in-depth phosphoproteome analysis. *Mol. Cell. Proteomics.* 7:1389–1396. doi:10.1074/mcp.M700468-MCP200.
- Alli-Balogun, G.O., and T.P. Levine. 2021. Fungal Ice2p is in the same superfamily as SERINC3s, restriction factors for HIV and other viruses. *Proteins.* 89:1240–1250. doi:10.1002/prot.26145.
- Amaya, C., C.J.F. Cameron, S.C. Devarkar, S.J.H. Seager, M.B. Gerstein, Y. Xiong, and C. Schlieker. 2021. Nodal modulator (NOMO) is required to sustain endoplasmic reticulum morphology. *J. Biol. Chem.* 297:100937. doi:10.1016/j.jbc.2021.100937.
- Ambroziak, J., and S.A. Henry. 1994. INO2 and INO4 gene products, positive regulators of phospholipid biosynthesis in *Saccharomyces cerevisiae*, form a complex that binds to the INO1 promoter. *J. Biol. Chem.* 269:15344–15349. doi:10.1016/S0021-9258(17)36612-7.
- Anwar, K., R.W. Klemm, A. Condon, K.N. Severin, M. Zhang, R. Ghirlando, J. Hu, T.A. Rapoport, and W.A. Prinz. 2012. The dynamin-like GTPase Sey1p mediates homotypic ER fusion in *S. cerevisiae*. *J. Cell Biol.* 197:209–217. doi:10.1083/jcb.201111115.
- Atkinson, K., S. Fogel, and S.A. Henry. 1980. Yeast mutant defective in phosphatidylserine synthesis. *J. Biol. Chem.* 255:6653–6661. doi:10.1016/S0021-9258(18)43619-8.
- Aviram, N., and M. Schuldiner. 2017. Targeting and translocation of proteins to the endoplasmic reticulum at a glance. *J. Cell Sci.* 130:4079–4085. doi:10.1242/jcs.204396.
- Bachhawat, N., Q. Ouyang, and S.A. Henry. 1995. Functional characterization of an inositol-sensitive upstream activation sequence in yeast. A cis-regulatory element responsible for inositol-choline mediated regulation of phospholipid biosynthesis. *J. Biol. Chem.* 270:25087–25095. doi:10.1074/jbc.270.42.25087.
- Bahmanyar, S., R. Biggs, A.L. Schuh, A. Desai, T. Müller-Reichert, A. Audhya, J.E. Dixon, and K. Oegema. 2014. Spatial control of phospholipid flux restricts endoplasmic reticulum sheet formation to allow nuclear envelope breakdown. *Genes Dev.* 28:121–126. doi:10.1101/gad.230599.113.
- Bahmanyar, S., L. Schroeder, A. Barentine, S. Schweighofer, D. Baddeley, and J. Bewersdorf. 2018. Nano-scale size holes in ER sheets provide an alternative to tubules for highly-curved membranes. *FASEB J.* 32. doi:10.1096/fasebj.2018.32.1_supplement.542.7.
- Bahmanyar, S. 2015. Spatial regulation of phospholipid synthesis within the nuclear envelope domain of the endoplasmic reticulum. *Nucleus.* 6:102–106. doi:10.1080/19491034.2015.1010942.
- Benton, L., L.X. Shan, and M.P. Hardy. 1995. Differentiation of adult Leydig cells. *J. Steroid Biochem. Mol. Biol.* 53:61–68. doi:10.1016/0960-0760(95)00022-r.
- Bertolotti, A., Y. Zhang, L.M. Hendershot, H.P. Harding, and D. Ron. 2000. Dynamic interaction of BiP and ER stress transducers in the unfolded-protein response. *Nat. Cell Biol.* 2:326–332. doi:10.1038/35014014.
- Bircham, P.W., D.R. Maass, C.A. Roberts, P.Y. Kiew, Y.S. Low, M. Yegambaram, J. Matthews, C.A. Jack, and P.H. Atkinson. 2011. Secretory pathway genes assessed by high-throughput microscopy and synthetic genetic array analysis. *Mol. Biosyst.* 7:2589–2598. doi:10.1039/c1mb05175j.
- Blackstone, C. 2012. Cellular pathways of hereditary spastic paraplegia. *Annu. Rev. Neurosci.* 35:25–47. doi:10.1146/annurev-neuro-062111-150400.
- Brady, J.P., J.K. Claridge, P.G. Smith, and J.R. Schnell. 2015. A conserved amphipathic helix is required for membrane tubule formation by Yop1p. *Proc Natl Acad Sci USA.* 112:E639-48. doi:10.1073/pnas.1415882112.

- Branon, T.C., J.A. Bosch, A.D. Sanchez, N.D. Udeshi, T. Svinkina, S.A. Carr, J.L. Feldman, N. Perrimon, and A.Y. Ting. 2018. Efficient proximity labeling in living cells and organisms with TurboID. *Nat. Biotechnol.* 36:880–887. doi:10.1038/nbt.4201
- Brickner, J.H., and P. Walter. 2004. Gene recruitment of the activated INO1 locus to the nuclear membrane. *PLoS Biol.* 2:e342. doi:10.1371/journal.pbio.0020342.
- Carman, G.M., and G.-S. Han. 2019. Fat-regulating phosphatidic acid phosphatase: a review of its roles and regulation in lipid homeostasis. *J. Lipid Res.* 60:2–6. doi:10.1194/jlr.S087452.
- Carman, G.M., and S.A. Henry. 1989. Phospholipid biosynthesis in yeast. *Annu. Rev. Biochem.* 58:635–669. doi:10.1146/annurev.bi.58.070189.003223.
- Carman, G.M., and S.A. Henry. 1999. Phospholipid biosynthesis in the yeast *Saccharomyces cerevisiae* and interrelationship with other metabolic processes. *Prog. Lipid Res.* 38:361–399. doi:10.1016/S0163-7827(99)00010-7.
- Carman, G.M., and S.A. Henry. 2007. Phosphatidic acid plays a central role in the transcriptional regulation of glycerophospholipid synthesis in *Saccharomyces cerevisiae*. *J. Biol. Chem.* 282:37293–37297. doi:10.1074/jbc.R700038200.
- Chawla, A., S. Chakrabarti, G. Ghosh, and M. Niwa. 2011. Attenuation of yeast UPR is essential for survival and is mediated by IRE1 kinase. *J. Cell Biol.* 193:41–50. doi:10.1083/jcb.201008071.
- Chen, S., P. Novick, and S. Ferro-Novick. 2012. ER network formation requires a balance of the dynamin-like GTPase Sey1p and the Lunapark family member Lnp1p. *Nat. Cell Biol.* 14:707–716. doi:10.1038/ncb2523.
- Chen, Y.-C., P.-H. Jiang, H.-M. Chen, C.-H. Chen, Y.-T. Wang, Y.-J. Chen, C.-J. Yu, and S.-C. Teng. 2018. Glucose intake hampers PKA-regulated HSP90 chaperone activity. *eLife.* 7. doi:10.7554/eLife.39925.
- Clancey, C.J., S.C. Chang, and W. Dowhan. 1993. Cloning of a gene (PSD1) encoding phosphatidylserine decarboxylase from *Saccharomyces cerevisiae* by complementation of an *Escherichia coli* mutant. *J. Biol. Chem.* 268:24580–24590. doi:10.1016/S0021-9258(19)74506-2.
- Cohen, N., M. Breker, A. Bakunts, K. Pesek, A. Chas, J. Argemí, A. Orsi, L. Gal, S. Chuartzman, Y. Wigelman, F. Jonas, P. Walter, R. Ernst, T. Aragón, E. van Anken, and M. Schuldiner. 2017. Iron affects Ire1 clustering propensity and the amplitude of endoplasmic reticulum stress signaling. *J. Cell Sci.* 130:3222–3233. doi:10.1242/jcs.201715.
- Collart, M.A., and S. Oliviero. 2001. Preparation of yeast RNA. *Curr. Protoc. Mol. Biol.* Chapter 13:Unit13.12. doi:10.1002/0471142727.mb1312s23.
- Costanzo, M., A. Baryshnikova, J. Bellay, Y. Kim, E.D. Spear, C.S. Sevier, H. Ding, J.L.Y. Koh, K. Toufighi, S. Mostafavi, J. Prinz, R.P. St Onge, B. VanderSluis, T. Makhnevych, F.J. Vizeacoumar, S. Alizadeh, S. Bahr, R.L. Brost, Y. Chen, M. Cokol, and C. Boone. 2010. The genetic landscape of a cell. *Science.* 327:425–431. doi:10.1126/science.1180823.
- Costanzo, M., E. Kuzmin, J. van Leeuwen, B. Mair, J. Moffat, C. Boone, and B. Andrews. 2019. Global Genetic Networks and the Genotype-to-Phenotype Relationship. *Cell.* 177:85–100. doi:10.1016/j.cell.2019.01.033.
- Costanzo, M., B. VanderSluis, E.N. Koch, A. Baryshnikova, C. Pons, G. Tan, W. Wang, M. Usaj, J. Hanchard, S.D. Lee, V. Pelechano, E.B. Styles, M. Billmann, J. van Leeuwen, N. van Dyk, Z.-Y. Lin, E. Kuzmin, J. Nelson, J.S. Piotrowski, T. Srikumar, and C. Boone. 2016. A global genetic interaction network maps a wiring diagram of cellular function. *Science.* 353. doi:10.1126/science.aaf1420.
- Cox, J.S., R.E. Chapman, and P. Walter. 1997. The unfolded protein response coordinates the production of endoplasmic reticulum protein and endoplasmic reticulum membrane. *Mol. Biol. Cell.* 8:1805–1814. doi:10.1091/mbc.8.9.1805.
- Craddock, C.P., N. Adams, F.M. Bryant, S. Kurup, and P.J. Eastmond. 2015. PHOSPHATIDIC ACID PHOSPHOHYDROLASE Regulates Phosphatidylcholine Biosynthesis in Arabidopsis by Phosphatidic Acid-Mediated Activation of CTP:PHOSPHOCHOLINE CYTIDYLYLTRANSFERASE Activity. *Plant Cell.* 27:1251–1264. doi:10.1105/tpc.15.00037.

- Decottignies, A., A. Evain, and M. Ghislain. 2004. Binding of Cdc48p to a ubiquitin-related UBX domain from novel yeast proteins involved in intracellular proteolysis and sporulation. *Yeast*. 21:127–139. doi:10.1002/yea.1071.
- Dimopoulos, S., C.E. Mayer, F. Rudolf, and J. Stelling. 2014. Accurate cell segmentation in microscopy images using membrane patterns. *Bioinformatics*. 30:2644–2651. doi:10.1093/bioinformatics/btu302.
- Dubots, E., S. Cottier, M.-P. Péli-Gulli, M. Jaquenoud, S. Bontron, R. Schneider, and C. De Virgilio. 2014. TORC1 regulates Pah1 phosphatidate phosphatase activity via the Nem1/Spo7 protein phosphatase complex. *PLoS ONE*. 9:e104194. doi:10.1371/journal.pone.0104194.
- Ejsing, C.S., J.L. Sampaio, V. Surendranath, E. Duchoslav, K. Ekroos, R.W. Klemm, K. Simons, and A. Shevchenko. 2009. Global analysis of the yeast lipidome by quantitative shotgun mass spectrometry. *Proc Natl Acad Sci USA*. 106:2136–2141. doi:10.1073/pnas.0811700106.
- Emmerstorfer, A., M. Wimmer-Teubenbacher, T. Wriessnegger, E. Leitner, M. Müller, I. Kaluzna, M. Schürmann, D. Mink, G. Zellnig, H. Schwab, and H. Pichler. 2015. Over-expression of ICE2 stabilizes cytochrome P450 reductase in *Saccharomyces cerevisiae* and *Pichia pastoris*. *Biotechnol. J.* 10:623–635. doi:10.1002/biot.201400780.
- Ernst, R., S. Ballweg, and I. Levental. 2018. Cellular mechanisms of physicochemical membrane homeostasis. *Curr. Opin. Cell Biol.* 53:44–51. doi:10.1016/j.ceb.2018.04.013.
- Estrada de Martin, P., Y. Du, P. Novick, and S. Ferro-Novick. 2005. Ice2p is important for the distribution and structure of the cortical ER network in *Saccharomyces cerevisiae*. *J. Cell Sci.* 118:65–77. doi:10.1242/jcs.01583.
- Fakas, S., C. Konstantinou, and G.M. Carman. 2011. DGK1-encoded diacylglycerol kinase activity is required for phospholipid synthesis during growth resumption from stationary phase in *Saccharomyces cerevisiae*. *J. Biol. Chem.* 286:1464–1474. doi:10.1074/jbc.M110.194308.
- Fawcett, D.W. 1981. *The Cell*. Subsequent. W B Saunders Co, Philadelphia.
- Fei, W., H. Wang, X. Fu, C. Bielby, and H. Yang. 2009. Conditions of endoplasmic reticulum stress stimulate lipid droplet formation in *Saccharomyces cerevisiae*. *Biochem. J.* 424:61–67. doi:10.1042/BJ20090785.
- Ferreira, J.V., and P. Carvalho. 2021. Pex30-like proteins function as adaptors at distinct ER membrane contact sites. *J. Cell Biol.* 220. doi:10.1083/jcb.202103176.
- Fregno, I., and M. Molinari. 2018. Endoplasmic reticulum turnover: ER-phagy and other flavors in selective and non-selective ER clearance. [version 1; peer review: 2 approved]. *F1000Res*. 7:454. doi:10.12688/f1000research.13968.1.
- Garbarino, J., M. Padamsee, L. Wilcox, P.M. Oelkers, D. D'Ambrosio, K.V. Ruggles, N. Ramsey, O. Jabado, A. Turkish, and S.L. Sturley. 2009. Sterol and diacylglycerol acyltransferase deficiency triggers fatty acid-mediated cell death. *J. Biol. Chem.* 284:30994–31005. doi:10.1074/jbc.M109.050443.
- Gardner, B.M., and P. Walter. 2011. Unfolded proteins are Ire1-activating ligands that directly induce the unfolded protein response. *Science*. 333:1891–1894. doi:10.1126/science.1209126.
- Gonzalez-Enriquez, G.V., M. Escoto-Delgadillo, E. Vazquez-Valls, and B.M. Torres-Mendoza. 2017. SERINC as a Restriction Factor to Inhibit Viral Infectivity and the Interaction with HIV. *J. Immunol. Res.* 2017:1548905. doi:10.1155/2017/1548905.
- Gruber, A., D. Hornburg, M. Antonin, N. Kraemer, J. Collado, M. Schaffer, G. Zubaite, C. Lüchtenborg, T. Sachsenheimer, B. Brügger, M. Mann, W. Baumeister, F.U. Hartl, M.S. Hipp, and R. Fernández-Busnadiego. 2018. Molecular and structural architecture of polyQ aggregates in yeast. *Proc Natl Acad Sci USA*. 115:E3446–E3453. doi:10.1073/pnas.1717978115.
- Guna, A., N. Volkmar, J.C. Christianson, and R.S. Hegde. 2018. The ER membrane protein complex is a transmembrane domain insertase. *Science*. 359:470–473. doi:10.1126/science.aao3099.
- Halbleib, K., K. Pesek, R. Covino, H.F. Hofbauer, D. Wunnicke, I. Hänelt, G. Hummer, and R. Ernst. 2017. Activation of the unfolded protein response by lipid bilayer stress. *Mol. Cell*. 67:673–684.e8.

doi:10.1016/j.molcel.2017.06.012.

- Han, G.-S., L. O'Hara, G.M. Carman, and S. Siniosoglou. 2008. An unconventional diacylglycerol kinase that regulates phospholipid synthesis and nuclear membrane growth. *J. Biol. Chem.* 283:20433–20442. doi:10.1074/jbc.M802903200.
- Han, G.-S., W.-I. Wu, and G.M. Carman. 2006. The *Saccharomyces cerevisiae* Lipin homolog is a Mg²⁺-dependent phosphatidate phosphatase enzyme. *J. Biol. Chem.* 281:9210–9218. doi:10.1074/jbc.M600425200.
- Han, S., S. Bahmanyar, P. Zhang, N. Grishin, K. Oegema, R. Crooke, M. Graham, K. Reue, J.E. Dixon, and J.M. Goodman. 2012. Nuclear envelope phosphatase 1-regulatory subunit 1 (formerly TMEM188) is the metazoan Spo7p ortholog and functions in the lipin activation pathway. *J. Biol. Chem.* 287:3123–3137. doi:10.1074/jbc.M111.324350.
- Han, S.-H., G.-S. Han, W.M. Iwanyshyn, and G.M. Carman. 2005. Regulation of the PIS1-encoded phosphatidylinositol synthase in *Saccharomyces cerevisiae* by zinc. *J. Biol. Chem.* 280:29017–29024. doi:10.1074/jbc.M505881200.
- Hasslacher, M., A.S. Ivessa, F. Paltauf, and S.D. Kohlwein. 1993. Acetyl-CoA carboxylase from yeast is an essential enzyme and is regulated by factors that control phospholipid metabolism. *J. Biol. Chem.* 268:10946–10952. doi:10.1016/S0021-9258(18)82077-4.
- Hedskog, L., C.M. Pinho, R. Filadi, A. Rönnbäck, L. Hertwig, B. Wiehager, P. Larssen, S. Gellhaar, A. Sandebring, M. Westerlund, C. Graff, B. Winblad, D. Galter, H. Behbahani, P. Pizzo, E. Glaser, and M. Ankarcrona. 2013. Modulation of the endoplasmic reticulum-mitochondria interface in Alzheimer's disease and related models. *Proc Natl Acad Sci USA.* 110:7916–7921. doi:10.1073/pnas.1300677110.
- te Heesen, S., B. Janetzky, L. Lehle, and M. Aebi. 1992. The yeast WBP1 is essential for oligosaccharyl transferase activity in vivo and in vitro. *EMBO J.* 11:2071–2075.
- Henry, S.A., and J.L. Patton-Vogt. 1998. Genetic regulation of phospholipid metabolism: yeast as a model eukaryote. *Prog. Nucleic Acid Res. Mol. Biol.* 61:133–179. doi:10.1016/s0079-6603(08)60826-0.
- Heyken, W.-T., A. Repenning, J. Kumme, and H.-J. Schüller. 2005. Constitutive expression of yeast phospholipid biosynthetic genes by variants of Ino2 activator defective for interaction with Opi1 repressor. *Mol. Microbiol.* 56:696–707. doi:10.1111/j.1365-2958.2004.04499.x.
- Hirsch, J.P., and S.A. Henry. 1986. Expression of the *Saccharomyces cerevisiae* inositol-1-phosphate synthase (INO1) gene is regulated by factors that affect phospholipid synthesis. *Mol. Cell. Biol.* 6:3320–3328. doi:10.1128/mcb.6.10.3320-3328.1986.
- Hofbauer, H.F., M. Gecht, S.C. Fischer, A. Seybert, A.S. Frangakis, E.H.K. Stelzer, R. Covino, G. Hummer, and R. Ernst. 2018. The molecular recognition of phosphatidic acid by an amphipathic helix in Opi1. *J. Cell Biol.* 217:3109–3126. doi:10.1083/jcb.201802027.
- Hollien, J., and J.S. Weissman. 2006. Decay of endoplasmic reticulum-localized mRNAs during the unfolded protein response. *Science.* 313:104–107. doi:10.1126/science.1129631.
- Holt, L.J., B.B. Tuch, J. Villén, A.D. Johnson, S.P. Gygi, and D.O. Morgan. 2009. Global analysis of Cdk1 substrate phosphorylation sites provides insights into evolution. *Science.* 325:1682–1686. doi:10.1126/science.1172867.
- Homann, M.J., M.A. Poole, P.M. Gaynor, C.T. Ho, and G.M. Carman. 1987. Effect of growth phase on phospholipid biosynthesis in *Saccharomyces cerevisiae*. *J. Bacteriol.* 169:533–539. doi:10.1128/jb.169.2.533-539.1987.
- Hoppins, S., S.R. Collins, A. Cassidy-Stone, E. Hummel, R.M. Devay, L.L. Lackner, B. Westermann, M. Schuldiner, J.S. Weissman, and J. Nunnari. 2011. A mitochondrial-focused genetic interaction map reveals a scaffold-like complex required for inner membrane organization in mitochondria. *J. Cell Biol.* 195:323–340. doi:10.1083/jcb.201107053.
- Hosomi, A., K. Iida, T. Cho, H. Iida, M. Kaneko, and T. Suzuki. 2020. The ER-associated protease Ste24 prevents N-terminal signal peptide-independent translocation into the endoplasmic reticulum in

- Saccharomyces cerevisiae*. *J. Biol. Chem.* 295:10406–10419. doi:10.1074/jbc.RA120.012575.
- Ho, B., A. Baryshnikova, and G.W. Brown. 2018. Unification of Protein Abundance Datasets Yields a Quantitative *Saccharomyces cerevisiae* Proteome. *Cell Syst.* 6:192-205.e3. doi:10.1016/j.cels.2017.12.004.
- Hsieh, L.-S., W.-M. Su, G.-S. Han, and G.M. Carman. 2016. Phosphorylation of yeast pah1 phosphatidate phosphatase by casein kinase II regulates its function in lipid metabolism. *J. Biol. Chem.* 291:9974–9990. doi:10.1074/jbc.M116.726588.
- Hu, C.-C.A., S.K. Dougan, A.M. McGehee, J.C. Love, and H.L. Ploegh. 2009a. XBP-1 regulates signal transduction, transcription factors and bone marrow colonization in B cells. *EMBO J.* 28:1624–1636. doi:10.1038/emboj.2009.117.
- Hu, J., Y. Shibata, C. Voss, T. Shemesh, Z. Li, M. Coughlin, M.M. Kozlov, T.A. Rapoport, and W.A. Prinz. 2008. Membrane proteins of the endoplasmic reticulum induce high-curvature tubules. *Science.* 319:1247–1250. doi:10.1126/science.1153634.
- Hu, J., Y. Shibata, P.-P. Zhu, C. Voss, N. Rismanchi, W.A. Prinz, T.A. Rapoport, and C. Blackstone. 2009b. A class of dynamin-like GTPases involved in the generation of the tubular ER network. *Cell.* 138:549–561. doi:10.1016/j.cell.2009.05.025.
- Humphreys, I.R., J. Pei, M. Baek, A. Krishnakumar, I. Anishchenko, S. Ovchinnikov, J. Zhang, T.J. Ness, S. Banjade, S.R. Bagde, V.G. Stancheva, X.-H. Li, K. Liu, Z. Zheng, D.J. Barrero, U. Roy, J. Kuper, I.S. Fernández, B. Szakal, D. Branzei, and D. Baker. 2021. Computed structures of core eukaryotic protein complexes. *Science.* 374:eabm4805. doi:10.1126/science.abm4805.
- Inoue, T., and B. Tsai. 2013. How viruses use the endoplasmic reticulum for entry, replication, and assembly. *Cold Spring Harb. Perspect. Biol.* 5:a013250. doi:10.1101/cshperspect.a013250.
- Inuzuka, M., M. Hayakawa, and T. Ingi. 2005. Serinc, an activity-regulated protein family, incorporates serine into membrane lipid synthesis. *J. Biol. Chem.* 280:35776–35783. doi:10.1074/jbc.M505712200.
- Iwanyshyn, W.M., G.-S. Han, and G.M. Carman. 2004. Regulation of phospholipid synthesis in *Saccharomyces cerevisiae* by zinc. *J. Biol. Chem.* 279:21976–21983. doi:10.1074/jbc.M402047200.
- Jacquemyn, J., A. Cascalho, and R.E. Goodchild. 2017. The ins and outs of endoplasmic reticulum-controlled lipid biosynthesis. *EMBO Rep.* 18:1905–1921. doi:10.15252/embr.201643426.
- Jamieson, J.D. 2008. A tribute to George E. Palade. *J. Clin. Invest.* 118:3517–3518. doi:10.1172/jci37749.
- Janke, C., M.M. Magiera, N. Rathfelder, C. Taxis, S. Reber, H. Maekawa, A. Moreno-Borchart, G. Doenges, E. Schwob, E. Schiebel, and M. Knop. 2004. A versatile toolbox for PCR-based tagging of yeast genes: new fluorescent proteins, more markers and promoter substitution cassettes. *Yeast.* 21:947–962. doi:10.1002/yea.1142.
- Johnston, M. 1987. A model fungal gene regulatory mechanism: the GAL genes of *Saccharomyces cerevisiae*. *Microbiol. Rev.* 51:458–476. doi:10.1128/mr.51.4.458-476.1987.
- Jonikas, M.C., S.R. Collins, V. Denic, E. Oh, E.M. Quan, V. Schmid, J. Weibezahn, B. Schwappach, P. Walter, J.S. Weissman, and M. Schuldiner. 2009. Comprehensive characterization of genes required for protein folding in the endoplasmic reticulum. *Science.* 323:1693–1697. doi:10.1126/science.1167983.
- Karanasios, E., A.D. Barbosa, H. Sembongi, M. Mari, G.-S. Han, F. Reggiori, G.M. Carman, and S. Siniosoglou. 2013. Regulation of lipid droplet and membrane biogenesis by the acidic tail of the phosphatidate phosphatase Pah1p. *Mol. Biol. Cell.* 24:2124–2133. doi:10.1091/mbc.E13-01-0021.
- Karanasios, E., G.-S. Han, Z. Xu, G.M. Carman, and S. Siniosoglou. 2010. A phosphorylation-regulated amphipathic helix controls the membrane translocation and function of the yeast phosphatidate phosphatase. *Proc Natl Acad Sci USA.* 107:17539–17544. doi:10.1073/pnas.1007974107.
- Kinoshita, E., E. Kinoshita-Kikuta, K. Takiyama, and T. Koike. 2006. Phosphate-binding tag, a new tool to visualize phosphorylated proteins. *Mol. Cell. Proteomics.* 5:749–757. doi:10.1074/mcp.T500024-MCP200.
- Kiyono, K., K. Miura, Y. Kushima, T. Hikiji, M. Fukushima, I. Shibuya, and A. Ohta. 1987. Primary structure and product characterization of the *Saccharomyces cerevisiae* CHO1 gene that encodes phosphatidylserine

- synthase. *J. Biochem.* 102:1089–1100. doi:10.1093/oxfordjournals.jbchem.a122147.
- Klopfenstein, D.R., J. Klumperman, A. Lustig, R.A. Kammerer, V. Oorschot, and H.P. Hauri. 2001. Subdomain-specific localization of CLIMP-63 (p63) in the endoplasmic reticulum is mediated by its luminal alpha-helical segment. *J. Cell Biol.* 153:1287–1300. doi:10.1083/jcb.153.6.1287.
- Klug, L., and G. Daum. 2014. Yeast lipid metabolism at a glance. *FEMS Yeast Res.* 14:369–388. doi:10.1111/1567-1364.12141.
- Knop, M., K. Siegers, G. Pereira, W. Zachariae, B. Winsor, K. Nasmyth, and E. Schiebel. 1999. Epitope tagging of yeast genes using a PCR-based strategy: more tags and improved practical routines. *Yeast.* 15:963–972. doi:10.1002/(SICI)1097-0061(199907)15:10B<963::AID-YEA399>3.0.CO;2-W.
- Kodaki, T., K. Hosaka, J. Nikawa, and S. Yamashita. 1991. Identification of the upstream activation sequences responsible for the expression and regulation of the PEM1 and PEM2 genes encoding the enzymes of the phosphatidylethanolamine methylation pathway in *Saccharomyces cerevisiae*. *J. Biochem.* 109:276–287.
- Kodaki, T., and S. Yamashita. 1987. Yeast phosphatidylethanolamine methylation pathway. Cloning and characterization of two distinct methyltransferase genes. *J. Biol. Chem.* 262:15428–15435. doi:10.1016/S0021-9258(18)47744-7.
- Kukulski, W., M. Schorb, S. Welsch, A. Picco, M. Kaksonen, and J.A.G. Briggs. 2012. Precise, correlated fluorescence microscopy and electron tomography of lowicryl sections using fluorescent fiducial markers. *Methods Cell Biol.* 111:235–257. doi:10.1016/B978-0-12-416026-2.00013-3.
- Kushnirov, V.V. 2000. Rapid and reliable protein extraction from yeast. *Yeast.* 16:857–860. doi:10.1002/1097-0061(20000630)16:9<857::AID-YEA561>3.0.CO;2-B.
- Kwiatk, J.M., G.-S. Han, and G.M. Carman. 2020. Phosphatidate-mediated regulation of lipid synthesis at the nuclear/endoplasmic reticulum membrane. *Biochim. Biophys. Acta Mol. Cell Biol. Lipids.* 1865:158434. doi:10.1016/j.bbalip.2019.03.006.
- Lamping, E., J. Lückl, F. Paltauf, S.A. Henry, and S.D. Kohlwein. 1994. Isolation and characterization of a mutant of *Saccharomyces cerevisiae* with pleiotropic deficiencies in transcriptional activation and repression. *Genetics.* 137:55–65. doi:10.1093/genetics/137.1.55.
- Lanz, M.C., K. Yugandhar, S. Gupta, E.J. Sanford, V.M. Faça, S. Vega, A.M.N. Joiner, J.C. Fromme, H. Yu, and M.B. Smolka. 2021. In-depth and 3-dimensional exploration of the budding yeast phosphoproteome. *EMBO Rep.* 22:e51121. doi:10.15252/embr.202051121.
- Lee, A.-H., G.C. Chu, N.N. Iwakoshi, and L.H. Glimcher. 2005. XBP-1 is required for biogenesis of cellular secretory machinery of exocrine glands. *EMBO J.* 24:4368–4380. doi:10.1038/sj.emboj.7600903.
- Li, L., Y. Li, C. Sottas, M. Culty, J. Fan, Y. Hu, G. Cheung, H.E. Chemes, and V. Papadopoulos. 2019. Directing differentiation of human induced pluripotent stem cells toward androgen-producing Leydig cells rather than adrenal cells. *Proc Natl Acad Sci USA.* 116:23274–23283. doi:10.1073/pnas.1908207116.
- Loewen, C.J.R., M.L. Gaspar, S.A. Jesch, C. Delon, N.T. Ktistakis, S.A. Henry, and T.P. Levine. 2004. Phospholipid metabolism regulated by a transcription factor sensing phosphatidic acid. *Science.* 304:1644–1647. doi:10.1126/science.1096083.
- Loewen, C.J.R., and T.P. Levine. 2005. A highly conserved binding site in vesicle-associated membrane protein-associated protein (VAP) for the FFAT motif of lipid-binding proteins. *J. Biol. Chem.* 280:14097–14104. doi:10.1074/jbc.M500147200.
- Loewen, C.J.R., A. Roy, and T.P. Levine. 2003. A conserved ER targeting motif in three families of lipid binding proteins and in Opi1p binds VAP. *EMBO J.* 22:2025–2035. doi:10.1093/emboj/cdg201.
- Loewen, C.J.R., B.P. Young, S. Tavassoli, and T.P. Levine. 2007. Inheritance of cortical ER in yeast is required for normal septin organization. *J. Cell Biol.* 179:467–483. doi:10.1083/jcb.200708205.
- Longtine, M.S., A. McKenzie, D.J. Demarini, N.G. Shah, A. Wach, A. Brachat, P. Philippsen, and J.R. Pringle. 1998. Additional modules for versatile and economical PCR-based gene deletion and modification in *Saccharomyces cerevisiae*. *Yeast.* 14:953–961. doi:10.1002/(SICI)1097-0061(199807)14:10<953::AID-

YEA293>3.0.CO;2-U.

- Lyman, S.K., and R. Schekman. 1995. Interaction between BiP and Sec63p is required for the completion of protein translocation into the ER of *Saccharomyces cerevisiae*. *J. Cell Biol.* 131:1163–1171. doi:10.1083/jcb.131.5.1163.
- MacGilvray, M.E., E. Shishkova, M. Place, E.R. Wagner, J.J. Coon, and A.P. Gasch. 2020. Phosphoproteome Response to Dithiothreitol Reveals Unique Versus Shared Features of *Saccharomyces cerevisiae* Stress Responses. *J. Proteome Res.* 19:3405–3417. doi:10.1021/acs.jproteome.0c00253.
- Maclsaac, K.D., T. Wang, D.B. Gordon, D.K. Gifford, G.D. Stormo, and E. Fraenkel. 2006. An improved map of conserved regulatory sites for *Saccharomyces cerevisiae*. *BMC Bioinformatics.* 7:113. doi:10.1186/1471-2105-7-113.
- Markgraf, D.F., R.W. Klemm, M. Junker, H.K. Hannibal-Bach, C.S. Ejsing, and T.A. Rapoport. 2014. An ER protein functionally couples neutral lipid metabolism on lipid droplets to membrane lipid synthesis in the ER. *Cell Rep.* 6:44–55. doi:10.1016/j.celrep.2013.11.046.
- Mastronarde, D.N. 2005. Automated electron microscope tomography using robust prediction of specimen movements. *J. Struct. Biol.* 152:36–51. doi:10.1016/j.jsb.2005.07.007.
- Mazzarello, P., A. Calligaro, V. Vannini, and U. Muscatello. 2003. The sarcoplasmic reticulum: its discovery and rediscovery. *Nat. Rev. Mol. Cell Biol.* 4:69–74. doi:10.1038/nrm1003.
- Merta, H., J.W. Carrasquillo Rodriguez, M.I. Anjur-Dietrich, M.E. Granade, T. Vitale, T.E. Harris, D.J. Needleman, and S. Bahmanyar. 2021. A CTDNEP1-lipin 1-mTOR regulatory network restricts ER membrane biogenesis to enable chromosome motions necessary for mitotic fidelity. *BioRxiv*. doi:10.1101/2021.03.02.433553.
- Mirheydari, M., P. Dey, G.J. Stuke, Y. Park, G.-S. Han, and G.M. Carman. 2020. The Spo7 sequence LLI is required for Nem1-Spo7/Pah1 phosphatase cascade function in yeast lipid metabolism. *J. Biol. Chem.* 295:11473–11485. doi:10.1074/jbc.RA120.014129.
- Mochida, K., Y. Oikawa, Y. Kimura, H. Kirisako, H. Hirano, Y. Ohsumi, and H. Nakatogawa. 2015. Receptor-mediated selective autophagy degrades the endoplasmic reticulum and the nucleus. *Nature.* 522:359–362. doi:10.1038/nature14506.
- Mori, K., N. Ogawa, T. Kawahara, H. Yanagi, and T. Yura. 1998. Palindrome with spacer of one nucleotide is characteristic of the cis-acting unfolded protein response element in *Saccharomyces cerevisiae*. *J. Biol. Chem.* 273:9912–9920. doi:10.1074/jbc.273.16.9912.
- Murthi, A., and A.K. Hopper. 2005. Genome-wide screen for inner nuclear membrane protein targeting in *Saccharomyces cerevisiae*: roles for N-acetylation and an integral membrane protein. *Genetics.* 170:1553–1560. doi:10.1534/genetics.105.043620.
- Nagy, Z., S. Comer, and A. Smolenski. 2018. Analysis of Protein Phosphorylation Using Phos-Tag Gels. *Curr. Protoc. Protein Sci.* 93:e64. doi:10.1002/cpps.64.
- Nikawa, J., T. Kodaki, and S. Yamashita. 1987. Primary structure and disruption of the phosphatidylinositol synthase gene of *Saccharomyces cerevisiae*. *J. Biol. Chem.* 262:4876–4881.
- Nikawa, J., and S. Yamashita. 1984. Molecular cloning of the gene encoding CDPdiacylglycerol-inositol 3-phosphatidyl transferase in *Saccharomyces cerevisiae*. *Eur. J. Biochem.* 143:251–256. doi:10.1111/j.1432-1033.1984.tb08366.x.
- Nixon-Abell, J., C.J. Obara, A.V. Weigel, D. Li, W.R. Legant, C.S. Xu, H.A. Pasolli, K. Harvey, H.F. Hess, E. Betzig, C. Blackstone, and J. Lippincott-Schwartz. 2016. Increased spatiotemporal resolution reveals highly dynamic dense tubular matrices in the peripheral ER. *Science.* 354. doi:10.1126/science.aaf3928.
- North, M., J. Steffen, A.V. Loguinov, G.R. Zimmerman, C.D. Vulpe, and D.J. Eide. 2012. Genome-wide functional profiling identifies genes and processes important for zinc-limited growth of *Saccharomyces cerevisiae*. *PLoS Genet.* 8:e1002699. doi:10.1371/journal.pgen.1002699.
- O'Hara, L., G.-S. Han, S. Peak-Chew, N. Grimsey, G.M. Carman, and S. Siniosoglou. 2006. Control of phospholipid synthesis by phosphorylation of the yeast lipin Pah1p/Smp2p Mg²⁺-dependent

- phosphatidate phosphatase. *J. Biol. Chem.* 281:34537–34548. doi:10.1074/jbc.M606654200.
- Ohtake, Y., K. Matsuhisa, M. Kaneko, S. Kanemoto, R. Asada, K. Imaizumi, and A. Saito. 2018. Axonal activation of the unfolded protein response promotes axonal regeneration following peripheral nerve injury. *Neuroscience*. 375:34–48. doi:10.1016/j.neuroscience.2018.02.003.
- Okamura, K., Y. Kimata, H. Higashio, A. Tsuru, and K. Kohno. 2000. Dissociation of Kar2p/BiP from an ER sensory molecule, Ire1p, triggers the unfolded protein response in yeast. *Biochem. Biophys. Res. Commun.* 279:445–450. doi:10.1006/bbrc.2000.3987.
- Oñate, M., A. Catenaccio, G. Martínez, D. Armentano, G. Parsons, B. Kerr, C. Hetz, and F.A. Court. 2016. Activation of the unfolded protein response promotes axonal regeneration after peripheral nerve injury. *Sci. Rep.* 6:21709. doi:10.1038/srep21709.
- Orso, G., D. Pendin, S. Liu, J. Tassetto, T.J. Moss, J.E. Faust, M. Micaroni, A. Egorova, A. Martinuzzi, J.A. McNew, and A. Daga. 2009. Homotypic fusion of ER membranes requires the dynamin-like GTPase atlastin. *Nature*. 460:978–983. doi:10.1038/nature08280.
- Özbalci, C., T. Sachsenheimer, and B. Brügger. 2013. Quantitative analysis of cellular lipids by nano-electrospray ionization mass spectrometry. *Methods Mol. Biol.* 1033:3–20. doi:10.1007/978-1-62703-487-6_1.
- Palade, G.E., and K.R. Porter. 1954. Studies on the endoplasmic reticulum. I. Its identification in cells in situ. *J. Exp. Med.* 100:641–656. doi:10.1084/jem.100.6.641.
- Palade, G.E. 1955. A small particulate component of the cytoplasm. *J. Biophys. Biochem. Cytol.* 1:59–68. doi:10.1083/jcb.1.1.59.
- Palade, G.E. 1956. The endoplasmic reticulum. *J. Biophys. Biochem. Cytol.* 2:85–98. doi:10.1083/jcb.2.4.85.
- Papagiannidis, D., P.W. Bircham, C. Lüchtenborg, O. Pajonk, G. Ruffini, B. Brügger, and S. Schuck. 2021. Ice2 promotes ER membrane biogenesis in yeast by inhibiting the conserved lipin phosphatase complex. *EMBO J.* 40:e107958. doi:10.15252/embj.2021107958.
- Pascual, F., A. Soto-Cardalda, and G.M. Carman. 2013. PAH1-encoded phosphatidate phosphatase plays a role in the growth phase- and inositol-mediated regulation of lipid synthesis in *Saccharomyces cerevisiae*. *J. Biol. Chem.* 288:35781–35792. doi:10.1074/jbc.M113.525766.
- Paul-Gilloteaux, P., X. Heiligenstein, M. Belle, M.-C. Domart, B. Larjani, L. Collinson, G. Raposo, and J. Salamero. 2017. eC-CLEM: flexible multidimensional registration software for correlative microscopies. *Nat. Methods*. 14:102–103. doi:10.1038/nmeth.4170.
- Petschnigg, J., H. Wolinski, D. Kolb, G. Zellnig, C.F. Kurat, K. Natter, and S.D. Kohlwein. 2009. Good fat, essential cellular requirements for triacylglycerol synthesis to maintain membrane homeostasis in yeast. *J. Biol. Chem.* 284:30981–30993. doi:10.1074/jbc.M109.024752.
- Phillips, M.J., and G.K. Voeltz. 2016. Structure and function of ER membrane contact sites with other organelles. *Nat. Rev. Mol. Cell Biol.* 17:69–82. doi:10.1038/nrm.2015.8.
- Pincus, D., A. Aranda-Díaz, I.A. Zuleta, P. Walter, and H. El-Samad. 2014. Delayed Ras/PKA signaling augments the unfolded protein response. *Proc Natl Acad Sci USA*. 111:14800–14805. doi:10.1073/pnas.1409588111.
- Pincus, D., M.W. Chevalier, T. Aragón, E. van Anken, S.E. Vidal, H. El-Samad, and P. Walter. 2010. BiP binding to the ER-stress sensor Ire1 tunes the homeostatic behavior of the unfolded protein response. *PLoS Biol.* 8:e1000415. doi:10.1371/journal.pbio.1000415.
- Porter, K.R., A. Claude, and E.F. Fullam. 1945. A study of tissue culture cells by electron microscopy: methods and preliminary observations. *J. Exp. Med.* 81:233–246. doi:10.1084/jem.81.3.233.
- Porter, K.R., and G.E. Palade. 1957. Studies on the endoplasmic reticulum. III. Its form and distribution in striated muscle cells. *J. Biophys. Biochem. Cytol.* 3:269–300.
- Powers, R.E., S. Wang, T.Y. Liu, and T.A. Rapoport. 2017. Reconstitution of the tubular endoplasmic reticulum network with purified components. *Nature*. 543:257–260. doi:10.1038/nature21387.

- Prinz, W.A., L. Grzyb, M. Veenhuis, J.A. Kahana, P.A. Silver, and T.A. Rapoport. 2000. Mutants affecting the structure of the cortical endoplasmic reticulum in *Saccharomyces cerevisiae*. *J. Cell Biol.* 150:461–474. doi:10.1083/jcb.150.3.461.
- Puhka, M., M. Joensuu, H. Vihinen, I. Belevich, and E. Jokitalo. 2012. Progressive sheet-to-tubule transformation is a general mechanism for endoplasmic reticulum partitioning in dividing mammalian cells. *Mol. Biol. Cell.* 23:2424–2432. doi:10.1091/mbc.E10-12-0950.
- Qiu, Y., A. Hassaninasab, G.-S. Han, and G.M. Carman. 2016. Phosphorylation of Dgk1 Diacylglycerol Kinase by Casein Kinase II Regulates Phosphatidic Acid Production in *Saccharomyces cerevisiae*. *J. Biol. Chem.* 291:26455–26467. doi:10.1074/jbc.M116.763839.
- Quon, E., Y.Y. Sere, N. Chauhan, J. Johansen, D.P. Sullivan, J.S. Dittman, W.J. Rice, R.B. Chan, G. Di Paolo, C.T. Beh, and A.K. Menon. 2018. Endoplasmic reticulum-plasma membrane contact sites integrate sterol and phospholipid regulation. *PLoS Biol.* 16:e2003864. doi:10.1371/journal.pbio.2003864.
- Radanović, T., and R. Ernst. 2021. The unfolded protein response as a guardian of the secretory pathway. *Cells.* 10. doi:10.3390/cells10112965.
- Rapoport, T.A. 2007. Protein translocation across the eukaryotic endoplasmic reticulum and bacterial plasma membranes. *Nature.* 450:663–669. doi:10.1038/nature06384.
- Ravindran, M.S., P. Bagchi, C.N. Cunningham, and B. Tsai. 2016. Opportunistic intruders: how viruses orchestrate ER functions to infect cells. *Nat. Rev. Microbiol.* 14:407–420. doi:10.1038/nrmicro.2016.60.
- Renvoisé, B., and C. Blackstone. 2010. Emerging themes of ER organization in the development and maintenance of axons. *Curr. Opin. Neurobiol.* 20:531–537. doi:10.1016/j.conb.2010.07.001.
- Rødskær, S.V., D. Pultz, M. Bruschi, M.V. Bennetzen, L.G. Falkenby, J.S. Andersen, and N.J. Færgeman. 2014. Quantitative proteomics identifies unanticipated regulators of nitrogen- and glucose starvation. *Mol. Biosyst.* 10:2176–2188. doi:10.1039/c4mb00207e.
- Ron, D., and P. Walter. 2007. Signal integration in the endoplasmic reticulum unfolded protein response. *Nat. Rev. Mol. Cell Biol.* 8:519–529. doi:10.1038/nrm2199.
- Rosa, A., A. Chande, S. Ziglio, V. De Sanctis, R. Bertorelli, S.L. Goh, S.M. McCauley, A. Nowosielska, S.E. Antonarakis, J. Luban, F.A. Santoni, and M. Pizzato. 2015. HIV-1 Nef promotes infection by excluding SERINC5 from virion incorporation. *Nature.* 526:212–217. doi:10.1038/nature15399.
- Ruggiano, A., O. Foresti, and P. Carvalho. 2014. ER-associated degradation: protein quality control and beyond. *J. Cell Biol.* 204:869–879. doi:10.1083/jcb.201312042.
- Ruotolo, R., G. Marchini, and S. Ottonello. 2008. Membrane transporters and protein traffic networks differentially affecting metal tolerance: a genomic phenotyping study in yeast. *Genome Biol.* 9:R67. doi:10.1186/gb-2008-9-4-r67.
- Rutkowski, D.T., and R.S. Hegde. 2010. Regulation of basal cellular physiology by the homeostatic unfolded protein response. *J. Cell Biol.* 189:783–794. doi:10.1083/jcb.201003138.
- Santos-Rosa, H., J. Leung, N. Grimsey, S. Peak-Chew, and S. Siniosoglou. 2005. The yeast lipin Smp2 couples phospholipid biosynthesis to nuclear membrane growth. *EMBO J.* 24:1931–1941. doi:10.1038/sj.emboj.7600672.
- Schäfer, J.A., J.P. Schessner, P.W. Bircham, T. Tsuji, C. Funaya, O. Pajonk, K. Schaeff, G. Ruffini, D. Papagiannidis, M. Knop, T. Fujimoto, and S. Schuck. 2020. ESCRT machinery mediates selective microautophagy of endoplasmic reticulum in yeast. *EMBO J.* 39:e102586. doi:10.15252/embj.2019102586.
- Schekman, R.W. 2008. Retrospective: George E. Palade (1912-2008). *Science.* 322:695. doi:10.1126/science.1167174.
- Schindelin, J., I. Arganda-Carreras, E. Frise, V. Kaynig, M. Longair, T. Pietzsch, S. Preibisch, C. Rueden, S. Saalfeld, B. Schmid, J.-Y. Tinevez, D.J. White, V. Hartenstein, K. Eliceiri, P. Tomancak, and A. Cardona. 2012. Fiji: an open-source platform for biological-image analysis. *Nat. Methods.* 9:676–682. doi:10.1038/nmeth.2019.

- Schroeder, L.K., A.E.S. Barentine, H. Merta, S. Schweighofer, Y. Zhang, D. Baddeley, J. Bewersdorf, and S. Bahmanyar. 2019. Dynamic nanoscale morphology of the ER surveyed by STED microscopy. *J. Cell Biol.* 218:83–96. doi:10.1083/jcb.201809107.
- Schuck, S., C.M. Gallagher, and P. Walter. 2014. ER-phagy mediates selective degradation of endoplasmic reticulum independently of the core autophagy machinery. *J. Cell Sci.* 127:4078–4088. doi:10.1242/jcs.154716.
- Schuck, S., W.A. Prinz, K.S. Thorn, C. Voss, and P. Walter. 2009. Membrane expansion alleviates endoplasmic reticulum stress independently of the unfolded protein response. *J. Cell Biol.* 187:525–536. doi:10.1083/jcb.200907074.
- Schuck, S. 2020. Microautophagy - distinct molecular mechanisms handle cargoes of many sizes. *J. Cell Sci.* 133. doi:10.1242/jcs.246322.
- Schuldiner, M., S.R. Collins, N.J. Thompson, V. Denic, A. Bhamidipati, T. Punna, J. Ihmels, B. Andrews, C. Boone, J.F. Greenblatt, J.S. Weissman, and N.J. Krogan. 2005. Exploration of the function and organization of the yeast early secretory pathway through an epistatic miniarray profile. *Cell.* 123:507–519. doi:10.1016/j.cell.2005.08.031.
- Schuldiner, M., J. Metz, V. Schmid, V. Denic, M. Rakwalska, H.D. Schmitt, B. Schwappach, and J.S. Weissman. 2008. The GET complex mediates insertion of tail-anchored proteins into the ER membrane. *Cell.* 134:634–645. doi:10.1016/j.cell.2008.06.025.
- Schüller, H.J., A. Hahn, F. Tröster, A. Schütz, and E. Schweizer. 1992. Coordinate genetic control of yeast fatty acid synthase genes FAS1 and FAS2 by an upstream activation site common to genes involved in membrane lipid biosynthesis. *EMBO J.* 11:107–114. doi:10.1002/j.1460-2075.1992.tb05033.x.
- Schwarz, D.S., and M.D. Blower. 2016. The endoplasmic reticulum: structure, function and response to cellular signaling. *Cell. Mol. Life Sci.* 73:79–94. doi:10.1007/s00018-015-2052-6.
- Shaffer, A.L., M. Shapiro-Shelef, N.N. Iwakoshi, A.-H. Lee, S.-B. Qian, H. Zhao, X. Yu, L. Yang, B.K. Tan, A. Rosenwald, E.M. Hurt, E. Petroulakis, N. Sonenberg, J.W. Yewdell, K. Calame, L.H. Glimcher, and L.M. Staudt. 2004. XBP1, downstream of Blimp-1, expands the secretory apparatus and other organelles, and increases protein synthesis in plasma cell differentiation. *Immunity.* 21:81–93. doi:10.1016/j.immuni.2004.06.010.
- Shaner, N.C., R.E. Campbell, P.A. Steinbach, B.N.G. Giepmans, A.E. Palmer, and R.Y. Tsien. 2004. Improved monomeric red, orange and yellow fluorescent proteins derived from *Discosoma* sp. red fluorescent protein. *Nat. Biotechnol.* 22:1567–1572. doi:10.1038/nbt1037.
- Shaner, N.C., G.G. Lambert, A. Chamma, Y. Ni, P.J. Cranfill, M.A. Baird, B.R. Sell, J.R. Allen, R.N. Day, M. Israelsson, M.W. Davidson, and J. Wang. 2013. A bright monomeric green fluorescent protein derived from *Branchiostoma lanceolatum*. *Nat. Methods.* 10:407–409. doi:10.1038/nmeth.2413.
- Shemesh, T., R.W. Klemm, F.B. Romano, S. Wang, J. Vaughan, X. Zhuang, H. Tukachinsky, M.M. Kozlov, and T.A. Rapoport. 2014. A model for the generation and interconversion of ER morphologies. *Proc Natl Acad Sci USA.* 111:E5243–51. doi:10.1073/pnas.1419997111.
- Shen, H., P.N. Heacock, C.J. Clancey, and W. Dowhan. 1996. The CDS1 gene encoding CDP-diacylglycerol synthase in *Saccharomyces cerevisiae* is essential for cell growth. *J. Biol. Chem.* 271:789–795. doi:10.1074/jbc.271.2.789.
- Shibata, Y., T. Shemesh, W.A. Prinz, A.F. Palazzo, M.M. Kozlov, and T.A. Rapoport. 2010. Mechanisms determining the morphology of the peripheral ER. *Cell.* 143:774–788. doi:10.1016/j.cell.2010.11.007.
- Shibata, Y., G.K. Voeltz, and T.A. Rapoport. 2006. Rough sheets and smooth tubules. *Cell.* 126:435–439. doi:10.1016/j.cell.2006.07.019.
- Shibata, Y., C. Voss, J.M. Rist, J. Hu, T.A. Rapoport, W.A. Prinz, and G.K. Voeltz. 2008. The reticulon and DP1/Yop1p proteins form immobile oligomers in the tubular endoplasmic reticulum. *J. Biol. Chem.* 283:18892–18904. doi:10.1074/jbc.M800986200.
- Siniosoglou, S., H. Santos-Rosa, J. Rappsilber, M. Mann, and E. Hurt. 1998. A novel complex of membrane

- proteins required for formation of a spherical nucleus. *EMBO J.* 17:6449–6464.
doi:10.1093/emboj/17.22.6449.
- Soto-Cardalda, A., S. Fakas, F. Pascual, H.-S. Choi, and G.M. Carman. 2012. Phosphatidate phosphatase plays role in zinc-mediated regulation of phospholipid synthesis in yeast. *J. Biol. Chem.* 287:968–977.
doi:10.1074/jbc.M111.313130.
- Sprouffske, K., and A. Wagner. 2016. Growthcurver: an R package for obtaining interpretable metrics from microbial growth curves. *BMC Bioinformatics.* 17:172. doi:10.1186/s12859-016-1016-7.
- Sun, Z., and J.L. Brodsky. 2019. Protein quality control in the secretory pathway. *J. Cell Biol.* 218:3171–3187.
doi:10.1083/jcb.201906047.
- Surma, M.A., C. Klose, D. Peng, M. Shales, C. Mrejen, A. Stefanko, H. Braberg, D.E. Gordon, D. Vorkel, C.S. Ejsing, R. Farese, K. Simons, N.J. Krogan, and R. Ernst. 2013. A lipid E-MAP identifies Ubx2 as a critical regulator of lipid saturation and lipid bilayer stress. *Mol. Cell.* 51:519–530.
doi:10.1016/j.molcel.2013.06.014.
- Su, W.-M., G.-S. Han, and G.M. Carman. 2014. Yeast Nem1-Spo7 protein phosphatase activity on Pah1 phosphatidate phosphatase is specific for the Pho85-Pho80 protein kinase phosphorylation sites. *J. Biol. Chem.* 289:34699–34708. doi:10.1074/jbc.M114.614883.
- Su, W.-M., G.-S. Han, P. Dey, and G.M. Carman. 2018. Protein kinase A phosphorylates the Nem1-Spo7 protein phosphatase complex that regulates the phosphorylation state of the phosphatidate phosphatase Pah1 in yeast. *J. Biol. Chem.* 293:15801–15814. doi:10.1074/jbc.RA118.005348.
- Swaney, D.L., P. Beltrao, L. Starita, A. Guo, J. Rush, S. Fields, N.J. Krogan, and J. Villén. 2013. Global analysis of phosphorylation and ubiquitylation cross-talk in protein degradation. *Nat. Methods.* 10:676–682.
doi:10.1038/nmeth.2519.
- Szoradi, T., K. Schaeff, E.M. Garcia-Rivera, D.N. Itzhak, R.M. Schmidt, P.W. Bircham, K. Leiss, J. Diaz-Miyar, V.K. Chen, D. Muzzey, G.H.H. Borner, and S. Schuck. 2018. SHRED Is a Regulatory Cascade that Reprograms Ubr1 Substrate Specificity for Enhanced Protein Quality Control during Stress. *Mol. Cell.* 70:1025-1037.e5. doi:10.1016/j.molcel.2018.04.027.
- Tavassoli, S., J.T. Chao, B.P. Young, R.C. Cox, W.A. Prinz, A.I.P.M. de Kroon, and C.J.R. Loewen. 2013. Plasma membrane--endoplasmic reticulum contact sites regulate phosphatidylcholine synthesis. *EMBO Rep.* 14:434–440. doi:10.1038/embor.2013.36.
- Tong, A.H.Y., and C. Boone. 2007. 16 High-Throughput Strain Construction and Systematic Synthetic Lethal Screening in. *In Yeast Gene Analysis - Second Edition.* Elsevier. 369–707.
- Trezise, S., and S.L. Nutt. 2021. The gene regulatory network controlling plasma cell function. *Immunol. Rev.* 303:23–34. doi:10.1111/imr.12988.
- Usaj, M., Y. Tan, W. Wang, B. VanderSluis, A. Zou, C.L. Myers, M. Costanzo, B. Andrews, and C. Boone. 2017. TheCellMap.org: A Web-Accessible Database for Visualizing and Mining the Global Yeast Genetic Interaction Network. *G3 (Bethesda).* 7:1539–1549. doi:10.1534/g3.117.040220.
- Velázquez, A.P., T. Tatsuta, R. Ghillebert, I. Drescher, and M. Graef. 2016. Lipid droplet-mediated ER homeostasis regulates autophagy and cell survival during starvation. *J. Cell Biol.* 212:621–631.
doi:10.1083/jcb.201508102.
- Venters, B.J., S. Wachi, T.N. Mavrich, B.E. Andersen, P. Jena, A.J. Sinnamon, P. Jain, N.S. Rolleri, C. Jiang, C. Hemeryck-Walsh, and B.F. Pugh. 2011. A comprehensive genomic binding map of gene and chromatin regulatory proteins in *Saccharomyces*. *Mol. Cell.* 41:480–492. doi:10.1016/j.molcel.2011.01.015.
- Veratti, E. 1961. Investigations on the fine structure of striated muscle fiber read before the Reale Istituto Lombardo, 13 March 1902. *J. Biophys. Biochem. Cytol.* 10(4)Suppl:1–59. doi:10.1083/jcb.10.4.1.
- Voeltz, G.K., W.A. Prinz, Y. Shibata, J.M. Rist, and T.A. Rapoport. 2006. A class of membrane proteins shaping the tubular endoplasmic reticulum. *Cell.* 124:573–586. doi:10.1016/j.cell.2005.11.047.
- Voeltz, G.K., M.M. Rolls, and T.A. Rapoport. 2002. Structural organization of the endoplasmic reticulum. *EMBO*

- Rep. 3:944–950. doi:10.1093/embo-reports/kvf202.
- Volmer, R., K. van der Ploeg, and D. Ron. 2013. Membrane lipid saturation activates endoplasmic reticulum unfolded protein response transducers through their transmembrane domains. *Proc Natl Acad Sci USA*. 110:4628–4633. doi:10.1073/pnas.1217611110.
- Walter, P., and D. Ron. 2011. The unfolded protein response: from stress pathway to homeostatic regulation. *Science*. 334:1081–1086. doi:10.1126/science.1209038.
- Wang, B., Z. Zhao, M. Xiong, R. Yan, and K. Xu. 2021a. The endoplasmic reticulum adopts two distinct tubule forms. *BioRxiv*. doi:10.1101/2021.10.26.465969.
- Wang, N., L.D. Clark, Y. Gao, M.M. Kozlov, T. Shemesh, and T.A. Rapoport. 2021b. Mechanism of membrane-curvature generation by ER-tubule shaping proteins. *Nat. Commun.* 12:568. doi:10.1038/s41467-020-20625-y.
- Weinert, B.T., C. Schölz, S.A. Wagner, V. Iesmantavicius, D. Su, J.A. Daniel, and C. Choudhary. 2013. Lysine succinylation is a frequently occurring modification in prokaryotes and eukaryotes and extensively overlaps with acetylation. *Cell Rep.* 4:842–851. doi:10.1016/j.celrep.2013.07.024.
- Westrate, L.M., J.E. Lee, W.A. Prinz, and G.K. Voeltz. 2015. Form follows function: the importance of endoplasmic reticulum shape. *Annu. Rev. Biochem.* 84:791–811. doi:10.1146/annurev-biochem-072711-163501.
- West, M., N. Zurek, A. Hoenger, and G.K. Voeltz. 2011. A 3D analysis of yeast ER structure reveals how ER domains are organized by membrane curvature. *J. Cell Biol.* 193:333–346. doi:10.1083/jcb.201011039.
- White, M.J., J.P. Hirsch, and S.A. Henry. 1991. The OPI1 gene of *Saccharomyces cerevisiae*, a negative regulator of phospholipid biosynthesis, encodes a protein containing polyglutamine tracts and a leucine zipper. *J. Biol. Chem.* 266:863–872.
- Wu, X., and T.A. Rapoport. 2018. Mechanistic insights into ER-associated protein degradation. *Curr. Opin. Cell Biol.* 53:22–28. doi:10.1016/j.ceb.2018.04.004.
- Yamamoto, K., K. Takahara, S. Oyadomari, T. Okada, T. Sato, A. Harada, and K. Mori. 2010. Induction of liver steatosis and lipid droplet formation in ATF6alpha-knockout mice burdened with pharmacological endoplasmic reticulum stress. *Mol. Biol. Cell.* 21:2975–2986. doi:10.1091/mbc.E09-02-0133.
- Yang, C., X. Wang, J. Wang, X. Wang, W. Chen, N. Lu, S. Siniosoglou, Z. Yao, and K. Liu. 2020. Rewiring neuronal glycerolipid metabolism determines the extent of axon regeneration. *Neuron*. 105:276–292.e5. doi:10.1016/j.neuron.2019.10.009.
- Zhang, P., L.S. Csaki, E. Ronquillo, L.J. Baufeld, J.Y. Lin, A. Gutierrez, J.R. Dwyer, D.N. Brindley, L.G. Fong, P. Tontonoz, S.G. Young, and K. Reue. 2019. Lipin 2/3 phosphatidic acid phosphatases maintain phospholipid homeostasis to regulate chylomicron synthesis. *J. Clin. Invest.* 129:281–295. doi:10.1172/JCI122595.
- Zucker-Franklin. 1988. Atlas of blood cells: function and pathology atlas of blood cells in health and disease. *Ann. Intern. Med.* 109:352. doi:10.7326/0003-4819-109-4-352_1.